Zoological Journal of the Linnean Society, 2024, **201**, zlae090
https://doi.org/10.1093/zoolinnean/zlae090
Advance access publication 20 August 2024
Original Article

Original Article

A new theropod dinosaur from the Callovian Balabansai Formation of Kyrgyzstan

Oliver W.M. Rauhut[1,2,3,*], Aizek A. Bakirov[4], Oliver Wings[5], Alexandra E. Fernandes[1,2], Tom R. Hübner[6]

[1]SNSB – Bayerische Staatssammlung für Paläontologie und Geologie, Munich, Germany
[2]Department für Geo- und Umweltwissenschaften, Ludwig-Maximilians-Universität, Munich, Germany
[3]GeoBioCenter, Ludwig-Maximilians-Universität, Munich, Germany
[4]Institute of Geology n.a. M.M. Adyshev, National Academy of Sciences of Kyrgyz Republic, Bishkek, Kyrgyzstan
[5]SNSB – Naturkundemuseum Bamberg, Bamberg, Germany
[6]Friedenstein Stiftung Gotha, Gotha, Germany

[*]Corresponding author. SNSB - Bayerische Staatssammlung für Paläontologie und Geologie, Richard-Wagner-Str. 10, 80333 München, Germany. E-mail: rauhut@snsb.de

ABSTRACT

Recent fieldwork in the late Middle Jurassic Balabansai Formation of Kyrgyzstan has yielded a partial skeleton of a large theropod dinosaur. The material includes a few bones of the skull (postorbital, quadratojugal), dorsal and sacral vertebrae, fragments of the pectoral girdle and forelimbs, and an almost complete pelvic girdle and hindlimbs, and is here made the type of a new theropod taxon, *Alpkarakush kyrgyzicus* gen. et sp. nov. *Alpkarakush* can be diagnosed by an extremely developed orbital brow on the postorbital, a pneumatic opening leading into cavities in the neural arch from the centroprezygodiapophyseal fossa in the posterior dorsal vertebrae, an almost enclosed ventral sulcus in manual phalanx II-1, a narrow and deep intercondylar groove on the anterior side of the distal femur, and an epicondylar crest on the distal femur that is offset from the distal end. A second, fragmentary, and smaller specimen from the same site represents the same taxon. Based on long bone histology, the type of *Alpkarakush* represents a late subadult individual, whereas the smaller specimen is a juvenile, possibly indicating gregarious behaviour. Phylogenetic analysis places *Alpkarakush* in the Metriacanthosauridae, underlining the diversity and wide distribution of this clade in the Jurassic of Asia.

Keywords: Central Asia; Middle Jurassic; Tetanurae; Metriacanthosauridae; bone histology

INTRODUCTION

During the Jurassic, many dinosaur clades experienced their most important radiations, and many new clades arose and spread. At the same time, the beginning of the fragmentation of the supercontinent Pangea, first by the formation of epicontinental seas and later also by seafloor spreading, has been argued to have led to increased endemism and faunal differentiation (e.g. Bonaparte 1980, 1995, Upchurch *et al.* 2002, Rauhut and López-Arbarello 2008, Wilson and Upchurch 2009, Foth and Rauhut 2017, Xu *et al.* 2018).

Apart from a few localities in the Asian parts of Russia (e.g. Averianov and Krasnolutskii 2009, Averianov *et al.* 2010, Godefroit *et al.* 2014), dinosaur faunas from the Middle to Late Jurassic of Asia are so far mainly known from localities in China. Up to 30 years ago, only the dinosaurs of the Shaximiao Formation (and equivalent beds) of Sichuan were known (see Dong *et al.* 1983, He 1984, Peng *et al.* 2005). The faunas from this unit still represent the most important reference faunas for this time from Asia, but their exact ages remain debated. Usually, two different faunas are distinguished, the lower *Shunosaurus-Omeisaurus* fauna from the Lower Shaximiao Formation (= Xiashaximiao Formation of some authors) and the upper *Mamenchisaurus* fauna from the Upper Shaximiao Formation (Shangshaximiao Formation of some authors; see Dong *et al.* 1983, Peng *et al.* 2005, Li *et al.* 2011). Most authors assumed a Middle Jurassic age for the *Shunosaurus-Omeisaurus* assemblage, and a Late Jurassic age for the *Mamenchisaurus* assemblage (e.g. Dong *et al.* 1983, Peng *et al.* 2005), but Li *et al.* (2011) argued for a Middle Jurassic age for both assemblages. In contrast, Wang *et al.* (2018) found radiometric evidence for an Oxfordian

---

Received 12 February 2024; revised 27 May 2024; accepted 1 July 2024

age for the Lower Shaximiao Formation at the famous Zigong Quarry, based on detrital zircons, indicating an entirely Upper Jurassic placement of the Shaximiao Formation. Even more recently, Zhou *et al.* (2022) reported a Late Middle Jurassic age (Callovian, 166 Mya) for the Lower Shaximiao Formation in the Chongqing area, based on a tuffaceous siltstone some 17 m below the dinosaur-bearing horizons. Thus, the Shaximiao faunas are most probably latest Middle to Late Jurassic in age.

In the past 30 years, more Middle and Late Jurassic dinosaur remains have been described from China. Especially noteworthy here are the Shishugou Formation of Xinjiang (Callovian–Oxfordian; Xu *et al.* 2022) and the Yanliao Biota of north-eastern China (?Callovian–Oxfordian; Xu *et al.* 2016, Zhou and Wang 2017), although important isolated finds have also been made in other Middle and Late Jurassic units (e.g. Wu *et al.* 2009, Xing *et al.* 2015, Xu *et al.* 2018, 2023).

Concerning theropod dinosaurs, the eastern Asian Middle to Late Jurassic faunas are dominated by tetanurans, with the only non-tetanuran theropod reported being the ceratosaur *Limusaurus* (Xu *et al.* 2009). Tetanurans from the Middle Jurassic of China include the early Middle Jurassic metriacanthosaurid *Shidaisaurus* (Wu *et al.* 2009, see also Carrano *et al.* 2012, note that this specimen was originally considered to be from the upper part of the Lufeng Formation, but the locality has recently been considered to be in the Chuanjie Formation; Ren *et al.* 2021), the either early branching tetanuran (Carrano *et al.* 2012) or megalosauroid (Rauhut *et al.* 2016, Schade *et al.* 2023) *Monolophosaurus*, and an array of poorly known taxa of uncertain affinities from the Lower Shaximiao Formation. The latter include the probably early branching tetanuran *Chuandongocoelurus* (He 1984, see Carrano *et al.* 2012), the either early branching tetanuran or metriacanthosaurid '*Szechuanosaurus*' *zigongensis* (Gao 1993, see Rauhut 2003, Carrano *et al.* 2012), the piatnitzkysaurid or metriacanthosaurid *Xuanhanosaurus* (Dong 1984, see Carrano *et al.* 2012, Rauhut *et al.* 2016), and the poorly known *Gasosaurus* (Dong and Tang 1985) and *Kaijiangosaurus* (He 1984). From the Late Jurassic of China, a large array of usually small-bodied coelurosaurs has been described in the past 20 years, including early branching taxa (Choiniere *et al.* 2010a), tyrannosauroids (Xu *et al.* 2004, 2006), alvarezsauroids (Choiniere *et al.* 2010b, Qin *et al.* 2019), and an array of pennaraptorans (e.g. Zhang *et al.* 2008, Hu *et al.* 2009, 2018, Xu *et al.* 2011, 2015, 2023). Large-bodied theropods from that time are mainly represented by metriacanthosaurids, with two species of *Yangchuanosaurus*, a so far unnamed third taxon ('*Szechuanosaurus campi*', CV 00214; Dong *et al.* 1983, see Carrano *et al.* 2012) from the Upper Shaximiao Formation, and *Sinraptor dongi* from the Shishugou Formation (Currie and Zhao 1993). Outside China, the only Jurassic metriacanthosaurid known is the poorly known name-giving genus of the clade, *Metriacanthosaurus*, from the Oxfordian of England (Huene 1926, Walker 1964, see Carrano *et al.* 2012). The so far youngest and only Cretaceous representative of this clade is the Barremian *Siamotyrannus isanensis* from the Sao Khua Formation of Thailand (Buffetaut *et al.* 1996, Carrano *et al.* 2012).

Metriacanthosaurids are a clade of medium to large-sized (5–8 m body length) allosauroid theropods that are characterized by high arched skulls, plate-like elongate dorsal neural spines, and rather slender hindlimbs (see Huene 1926, Dong *et al.* 1983, Currie and Zhao 1993, Gao 1999). Synapomorphies of the clade include the absence of an anterior ramus of the maxilla, the presence of at least a small suborbital flange on the ventral process of the postorbital, the presence of a pronounced orbital brow on the postorbital, a large and unconstricted infratemporal fenestra, an anterodorsally sloping occiput in the braincase, dorsal neural spines that are more than twice the height of their respective centra, a narrow brevis fossa in the ilium, a heart-shaped cross section of the articulated ischia, distally fused ischia, and a bulbous fibular crest on the tibia (Carrano *et al.* 2012).

In Central Asia, the Middle Jurassic Balabansai Formation in the northern part of the Fergana Depression, Kyrgyzstan, is known for a rich vertebrate fauna, including dinosaurs (Averianov 2000, and references therein, Averianov and Bakirov 2000, Averianov *et al.* 2005, 2006, 2007, 2008). In July 1966, a geological team of the Leningrad State University (now Saint Petersburg State University), led by N.N. Verzilin, found a partial sauropod skeleton in the upper part of the Balabansai Formation at the Balabansai ravine in the southern foothills of the Chatkal Range, 5 km west of Tashkumyr City, in western Kyrgyzstan. This was the first sauropod skeleton found in the former USSR (Rozhdestvensky 1968). It was excavated in August 1966 and July 1967 by a team from the Moscow Paleontological Institute, led by A.K. Rozhdestvensky, which recovered an articulated skeleton, lacking the skull, cervical and posterior caudal vertebrae, both hind feet, and the right manus. This skeleton was described as the first valid dinosaur taxon from Kyrgyzstan, the eusauropod *Ferganasaurus verzilini*, although the dorsal vertebrae, some of the caudal vertebrae, the scapulocoracoid, and the manus can no longer be found in the collections of the Paleontological Institute (Alifanov and Averianov 2003).

In 1967, N.N. Verzilin found another partial sauropod skeleton in the middle-upper part of the Balabansai Formation at Balabansai, including pelvis bones, a sacrum, a partial femur, and some dorsal, sacral, and caudal vertebrae (Nessov 1995). The fate of this skeleton is unknown, and it is possible that it was not excavated (Alifanov and Averianov 2003). Since then, mostly finds of isolated bones and teeth of sauropod and theropod dinosaurs have been documented (Nessov 1995).

The next phase of palaeontological fieldwork took place between 2000 and 2006, when a combined Kyrgyz-Russian-German field team worked in northern Fergana. Thanks to their successful work, the Balabansai Formation is now known for often fragmented or isolated remains of a diverse fossil vertebrate fauna, including sharks, bony fish, primitive salamanders, the turtle *Xinjiangchelys*, a lizard, a choristodere reptile, the mesoeucrocodyle *Sunosuchus*, pterosaurs, several dinosaurs, and up to 10 mammal species (see Nessov 1995, Averianov 2000, Averianov and Bakirov 2000, Alifanov and Averianov 2003, Averianov *et al.* 2005, 2006, 2007, 2008, Martin and Averianov 2010).

Apart from the eusauropod *Ferganasaurus verzilini* (Alifanov and Averianov 2003, Averianov *et al.* 2005, Ksepka and Norell 2010) and a named but challenged ornithischian taxon based on teeth only (Averianov *et al.* 2005, Sullivan 2006), further dinosaur finds up to now were too incomplete to be named. The fauna comprises a diverse assemblage though, including one of the oldest known and westernmost Asian stegosaurs (Averianov *et al.* 2007) and probable tetanuran theropods, so far only represented by teeth (Nessov 1995, Averianov *et al.* 2005, Carrano *et al.* 2012).

More recent excavations led by one of the authors (AAB) in 2005 and 2006 at two localities close to Tashkumyr (the Sarykamyshsai and Uurusai valleys) have produced more complete dinosaur remains (Averianov *et al.* 2007). One partial skeleton consists of 12 articulated caudal vertebrae and other bone fragments of a sauropod dinosaur, which were already excavated and partly prepared. The second find, from the FTU-1 site (FTU for Fergana-Tashkumyr-Uurusai) in the Uurusai Valley (Figs 1, 2), located west of Tashkumyr, is from the upper (red-coloured) part of the Balabansai Formation and comprises the partial remains of two theropod dinosaurs. In 2006, one of the authors (AAB) found a vertebra and a carpal phalanx on the weathered surface. During the excavation of this site, some limb bones and ribs were recovered. In 2009, no further bone remains could be found at this site. In 2014, during an extended and deepened excavation at this site, it was possible to extract some bones of

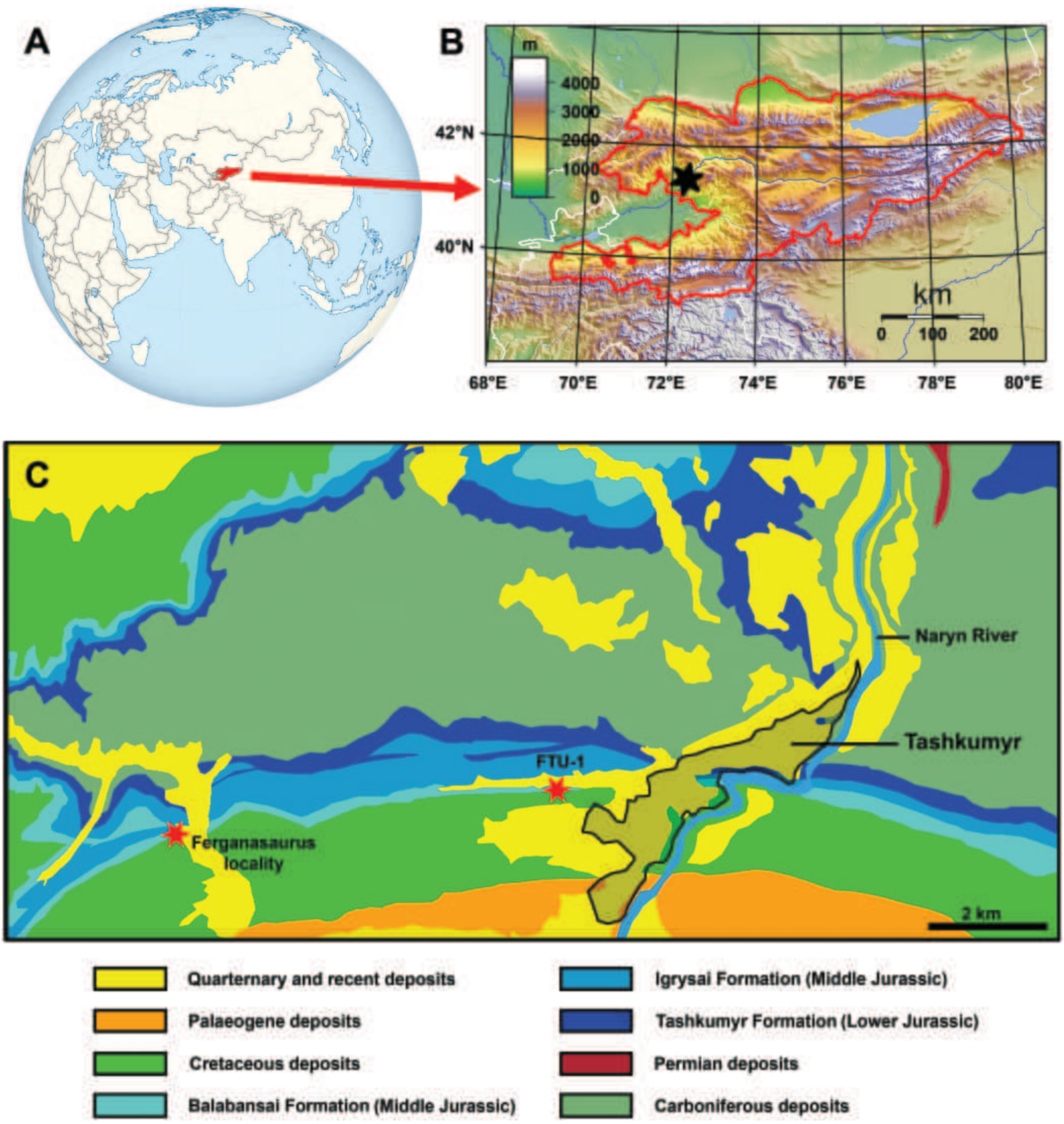

Figure 1. Geographic location of the locality FTU-1 within Kyrgyzstan (A, B) and general geological map of the area around the city of Tashkumyr (C).

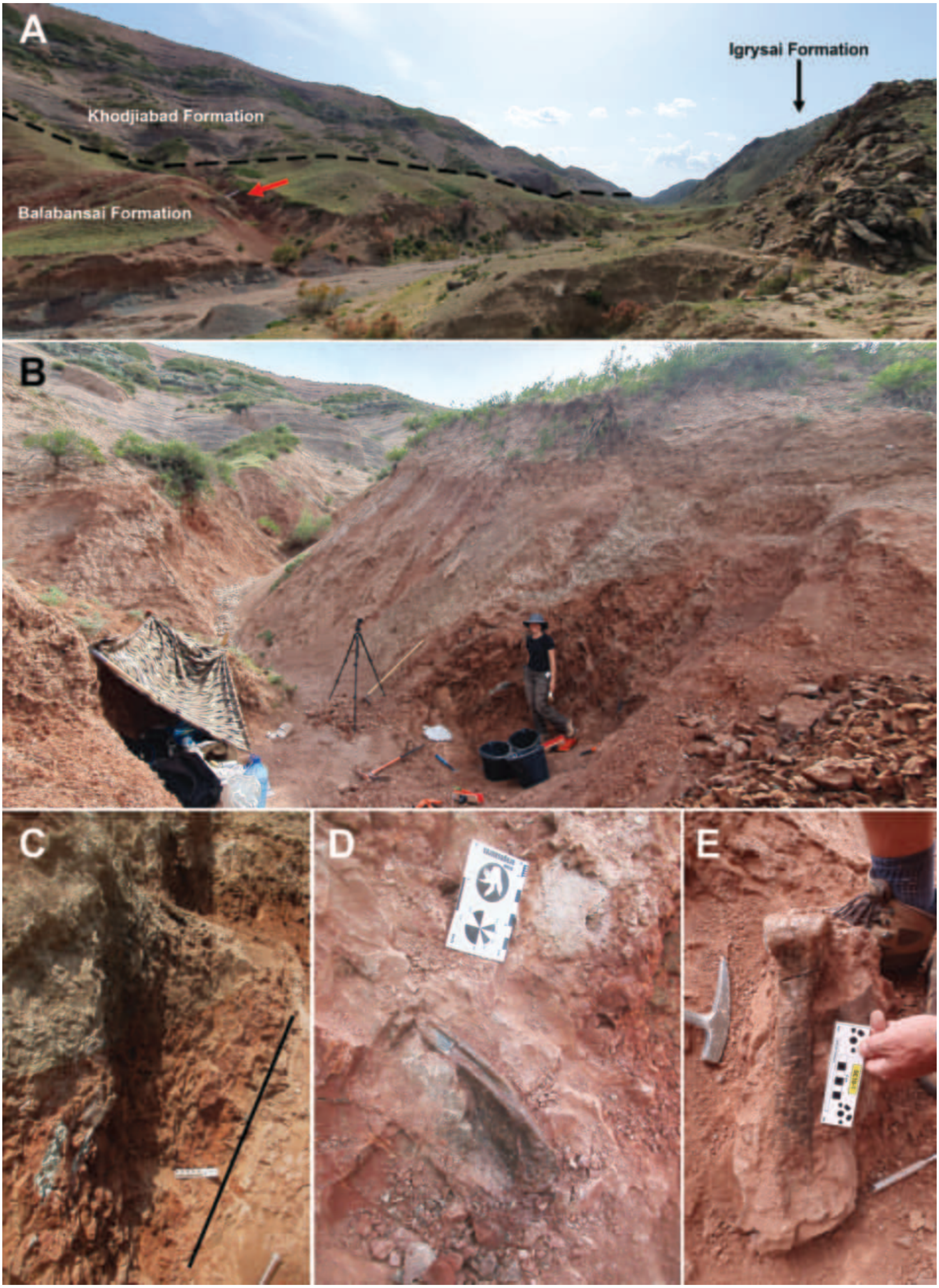

Figure 2. Excavation site FTU-1. A, position of the site within the Uurusai Valley west of Tashkumyr (red arrow). B, overview of the site, with one of the authors (A.E.F.) for scale. C, section of the excavation site. Black line indicates approximate dip of the sediments. D, quadratojugal of the new theropod as discovered in the field. E, metatarsal III of the new theropod during the excavation.

the limbs in anatomical order, as well as vertebrae and ribs. The pelvic bones and sacral vertebrae were exposed in articulation, but the excavation had to be stopped because the steeply inclined bone-bearing layer went deep into the slope, which required the removal of a large amount of overburden. For this reason and the lack of funding for fieldwork, the site was mothballed. In 2016–2017 excavations could continue and the remaining bones were recovered (Bakirov 2009, 2013, 2019). Finally, a Kyrgyz-German expedition consisting of all participating authors re-opened and deepened the FTU-1 site in 2023, resulting in the finding of several additional isolated bones and teeth (Fig. 2).

In total, a considerable part of an associated theropod skeleton and some additional vertebrate remains, including a fragmentary second theropod specimen could be extracted from the FTU-1 site over the years. This important material is described and analysed in detail here.

Geological setting

Three Jurassic formations of terrestrial sediments are exposed in the surroundings of the city of Tashkumyr in the western part of Kyrgyzstan. The Tashkumyr, Igrysai, and Balabansai formations (from bottom to top) form a continuous succession without obvious unconformities in between. The succession starts with the lowermost, coal-bearing Tashkumyr Formation, followed by the Igrysai Formation, which is composed of alternating brightly coloured sandstones and dark-coloured mudstones, and is completed by the Balabansai Formation at the top, which mainly consists of reddish-brown and grey mudstones with intercalated siltstones and sandstones. Thus, within these Jurassic deposits, there is a clear tendency from humid to more arid climatic conditions (Averianov *et al.* 2005). The Balabansai Formation is finally unconformably overlain by Lower Cretaceous conglomerates of the Khodjiabad Formation, with an erosional base (Fig. 2A). For an overview of the geology of the Balabansai Formation, see Averianov *et al.* (2005). The Balabansai Formation is currently dated by palynomorphs and vertebrate assemblages as late Middle Jurassic (Bathonian–Callovian; Aliev *et al.* 1981, Averianov and Bakirov 2000, Averianov *et al.* 2005, 2006).

The sedimentary rocks at the FTU-1 excavation site are composed of fine-scaled, up to 1 m-thick, fining-upward cycles of greyish fine sandstones to reddish mudstones (Fig. 2B, C). The steeply inclined strata dip with up to 80° southwards. Layers of fine sandstone and reddish mudstone also alternate within a millimetre scale. Isolated lenses of fine sandstone, sometimes housing microfossils, may be incorporated as well. Locally, the sediment layers have been secondarily bleached. These bleached zones often cross normal-coloured sediment layers. Green spots, indicating reducing chemical conditions, are locally abundant and are sometimes developed into hard concretions up to several centimetres in diameter, but without any fossil content.

All bones of the FTU-1-site were found at the base of a fining-upward cycle. During excavation of additional bones from that site in 2023, a lens with microfossils, including pieces of turtle carapace, lungfish tooth plates, and fish teeth, was found. Generally, the remains of the two theropod individuals were spread over several square metres with the still articulated pelvic region of the holotype of the new taxon (sacral vertebrae, pelvis, femur) in the centre and associated bones scattered around it.

MATERIAL AND METHODS

Material

All the fossils described here come from the single locality FTU-1 in the upper section of the Balabansai Formation close to the town of Tashkumyr, Jalal-Abad, Kyrgyzstan (Figs 1, 2). The excavation site FTU-1 at the Uurusai Valley is situated *c.* 1000 m west of the city centre of Tashkumyr (measured coordinates: N 41°20’25.5”, E 72°11’28.5”) at the floor of a small gully (Fig. 2A, B).

Vertebrate fossils retrieved from the FTU-1 locality include numerous elements of two large theropod dinosaurs. All the elements here referred to the holotype of the new taxon are consistent in size and, in the case of serial elements (vertebrae), morphology. Furthermore, elements known from the left and right side of the body (postorbitals, pubes, femora, tibiae, astragalocalcanea, metatarsal III) are virtually identical in size and morphology (apart from preservation-related deformation or damage), and the femoral head of the left femur was found in the acetabulum of the left ilium, with the articulated ischia placed in natural position behind the shaft of this bone in a separate jacket. Thus, there can be little doubt that all of this material represents a single individual. Apart from the holotype, a few elements of a smaller theropod (both pubes, partial ischium, right tibia) as well as additional microvertebrate remains were recovered from the site. The smaller theropod individual is interpreted as representing the same taxon as the large theropod (see discussion below). A few elements, including teeth and a furcula, cannot be confidently assigned to either of the two individuals. However, as there are no indications for any other larger vertebrates in the locality, apart from the two theropod specimens that represent the same taxon, these materials are here regarded as referred specimens. In the case of the teeth, this should be seen as tentative, especially for the possible premaxillary teeth, as it cannot be ruled out that these elements represent shed teeth of scavengers.

Preparation of the material was carried out by the authors in May 2023. Several field jackets in varying states of preservation were retrieved from the suboptimal long-term storage at the Geological Institute in Bishkekand opened there for fossil preparation (which was also performed in tandem on the finds retrieved from the current fieldwork expedition). All fossil elements were extracted completely from their jackets and field wrappings. Apart from the jackets, numerous elements were paper or tinfoil wrapped and stored in cardboard boxes, often in many separate pieces. All of these remains were unwrapped, cleaned, and puzzled together as much as possible.

Serious time constraints, limited resources, and the lack of availability of laboratory-grade glues, solvents, and other state-of-the-art tools (beyond what was brought along from outside Kyrgyzstan for intended fieldwork usage) demanded numerous compromises on the treatment standards applied to the fossils. No original surface consolidation of fossil elements had been performed *in situ* at the time of the original excavation years prior, and therefore preparation efforts were begun by surface consolidation of exposed bone surfaces with varying concentrations of Paraloid B-72 in a locally-sourced acetone-based solvent (marketed as acetone, but of unknown exact chemical composition). This solvent compromised the utility of the Paraloid B-72 to be used in any functional adhesive capacity, and therefore any further surface breaks or deep fissures were necessarily glued and reinforced with store-brand epoxies and cyanoacrylates, namely Starbond EM 150, Akfix 702 Super Glue, and Akfix E340 Epoxy, as required. Bone fragments that had undergone exceptional fracturing (e.g. the vertebral neural spines) were reinforced by facing the bone surfaces with surgical compresses cut to size, and soaked in Paraloid B-72 in acetone. Mechanical sediment cleaning of the fossils was first performed using an assortment of metal hand tools, wooden dowels, and soft-bristled brushes. In some cases, the dirt cover of clearly solid bones was brushed off with water. Mechanical cleaning was performed using an Aircraft Mobilboy 261/10S compressor with a Kranz W 224 pneumatic micro-hammer attachment. Customized housing and storage for the fossils was improvised in a pre-existing museum storage cabinet, using a locally-sourced polyethylene foam subfloor underlayment that was sourced from a construction supplier. Minimal interventions were performed overall on the fossils, in the hope that in the future, with more access to resources, remediations and upgrades can be made over time.

All of the specimens are housed in the Paleontological Collection of the Institute of Geology, National Academy of Sciences, Kyrgyz Republic, Bishkek, Kyrgyzstan (abbreviated as IGB).

Nomenclatural acts

The electronic edition of this article conforms to the requirements of the amended International Code of Zoological Nomenclature (ICZN), and hence the new names contained herein are available under that Code from the electronic edition of this article. This published work and the nomenclatural acts it contains have been registered in ZooBank, the online registration system for the ICZN.

Photogrammetry

High-resolution photogrammetric 3D-models were generated for the anatomically relevant bones from photographs taken after preparation following the procedures described by Mallison and Wings (2014). Photographs were taken by O.W. using a Samsung S10+ smartphone. Photogrammetric models were generated using the PC software programme Agisoft Metashape Professional v.2.0.1 (www.agisoft.com). Photographs and corresponding mesh data of the photogrammetric 3D-models are available online in PLY-format at https://www.morphosource.org/concern/biological_specimens/000630389/.

Histological sampling

Because weight-bearing bones in large to gigantic theropods are more informative in skeletochronology than non-weight bearing bones (Cullen *et al.* 2020), long bones of the hindlimb were chosen for a general insight into the assessment of skeletal maturity of both theropod individuals of the locality FTU-1. The right femur of the holotype of the new taxon (IGB 2/33) was sampled at the level of the smallest circumference of the shaft, *c.* 34 cm from the distal end. The shaft outline at this level was triangular. For handling reasons, only the posterior and lateral corners, including the posterolateral bone wall in between, were processed into two thin sections of *c.* 100 microns thickness. Fossil bones from FTU-1 were generally very hard, but also very brittle. In addition, there was a distinct mineralization present with a silvery-black metallic mineral. The elemental content of this mineral was analysed using a handheld XL3t X-ray fluorescence spectrometer. Most of the medullary cavity and the cracks within the bone wall were filled by dark minerals, but also several regions of the fossil tissue itself were stained black, hampering microscopic analysis. For reasons of better preservation and especially less staining of the skeletal tissue, the description of the femoral bone histology focuses mainly on the section incorporating the lateral corner and most of the posterolateral wall.

From the right tibia of the smaller individual (IGB 2-48), a piece from the posterior bone wall of the brittle shaft was extracted, approximately from the level of the border between the lower and middle third of the bone length. Only the bone wall itself could be extracted, whereas the sediment-filled free medullary cavity remained with the tibia. The staining of the bone tissue was less extensive than in the sampled large femur. Cracks were often filled by the dark mineral.

The processing of bone samples into thin sections was done in the lab in Friedenstein Stiftung Gotha, Germany. Before cutting of the long bone samples, casts were made to maintain the original dimensions. The sampling procedure generally followed Chinsamy and Raath (1992) and Lamm (2013). The cutting of the femur samples was performed using a Uniprec WOCO 50 abrasive cutoff machine, whereas for the tibia sample, a Bühler IsoMet was used. Specimens were ground and polished using a Bühler EcoMet 30 grinding machine. The impregnation of specimens before cutting as well as the gluing onto glass slides was done with the epoxy resin EPO-TEK 301-1. The thin sections were finally analysed, digitally measured, and images generated with a Zeiss Axioscope 5/7 combined with an axiocam 305 colour camera and the software ZEN Core v.3.3.

Phylogenetic analysis

In order to evaluate the phylogenetic position of the new theropod from Kyrgyzstan, we included it in the Mesozoic Tetrapod Group Theropod Matrix that is currently being developed at the Bayerische Staatssammlung für Paläontologie und Geologie in Munich, Germany, by an international team of theropod experts. This matrix is originally based on the phylogenetic dataset published by Wang *et al.* (2017), incorporating the changes implemented by Rauhut and Pol (2021). Since the publication of the latter paper, characters, coding, and taxon sampling has been constantly evaluated and expanded on by the work group. As the new taxon described clearly represents a basal, non-coelurosaurian tetanuran, we reduced the taxon sampling of the original matrix to keep only several, well-known representatives of more distantly related clades, such as abelisaurids, oviraptorosaurs, or paravians, among others. The final matrix thus had a total of 112 Operational Taxonomic Units (OTUs), scored for 841 morphological characters (see Supporting information, file D1). The data matrix was analyzed in the PC software TNT 1.6 (Goloboff and Morales 2023) both under equally weighted maximum parsimony criteria and using implied weights (Goloboff *et al.* 2018). In order to test the results for the sensitivity to character weighing, we used different concavities, with k = 12, k = 9, k = 6, and k = 3 (see Goloboff *et al.* 2018). All analyses were carried out using first a new technology search, aimed to find the shortest tree 30 times, followed by tree-bisection-and-reconnection (TBR) branch swapping. Character support of nodes and alternative topologies were explored using TNT and Mesquite 3.81 (Maddison and Maddison 2023).

Biogeographic analysis

In order to test the biogeographic implications of our phylogenetic analysis, we carried out a Statistical Dispersal-Vacariance-Analysis (S-DIVA; Yu *et al.* 2010), using the program RASP (Yu *et al.* 2015). For this analysis, we used the resulting trees from our implied weighing analysis with k = 12 (see discussion under results), which were read into RASP to produce a condensed (= consensus) tree for which the biogeographical reconstruction was calculated. In order to account for stratigraphic heterogeneity of geographical areas over the long time-scale covered by our phylogenetic dataset, we defined rather small, sub-continent-scale geographical areas for the analysis (unless only a single taxon was known from a continent or taxa are only known from a part of a continent). Areas that have not yielded taxa, either generally, or not taxa included in the analysis, may be missing from the areas as defined below. Thus, areas used included North Africa (the Sahel zone and the areas north of it), Central Africa (sub-Saharan Africa north of Namibia/Zimbabwe), South Africa (Africa south of the northern borders of Namibia/Zimbabwe), Antarctica, Central Asia (area from the Chinese province of Xinjiang to the Caspian Sea), North-Eastern Asia (Chinese provinces of Inner Mongolia, Liaoning, Hebei, and Shanxi, and Mongolia and Japan), South-Eastern Asia (Chinese provinces of Sichuan and Yunnan and areas south of this), Australia, North-Eastern Europe (central and northern Europe), South-Western Europe (Iberian Peninsula), western North America, central South America (Brazil), and southern South America (Argentina).

Institutional abbreviations

DINO, Dinosaur National Monument, Jensen, USA; IGB, Institute of Geology, National Academy of Sciences, Bishkek, Kyrgyzstan; IVPP, Institute for Vertebrate Paleontology and Paleoanthropology, Chinese Academy of Sciences, Beijing, China; MACN, Museo Argentino de Ciencias Naturales 'Bernardino Rivadavia', Buenos Aires, Argentina; MPEF, Museo Paleontológico Egidio Feruglio, Trelew, Argentina; NCSM, North Carolina Museum of Natural Sciences, Raleigh, USA; OUM, Oxford University Museum, Oxford, UK; SGM, Service Géologique du Maroc, Ministére de l'Energie et des Mines, Rabat, Morocco; USNM, United States National Museum, Smithsonian Institution, Washington D.C., USA.

RESULTS

SYSTEMATIC PALAEONTOLOGY

Dinosauria Owen, 1842

Saurischia Seeley, 1887

Theropoda Marsh, 1881

Tetanurae Gauthier, 1986

Metriacanthosauridae Paul, 1988

Alpkarakush gen. nov.

ZooBank LSID: urn:lsid::act:AEE2C533-04B8-45E9-90C1-D0DA2F90840E.

Etymology: Named after *Alpkarakush*, a mythological large bird that often comes to the help of heroes in critical moments in the 'Manas' epos, one of the central mythological elements in Kyrgyz culture (Seiilbek *et al.* 2018).

Diagnosis: As for species.

Type species: Alpkarakush kyrgyzicus sp. nov.

Alpkarakush kyrgyzicus sp. nov.

ZooBank LSID: urn:lsid:zoobank.org:act:2ABC5B5C-7119-4D12-842F-1CB9D88CF2CB.

Etymology: The species epithet refers to the Kyrgyz Republic, the provenance of the type specimen.

Holotype: Partial skeleton (Fig. 3), including both postorbitals (IGB 2-1, 2-2), the left quadratojugal (IGB 2-9), two posterior dorsal vertebral centra (IGB 2-10,2-11), two partial dorsal neural spines (IGB 2-12, 2-13) and a fragment of the dorsal neural arch (IGB 2-22), five sacral vertebrae (IGB 2-14, 2-15), several dorsal ribs (IGB 2-16, 2-17, 2-18, 2-19, 2-20, 2-21), a manual phalanx (IGB 2-24), a manual ungual (IGB 2-47), a partial left ilium (IGB 2-25), a partial pubes (IGB 2-26, 2-27, 2-28, 2-29),

Figure 3. Outline reconstruction of *Alpkarakush kyrgyzicus*, with recovered elements indicated. Scale bar is 1 m.

both articulated ischia (IGB 2-30, 2-31), a complete left (IGB 2-32) and right (IGB 2-33) femora, a complete left (IGB 2-34) and right tibiae (IGB 2-35), an almost complete left fibula (IGB 2-36, 2-37), left and right astragalocalcanea (IGB 2-38, 2-39), a partial left distal tarsal IV (IGB 2-40), a left metatarsal II (IGB 2-41), a left and right metatarsal III (IGB 2-42, 2-43), a pedal phalanx (IGB 2-44), and two pedal unguals (IGB 2-45, 2-46).

Paratype: Fragmentary postcranium of a smaller individual, from the same locality as the holotype, including the left and right pubes (IGB 2-49, 2-50, 2-51, 2-52), a proximal fragment of the right ischium (IGB 2-53), and a right tibia (IGB 2-48).

Referred material: Several isolated teeth (IGB 2-3, 2-4, 2-5, 2-6, 2-7, 2-8, 2-27) and a furcula (IGB 2-23) from the type locality are referred to the same taxon. In the case of the teeth IGB 2-6, 2-7, 2-8, and 2-27, this referral should be regarded as tentative (see below).

Type locality and horizon: Locality FTU-1, just west of the town of Tashkumyr, Jalal-Abad Oblast, Kyrgyzstan (Figs 1, 2). The specimens were found in the higher part of the Balabansai Formation, Callovian.

Diagnosis: Alpkarakush kyrgyzicus can be diagnosed by the following combination of characters (autapomorphies are indicated by *): extremely developed supraorbital brow on the postorbital, overhanging the orbit; posterior dorsal vertebrae with a channel leading from the centroprezygodiapophyseal fossa posteromedially into pneumatic chambers in the neural arch*; sacral vertebrae with fused neural spines that are approximately as high as the combined height of the vertebral centrum plus neural arch; manual phalanx II-1 with a ventral sulcus proximally that is almost completely enclosed by medial and lateral ventral flanges*; dorsal margin of the ilium slopes steeply posteroventrally*; brevis fossa on ilium reduced to a small medial shelf; shaft of pubis strongly bowed anteriorly; well-developed longitudinal depression on the posterolateral side of the pubic shaft adjacent to the pubic boot (based on paratype); unusually high pubis/tibia ratio (1.22 or higher); articulated ischia with pronounced ischial boots that are convex distally and fused anteriorly, but separated posteriorly; ischium with small obturator flange that is offset from the pubic peduncle; pubic peduncle of ischium very long; iliac articulation in proximal ischium cup-shaped; narrow and deep intercondylar groove on the anterior side of distal femur*; robust and well-developed medial epicondylar crest on distal femur, considerably offset proximally from distal end*; tibia with robust, bulbous fibular flange; astragalus and calcaneum fused.

Description

Cranium

Only both postorbitals and the left quadratojugal are preserved of the cranium. In addition, several teeth were collected from the site, at least several of which represent the same taxon with high certainty.

Postorbital: Both postorbitals are preserved (Fig. 4). The left element (IGB 2-1) is complete (Fig. 4A–D), while the right postorbital (IGB 2-2) has been reconstructed from numerous fragments and misses several of the finer margins (Fig. 4E, F). As in most non-maniraptoriform theropods, the postorbital is a triradiate, T-shaped bone, in which the ventral (jugal) process is considerably longer than either the anterior (frontal) or posterior (squamosal) processes. The postorbital is *c.* 20 cm high and 17.5 cm long over the anterior and posterior processes, of which the anterior process is longer (c. 8 cm) than the posterior process (5 cm).

The most conspicuous character of the postorbital is an extremely developed, rugose orbital brow that covers the posterior two-thirds of the anterior process and the anterior half of the junction of the three processes (Fig. 4A, D, E). This brow forms a massive lateral and dorsal swelling with a rugose lateral surface, composed of numerous small tubercles, giving it a granulate texture. It considerably overhangs the posterodorsal part of the orbital cavity, thus forming a mediolaterally deeply concave dorsomedial surface of this opening at the junction of the processes. Strongly developed postorbital brows are generally present in carcharodontosaurids (e.g. Sereno *et al.* 1996, Coria and Currie 2006, Canale *et al.* 2022), and also in the metriacanthosaurids (Dong *et al.* 1983, Currie and Zhao 1993, Gao 1999). However, whereas carcharodontosaurids usually have an ornamentation of ridges and grooves, metriacanthosaurids show a similar granulated structure as it is also present in *Alpkarakush*. From the posterior margin of the brow, a marked oblique step extends posteroventrally over the lateral surface of the ventral process (Fig. 4A), as in *Sinraptor* (Currie and Zhao 1993). This step meets the convex posterior margin of this process at approximately its half height and separates a smooth posterodorsal surface from a more rugose anteroventral surface, which covers most of the lateral surface of the ventral process, similar to the condition in many abelisaurids (e.g. Sampson and Witmer 2007, Cerroni *et al.* 2020). Similar low rugosities also cover the lateral and dorsal surfaces of the anterior process anterior to the orbital brow. The anterior end of the anterior process is turned ventrally, as in *Irritator* (Schade *et al.* 2023). The anterior margin of the anterior process is massive (*c.* 15 mm thick dorsoventrally), but lacks an articular facet for the lacrimal/prefrontal, indicating that the latter elements did not contact the postorbital, in contrast to abelisaurids (Bonaparte and Novas 1985, Bonaparte *et al.* 1990, Sampson and Witmer 2007) and carcharodontosaurids (Sereno *et al.* 1996, Coria and Currie 2002, Sereno and Brusatte 2008). The posterior process is short and spike like, being wider mediolaterally than dorsoventrally over its entire length, as in *Sinraptor* (Currie and Zhao 1993), but in contrast to most theropods, where this process usually forms a dorsoventrally oriented, triangular sheet of bone (e.g. Madsen 1976, Britt 1991, Brusatte *et al.* 2012, Rauhut *et al.* 2016). In dorsal view, this process tapers posteriorly and shows weak longitudinal striations where it was overlapped by the squamosal (Fig. 4D). There is a marked asymmetry in the development of the lateral surface of the posterior process of the left and right postorbital; whereas it is dorsoventrally narrow in the former, and was probably underlain by the ventral anterior process of the squamosal, the right element shows a deep longitudinal groove on the lateral surface of this process (Fig. 4E), in which the anterior process of the squamosal might have fitted. A similar groove on the lateral side of the posterior process of the postorbital is found in *Sinraptor* (Currie and Zhao 1993).

Figure 4. Postorbital of *A. kyrgyzicus*. A–D, left postorbital IGB 2-1 in lateral (A, stereophotographs), posterior (B), medial (C), and dorsal (D, stereophotographs) views. E, F, right postorbital IGB 2-2 in lateral (E) and medial (F) views. Abbreviations: g, groove; jf, jugal facet; ls, laterosphenoid contact; ob, orbital brow; pp, posterior process; sf, supratemporal fossa; sq, squamosal facet; st, step. Scale bar is 5 cm.

In medial view, a marked ridge forms the posterior and posterodorsal margins of the orbit and extends from the anteromedial end of the anterior process to the ventral end of the ventral process (Fig. 4C, F). A stout flange of bone extends from the ventral end of this ridge towards the base of the posterior process, thus forming the markedly convex dorsal part of the anterior margin of the infratemporal fenestra; the ventral part of this margin was formed by the dorsal process of the jugal, which the postorbital overlapped anteriorly in the ventral third of its height. The facet for the jugal is developed as a broad, posteriorly opening groove on the posterior surface of the orbital ridge (Fig. 4B), as in megalosauroids (e.g. Britt 1991, Sereno *et al.* 1994, Sadleir *et al.* 2008, Rauhut *et al.* 2016, Schade *et al.* 2023). Anterior to the orbital ridge, a small anterior flange intruding into the orbit was obviously present, similar to the situation in *Sinraptor* (Currie and Zhao 1993) and other metriacanthosaurids (Gao 1999), but is damaged on both sides. At the junction of the three processes, a deep, oval depression dorsal to the orbital ridge marks the contact with the laterosphenoid. (Fig. 4C, F)

In dorsal view, the supratemporal fossa extends onto the medial side of the anterior process of the postorbital and forms a smooth, dorsally facing shelf anterior to the laterosphenoid articulation (Fig. 4D), as in *Sinraptor* (Currie and Zhao 1993). Anteromedial to this shelf, the relatively thin articular surface for the frontal is marked by a groove in the anteromedial margin of the bone. Behind the laterosphenoid articulation, the margin of the supratemporal fossa extends onto the dorsal surface of the medial side of the junction of the three processes and is offset posteroventrally by a marked step from the medial surface of the posterior flange on the ventral process. Posterodorsally, an abrupt flexure separates the margin of the supratemporal fossa from the dorsal surface of the base of the posterior process. This surface is flat and marked by a sharp dorsal rim laterally. Apparently, all of this surface was overlapped by the dorsal process of the squamosal, as indicated by the sharp lateral rim and a small raised lip at the anterior end of this surface (Fig. 4D). If this really was the case, the dorsal anterior process of the squamosal would have reached considerably more anteriorly than the ventral process and would have reached the level of the posterior margin of the orbit, an unusual condition in theropods, including metriacanthosaurids (Currie and Zhao 1993).

Quadratojugal: The left quadratojugal (IGB 2-9) is almost completely preserved, missing only minor parts at the anterior end (Fig. 5). It has a long and slender anterior (jugal) process and a ventrally wide, dorsally tapering triangular dorsal (squamosal) process. The element is considerably longer anteroposteriorly (> 180 mm) than high dorsoventrally (128 mm), indicating a large, at least ventrally anteroposteriorly wide, infratemporal fenestra, as in other metriacanthosaurids (Dong *et al.* 1983, Currie and Zhao 1993, Gao 1999). There is a medial, laterally facing shelf in the anterior part of the anterior process for the reception of the dorsal posterior process of the jugal (Fig. 5A), and a ventromedially facing groove on the ventromedial surface for the ventral posterior process of the jugal (Fig. 5C). A similar, but more ventrally placed groove is present in *Allosaurus* (Madsen 1976), and Currie and Zhao (1993) described a medial groove on the anterior process of the quadratojugal for *Sinraptor*, but interpreted it as the articulation for a seemingly unique, medial posterior process of the jugal in this taxon. Whereas the shelf for the dorsal jugal process ends approximately 25–30 mm anterior to the dorsal quadratojugal process, the medioventral groove continues to the level of the posterior margin of the infratemporal fenestra, indicating that the ventral jugal process was considerably longer than the dorsal process, as in many theropods. The anterior process and the ventral margin of the main quadratojugal process are somewhat thickened, as is the posterior margin of the dorsal process. In contrast, the lamina spanning between the two processes forms a thin sheet of bone that is slightly depressed in medial view. Posteriorly, a flat, oval surface at the posteroventral end of the bone that faces medially and slightly ventrally marks the contact with the lateral surface of the lateral condyle of the quadrate (Fig. 5C). Above this facet, the posterior margin flexes slightly medially, probably for continued contact with the quadrate shaft. There is no medial indentation in this margin, indicating that, if a quadrate foramen was present, it was mainly or entirely enclosed by the quadrate. In

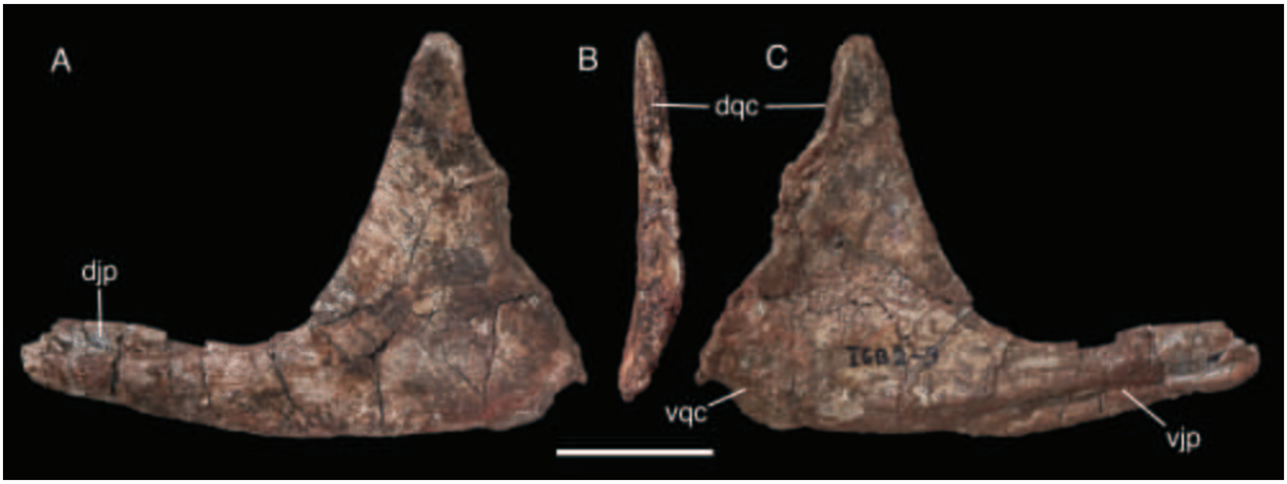

Figure 5. Left quadratojugal of *A. kyrgyzicus*, IGB 2-9, in lateral (A), posterior (B), and medial (C) views. Abbreviations: djp, articular facet for the dorsal jugal prong; dqc, dorsal quadrate contact; vjp, facet for the ventral jugal prong; vqc, ventral quadrat contact. Scale bar is 5 cm.

the dorsal third of the bone, there is a widened, posteriorly facing facet that was posteriorly overlapped by the lateral lamina of the quadrate (Fig. 5B), as e.g. in *Yangchuanosaurus* (Dong *et al.* 1983). In medial view, a very low, anterodorsally extending ridge delimits a medially facing, oval facet at the tip of the dorsal process that might have been overlapped by the ventral process of the squamosal. Overall, the quadratojugal of *Alpkarakush* seems to be more robust than that of *Sinraptor* or *Yangchuanosaurus*, especially in the more evenly tapering dorsal process (Dong *et al.* 1983, Currie and Zhao 1993, Gao 1999).

Teeth: Several partial to complete teeth have been collected from site FTU-1 (Fig. 6). Some are clearly theropod teeth, being labiolingually compressed, recurved, and showing serrated carinae (IGB 2-3, 2-4, 2-5). Only one of these teeth is complete (IGB 2-3; Fig. 6D, E), with a fore-aft basal length of approximately 21.5 mm and a crown height of *c.* 40 mm, and are thus in the size range of maxillary teeth of *Sinraptor* (Hendrickx *et al.* 2020), but slightly smaller than the larger lateral teeth of *Yangchuanosaurus hepingensis* (Gao 1999). The other two teeth are partial and were considerably smaller. As tooth size varies considerably in theropods, both taxonomically and also in respect to their position within the jaw, these teeth might belong to the same individual as the rest of the bones, although this cannot be shown with certainty. Even more problematic are the remaining four teeth or tooth fragments (IGB 2-6, 2-7, 2-8, 2-27), which have a rather round cross-section, are notably recurved, and lack carinae or serrations. The best preserved of these teeth (IGB 2-6; Fig. 6A–C) has a fore-aft basal length of 16 mm and a crown height of also *c.* 40 mm, and is thus very similar in size to the largest theropod lateral tooth present, and also within the size range of premaxillary teeth of *Sinraptor* (Hendrickx *et al.* 2020). These teeth resemble teeth of certain crocodyliforms (e.g. pholidosaurids), and a similar tooth from the Balabansai Formation was indeed briefly described and figured by Nessov *et al.* (1989: pl. 2, fig. 14) as a probable thalattosuchian crocodyliform. However, most Jurassic terrestrial crocodiles are considerably smaller than the animal that these teeth were derived from, which is also the case for the vast majority of the crocodyliform remains described from the Balabansai Formation, in which teeth or alveoli generally show fore-aft basal lengths of less than 10 mm (Nessov *et al.* 1989, Averianov 2000). It should be noted that Averianov (2000: 778) also mentioned a large partial crocodyliform tibia, but he neither figured this specimen nor described it in detail. Furthermore, no crocodyliform remains were found at the FTU-1 locality. Thus, we consider the possibility that these teeth represent premaxillary teeth of *Alpkarakush*, as such teeth are often more rounded and differ in morphology from the lateral teeth in other theropods (e.g. in *Ceratosaurus*, see Madsen 1976, Madsen and Welles 2000), and longitudinal striations are also known in the premaxillary teeth of some theropods (e.g. *Ceratosaurus*; see Madsen 1976, Madsen and Welles 2000, Soto and Perea 2008) and in all teeth in baryonichine spinosaurs (e.g. Charig and Milner 1997). However, although *Sinraptor* also has more labiolingually thickened premaxillary teeth, these lack striations and bear serrations in this taxon, thus differing from the teeth described here (Hendrickx *et al.* 2020). Thus, the interpretation as possible premaxillary teeth of *Alpkarakush* should be seen as very tentative until future finds might show that such teeth are indeed present in theropods, or confirm a crocodyliform identification of these teeth. The following descriptions are mainly based on the two most complete specimens, IGB 2-6 and IGB 2-3.

The possible premaxillary tooth IGB 2-6 has an almost round cross-section at the base (16 mm long, 14.5 mm wide) and is notably recurved, so that the apical tip would lie distal to the tooth base when the tooth was placed in the jaw (Fig. 6A–C). The cross-section remains round throughout the height of the tooth, as there are no mesial or distal carinae. Very fine longitudinal striations are present throughout the labial and lingual sides.

The lateral tooth IGB 2-3 is considerably labiolingually compressed, being 21.5 mm long and 11 mm wide at the base, but only moderately recurved (Fig. 6D, E), as it is the case also in *Sinraptor* (Hendrickx *et al.* 2020). Its cross-section here is drop shaped, being widest towards the mesial end and gradually tapering distally into a sharp carina. Both labial and lingual sides are mesiodistally convex up to the carinae, the probably lingual side more notably so than the labial side, as the distal carina is somewhat displaced towards the labial side. Both carinae extend all the way to the root of the tooth, as in *Sinraptor* (Hendrickx *et al.* 2020) and several other theropods (Hendrickx *et al.* 2019). Small serrations are present on both the mesial and distal carina, with 11–12 denticles per 5 mm on both the mesial and distal carinae, as in the mid-section of the carinae of the largest lateral teeth in *Sinraptor* (Hendrickx *et al.* 2020). The individual denticles are chisel shaped, approximately as long mesiodistally as apicobasally and lack interdenticular sulci, in contrast to *Sinraptor* (Hendrickx *et al.* 2020) and several other basal tetanurans (Hendrickx *et al.* 2019). Likewise, pronounced marginal enamel wrinkles are also absent, although a few weak bandings are visible under oblique light on the probable labial side next to the distal carina. The enamel has a very finely developed braided texture (*sensu* Hendrickx *et al.* 2015).

Axial skeleton

The axial skeleton of *Alpkarakush* is represented by two posterior dorsal vertebral centra with fragmentary neural arches, several fragments of dorsal neural arches and spines, the central and partial neural arches (including spines) of the sacrum, and several partial to almost complete dorsal ribs (Figs 7–10). For vertebral measurements see Table 1.

Dorsal vertebrae: Two posterior dorsal vertebral centra are preserved (IGB 2-10, 2-11; Figs 7A–F, 8A). The centra are higher than wide, with oval to almost round articular surfaces, and very slightly higher than long. The articular facets are slightly amphicoelous, more notably posteriorly than anteriorly. The centra are notably constricted to almost half the width of the articular facets in ventral view (Fig. 7C), and are ventrally broadly rounded to flattened, especially in the probably more posterior element IGB 2-11. Pleurocoels are absent, but there are large, oval pleurocentral depressions on the dorsal part of the lateral sides (Fig. 7A, D), as in many basal tetanuran theropods, including metriacanthosaurids (Currie and Zhao 1993, Gao 1999). Internally, the dorsal half of the centrum is made up of spongy bone, while there is an asymmetrically developed larger hollow present on the ventral half in IGB 2-11, filled with large calcite crystals. Notable, but short, striations are present on the lateral side along the edges of the articular facets.

Figure 6. Teeth referred to of *A. kyrgyzicus*. A–C, possible premaxillary tooth IGB 2-6 in mesial (A), labial or lingual (B), and distal (C) views. D, E, lateral tooth IGB 2-3 in (?)lingual (D) and distal (E) views. Scale bar is 1 cm.

Only the base of the neural arch is present in both specimens. It was apparently slightly more than half the height of the centrum and enclosed a large neural canal that is somewhat constricted ventrally. In IGB 2-10, the neural canal slightly indents the dorsal margin of the centrum, but that did not seem to be the case in IGB 2-11. Anteriorly, the broken bases of the stout, posterodorsally directed centroparapophyseal laminae are preserved. Dorsal to these laminae, a large, round foramen led from the centroprezygodiapophyseal fossa posteromedially into the neural arch (Fig. 7B, E, F), which here obviously had large chambers above the neural canal, separated medially by a robust median lamina. Elaborate pneumatization of the neural arch is also present in *Sinraptor*, where a pneumatic foramen enters the neural canal from the postzygocentrodiapophyseal fossa in the posterior dorsal vertebrae (Currie and Zhao 1993). An isolated fragment of a neural arch (IGB 2-22, which might belong

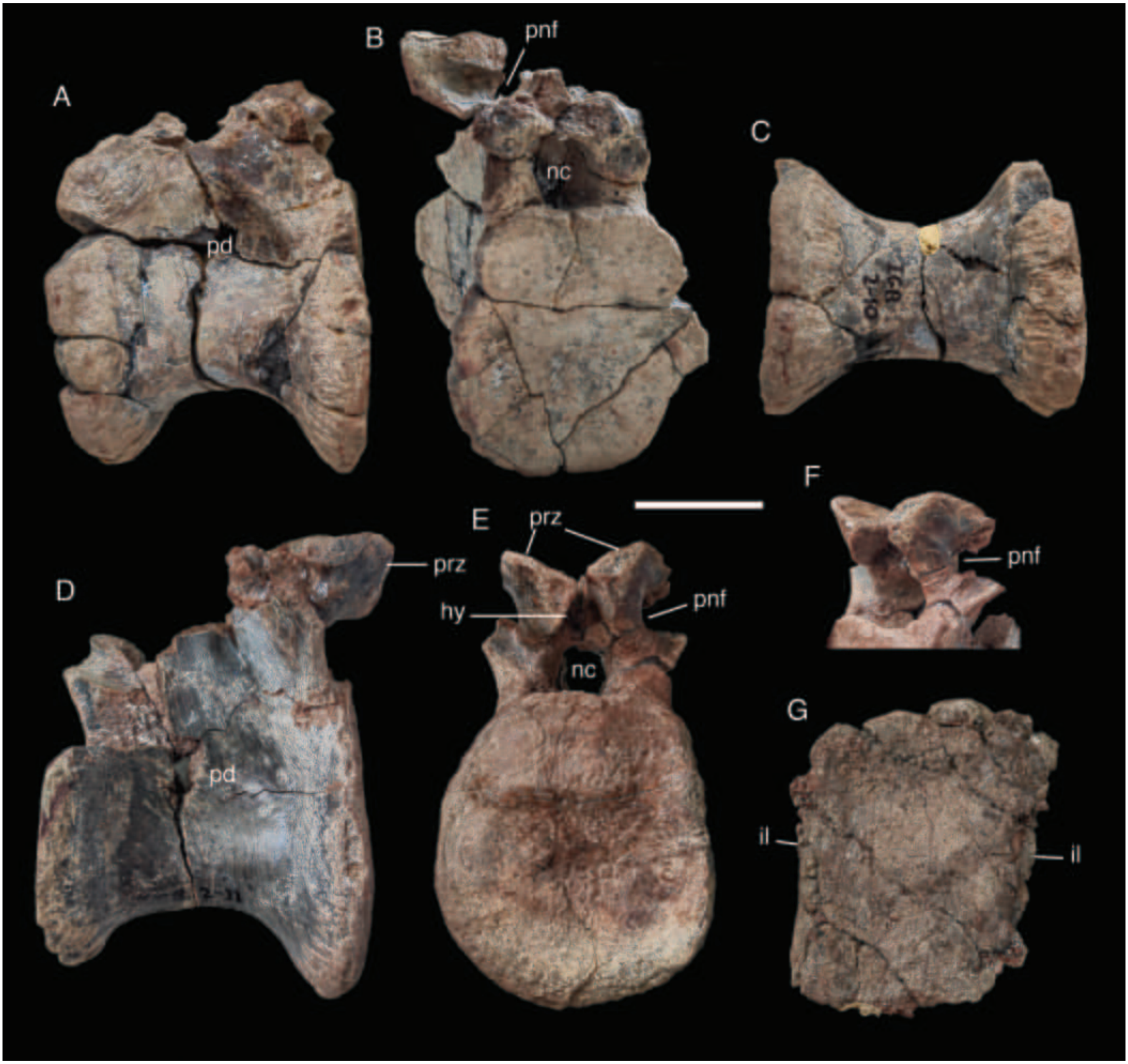

Figure 7. Dorsal vertebral remains of *A. kyrgyzicus*. A–C, posterior dorsal vertebral centrum IGB 2-10 in right lateral (A), anterior and slightly anterolaterodorsal (B, with neural arch fragment IGB 2-22 in approximate position), and ventral (C) views. D–F, probably last dorsal vertebra IGB 2-11 in right lateral (D) and anterior (E) views, and detail of partial neural arch in left anterolateral view (F). G, isolated dorsal neural spine IGB 2-12 in left lateral view. Abbreviations: hy, hypantrum; il, insertion of interspinal ligaments; nc, neural canal; pd, pleurocentral depression; pnf, pneumatic foramen; prz, prezygapophysis. Scale bar is 5 cm.

to IGB 2-10, but does not directly fit on the broken base of the centroparapophyseal lamina; Fig. 7B) shows the dorsal end of the thin centroparapophyseal lamina, the parapophysis, and the anteromedially directed stem of the prezygapophysis, which together form the lateral border of the large foramen leading into the neural arch. This fragment also shows that the parapophysis was placed anterodorsally on the neural arch and did not project strongly laterally, in contrast to abelisauroids (e.g. Bonaparte *et al.* 1990, O'Connor 2007, Carrano *et al.* 2011, Filippi *et al.* 2018) and piatnitzkysaurids (Bonaparte 1986). The prezygapophyses are preserved in IGB 2-11, though somewhat distorted (Fig. 7D, E). They are relatively large, standing at an angle of approximately 25–30° from the horizontal and have anterolaterally rounded articular surfaces that are approximately as wide as long. Anteriorly, the prezygapophyses form a robust, ventrally widening hypantrum (Fig. 7E). In contrast to some theropods, such as *Condorraptor* (Rauhut 2005), the interprezygapophyseal gap did not widen posterior to the hypantrum.

Parts of two probably dorsal neural spines are present (IGB 2-12, 2-13). They form thin, rectangular sheets of bone that slightly widen towards their dorsal end posteriorly. The anteroposteriorly larger and more complete spine (IGB 2-12;

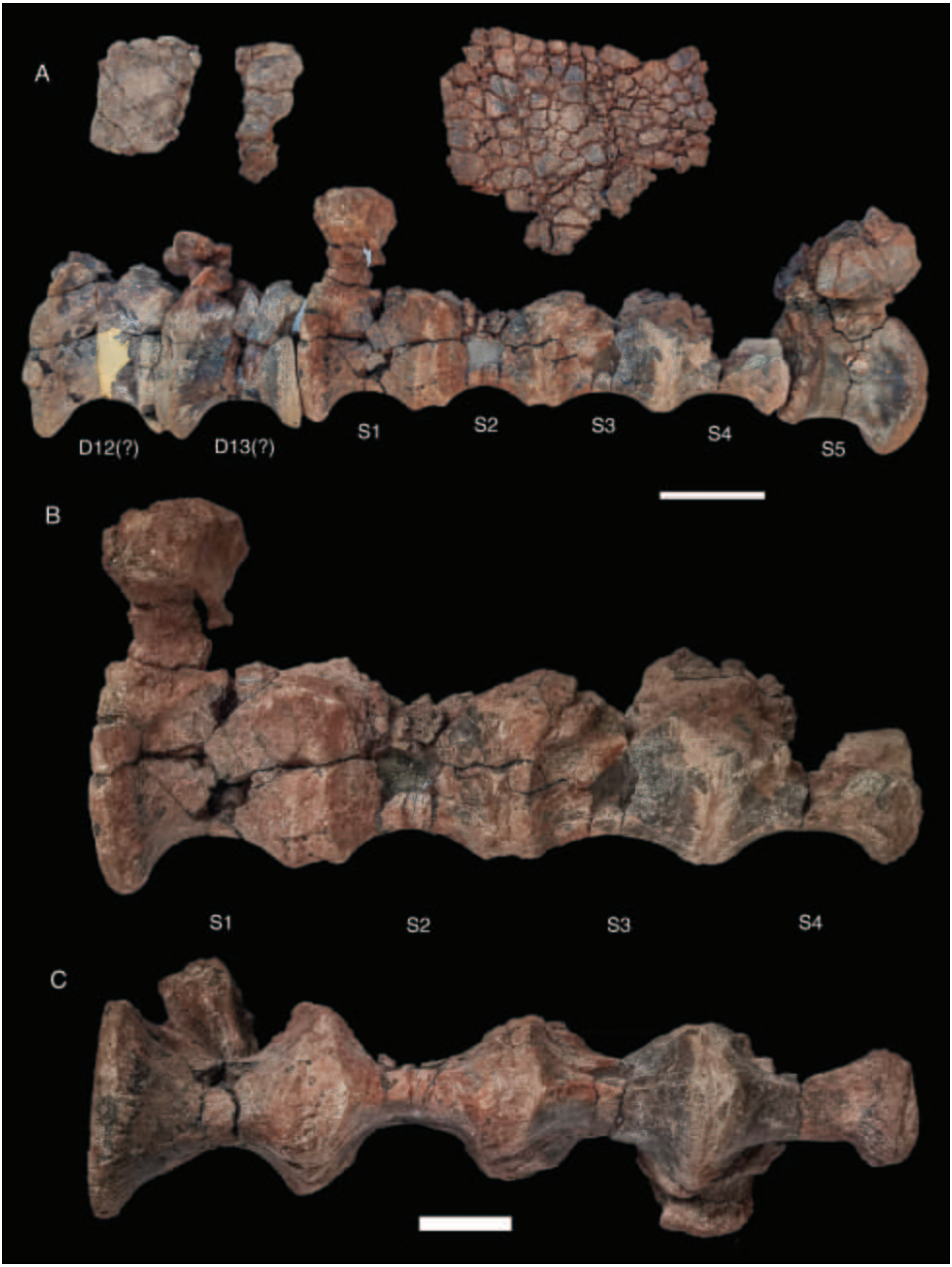

Figure 8. Dorsal and sacral vertebrae of *A. kyrgyzicus*. A, articulated posterior dorsal vertebrae and sacrum, with approximate position of neural spines, in left lateral view. B, C, articulated sacral vertebral centra of sacrals 1 to 4, IGB 2-14, in left lateral (B) and ventral (C) views. Abbreviations: D, dorsal vertebra, S, sacral vertebra. Scale bars are 10 cm (A) and 5 cm (B, C).

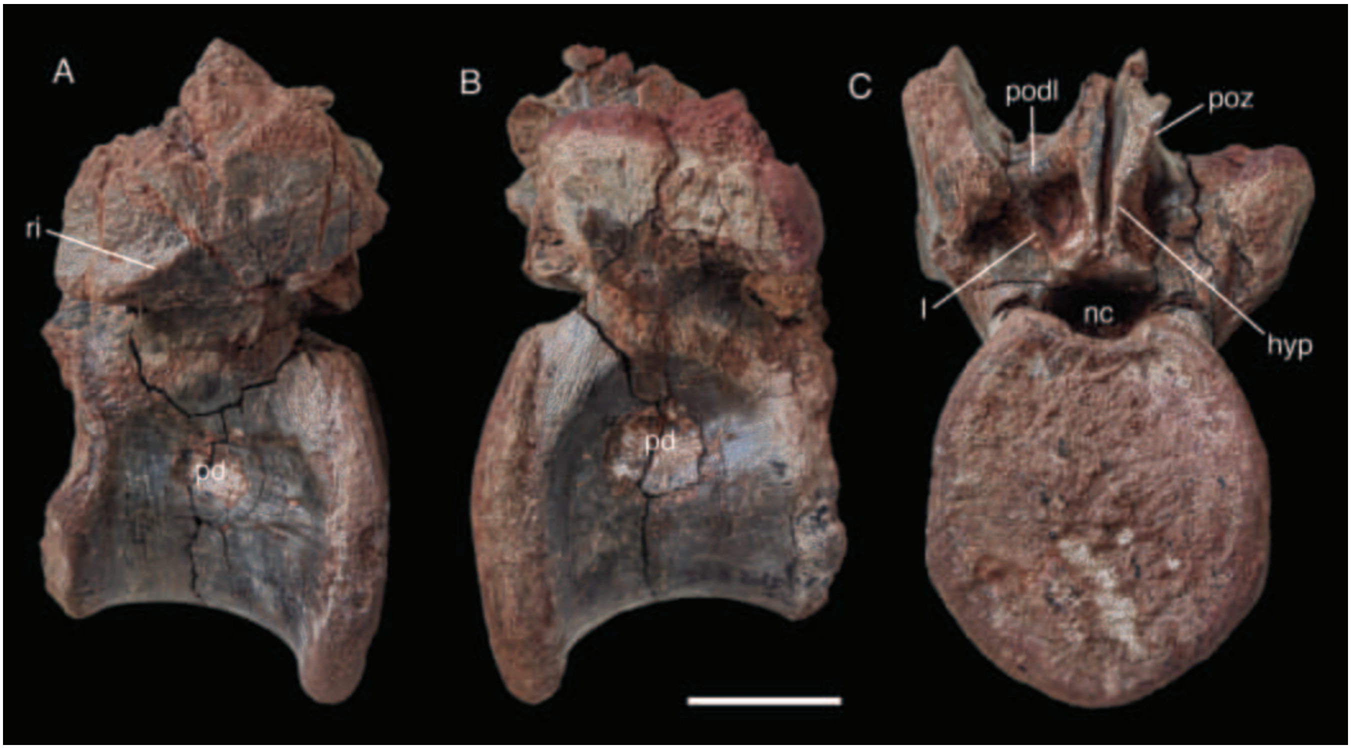

Figure 9. Last (5th) sacral vertebra of *A. kyrgyzicus*, IGB 2-15, in left lateral (A), right lateral (B), and posterior (C) views. Abbreviations: hyp, hypantrum; l, lamina; nc, neural canal; pd, pleurocentral depression; podl, postzygodiapophyseal lamina; poz, postzygapophysis; ri, ridge. Scale bar is 5 cm.

Fig. 7G) shows well-developed anterior and posterior ridges for the attachment of the interspinal ligaments, which almost reach the apex of the spine, as in *Yangchuanosaurus hepingensis* (Gao 1999).

Sacrum: Most of the sacrum is preserved, but in a very poor state of preservation (Fig. 8), as the articulated vertebrae were obviously collected from already largely eroded sediment at the surface. The anterior four sacral vertebrae were fused and collected in a jacket, together with their spines (IGB 2-14; Fig. 8), whereas the last sacral vertebra (IGB 2-15; Fig. 9) was isolated. The total length of the articulated sacrum is 54 cm, with the length of the individual vertebrae being all of subequal length ranging between 10.5 and 11 cm, unlike the situation in *Yangchuanosaurus hepingensis*, where the first and last sacral vertebrae are notably longer than sacrals 3 and 4 (Gao 1999). The anterior articular surface of the sacrum is subequal in size to the articular surfaces of the posterior dorsal vertebrae, but the articulations between the sacral vertebrae are reduced in width, as in *Yangchuanosaurus hepingensis* (Gao 1999), although not to the degree seen in *Siamotyrannus* (Samathi 2013) and many ceratosaurs (e.g. Gilmore 1920, Bonaparte *et al.* 1990, Rauhut and Carrano 2016), and, in contrast to the latter, the boundaries between the vertebrae are still visible (Fig. 8B, C). The centra are strongly constricted in the middle, especially in sacrals 2 and 3, with narrow, transversely rounded to flattened ventral surfaces. Pleurocoels or marked lateral depressions are absent in the vertebral centra, as it is also the case in *Sinraptor* (Currie and Zhao 1993).

The neural arches of these vertebrae are very poorly preserved, and little can be said about their morphology. Only the transverse process of the first sacral is present; it is massive, round in outline distally and placed on the neural arch over the anterior end of the centrum, as in *Sinraptor* (Currie and Zhao 1993) or *Piatnitzkysaurus* (MACN CH 895), but in contrast to *Allosaurus*, where the transverse process is dorsoventrally elongate (Madsen 1976). Otherwise, only the neural spines can be discerned. At least from sacral one to three, the neural spines are anteroposteriorly long, plate-like and seem to have been completely fused to each other (Fig. 8A), as in *Yangchuanosaurus hepingensis* (Gao 1999), whereas the spines seem to have been fused basally but remained separated distally in *Yangchuanosaurus magnus* (Dong *et al.* 1983) and are closely spaced but apparently separated over their entire height in *Shidaisaurus* (Wu *et al.* 2009). Their height approximately equals the height of the sacral centra plus the neural arch, and is thus similar to the relative height of the elongate posterior dorsal neural spines in other metriacanthosaurids (Huene 1926, Dong *et al.* 1983, Currie and Zhao 1993, Gao 1999, Wu *et al.* 2009).

The last sacral vertebra (IGB 2-15), which was found isolated from the rest of the sacrum, is largely preserved, but lacks the anterior end of the neural arch, the left postzygapophysis, and the neural spine (Fig. 9). The anterior articular surface is considerably smaller than the posterior surface, but the vertebra was obviously not fused to the rest of the sacrum. The centrum is considerably more massive than that of the middle sacrals, as in *Yangchuanosaurus hepingensis* (Gao 1999), and broadly rounded ventrally, although a very faint midline keel might be present in the anterior part; this keel is only visible under oblique light, but obvious to the touch of the surface. Laterally, relatively small, but marked pleurocentral depressions are present on the dorsal half

Figure 10. Right partial dorsal rib of *A. kyrgyzicus*, IGB 2-16, in posterior (A) and anterior (B) views. Scale bar is 5 cm.

Table 1. Vertebral measurements for *A. kyrgyzicus* (in mm)

Element	Number	Centrum length	Anterior height	Anterior width	Mid-centrum width	Posterior height	Posterior width
Dorsal	IGB 2-10	115	122	*c.* 105	*c.* 55	124	105
Dorsal	IGB 2-11	120	124	108	*c.* 64	*c.* 120	*c.* 107
Sacral 5	IGB 2-15	110	*c.* 100	*c.* 88	*c.* 60	127	106

of the centrum (Fig. 9A, B). However, although these depressions are rather sharply defined, they do not penetrate the cortex and do not lead into internal cavities. Such a sharply defined depression seems to be absent in *Sinraptor* (Currie and Zhao 1993) and *Shidaisaurus* (Wu *et al.* 2009).

The neural arch is narrow anteriorly and mainly formed by the massive bases of the transverse processes in lateral view. The latter are placed over approximately the half length of the centrum on the neural arch and they are higher dorsoventrally than long anteroposteriorly. No lateral lamina supporting the transverse process are present, but there is a very shallow depression anteriorly on the base of the transverse process, and posteriorly, a short, very stout ridge extends from the base of the postzygapophysis towards the roof of the transverse process. The processes itself seem to have been very short, and an anteroposteriorly expanded, largely vertically oriented bone that begins just a few centimetres lateral from the neural arch probably represent the fused sacral ribs, as in *Sinraptor* (Currie and Zhao 1993); the almost vertical dorsoventral orientation of these bones, especially on the better preserved left side, might be due to mediolateral compression of the obviously laterodorsally oriented ribs. A pronounced, sharp-edged ridge is present on the anteroventral part of the sacral rib on the left side, and fades rapidly posterodorsally into the surface of the bone (Fig. 9A); this part seems to be abraded on the right side. The neural canal is small anteriorly, but considerably wider posteriorly, where it slightly indents the dorsal margin of the articular facet posteriorly. The anterior side of the neural arch is largely damaged, but there did not seem to have been normal prezygapophyses developed, but the arch around the neural canal was narrow and probably in direct contact and possibly fused with the neural arch of the preceding vertebra. Above the neural canal, only a narrow (*c.* 10 mm), vertical strut of bone is present. Posteriorly, a large, triangular depression was present on the posterior side of the neural arch on either side of the base of the neural spine, above the neural canal and below the very dorsally placed postzygapophyses. This depression is subdivided by a thin lamina that extends from the lateral roof of the neural canal towards the dorsal base of the transverse process (Fig. 9C). An equivalent lamina seems to be also present in *Sinraptor* (Currie and Zhao 1993). The depression is bordered medially by a thin lamina that extends from the medial edge of the postzygapophysis ventrally and forms part of the hyposphene. The laminae extending down from the left and right postzygapophysis remain separated by the very narrow postspinal fossa over almost their entire length and only meet in a marked ventral mediolateral expansion of the hyposphene (Fig. 9C). The latter forms the ventral border of the triangular depression noted above, and its ventrolateral border is formed by a thin and low lamina that extends from the lateral end of the ventral expansion of the hyposphene dorsolaterally. Dorsally, the depression is bordered by the very stout postzygodiapophyseal lamina. The postzygapophysis is small (*c.* 23 by 17 mm), high oval in shape and placed high on the neural arch, at the level of the dorsal surface of the transverse process. As in the last sacral vertebra of *Allosaurus* (Madsen 1976) and *Sinraptor* (Currie and Zhao 1993), it is very steeply inclined, at an angle of *c.* 75° from the horizontal (Fig. 9C). The neural spine is missing. Its base is mediolaterally slender, and the spine was either anteroposteriorly short or largely placed over the anterior part of the centrum.

Dorsal ribs: Several partial to almost complete dorsal ribs are present, plus numerous isolated rib sections that cannot be fitted to any of the more complete elements. The following description is based on the more complete ribs IGB 2-16, 2-17, 2-18, 2-19, and 2-20, most, if not all of which seem to be derived from the right side (Fig. 10).

As in all dinosaurs, the dorsal ribs are double headed, with a short tuberculum and a long and slender capitulum. These two slightly thickened articular processes come together at the base of the rib shaft, but are connected above that by a thin web of bone that extends from the anteroventral edge of the tuberculum almost to the articular facet of the capitulum. Where the two proximal articular processes meet, the thickened bone extending distally from the tuberculum, which, at the rib head was more dorsoventrally oriented, twists to face more dorsally and thus forms a robust dorsal surface of the proximal rib shaft. Well-developed longitudinal furrows are present on both the anterior and posterior side of the proximal rib shaft (Fig. 10), resulting in a somewhat oblique, T-shaped cross-section of the proximal rib. The posterior one of these furrows extends somewhat further distally than the anterior one, but both disappear within 20 cm from the junction of the articular processes. Distal to this, the rib shaft becomes dorsoventrally high oval in cross-section, being slightly wider anteroposteriorly and dorsally flattened in its dorsal part. Even more distally, the ribs become thin and rod-like, and a very shallow longitudinal furrow appears again on the posterior and sometimes also the anterior side of the distal part of the rib. The proximal parts of the ribs have only a very moderate ventral curvature, indicating a rather deep ribcage in the posterior part of the body, as in *Wiehenvenator* (Rauhut *et al.* 2016).

Appendicular skeleton

The appendicular skeleton of *Alpkarakush* is mainly known from the pelvic girdle and hindlimbs. Of the forelimbs, only a furcula, a manual phalanx, and a manual ungual are preserved. The hindlimb is represented by a partial left ilium, partial pubes of the holotype and almost complete pubes of the paratype, complete ischia of the holotype and partial ischium of the paratype, both femora and tibiae of the holotype, the right tibia of the paratype, almost complete left fibula, both astragalocalcanea, a partial distal tarsal, left metatarsal II, left and right metatarsal III, and several pedal phalanges and unguals of the holotype. For measurements of the hindlimb elements see Table 2.

Furcula: A wide V-shaped bone represents a furcula (IGB 2-23; Fig. 11). With an overall transverse width of 17.5 cm (with maybe some 2–3 cm missing), the bone is rather small for an animal of the size as the holotype of *Alpkarakush*, but as there is considerable variation in the relative size (and shape) of furculae in theropods (Makovicky and Currie 1998, Nesbitt *et al.* 2009) and the vast majority of elements recovered from site FTU-1 seem to represent a single individual, we consider it likely that this element comes from the same animal. However, it cannot be excluded that it might represent the smaller, paratype individual.

The furcula is formed by two largely symmetrical rami that meet each other at an angle of approximately 140° (Fig. 11A, C). The lateral ends are slender, but the bone becomes dorsoventrally wider towards the median junction. Whereas the rami are narrowly rounded dorsally and more sharp-edged ventrally, the central part is rounded both dorsally and ventrally. The cross-section of the rami is thus roughly teardrop shaped. A hypocleidium, as it is found in a variety of other non-avian theropods (Nesbitt *et al.* 2009), is absent. Towards the lateral ends, the bone becomes slightly wider anteroposteriorly and there is a laterally widening posterodorsally facing facet on the posterior side of the bone on either side (Fig. 11C). This facet extends over almost half of the

Table 2. Measurements of hindlimb elements of *A. kyrgyzicus* (in cm).

Element	Number	Length	Proximal width	Proximal depth	Distal width	Distal depth	Shaft circumference
Femur right	IGB 2-33	90	15.5[a]	10.5	16	15.5	29
Femur left	IGB 2-32	88	18.5	10	15.5[b]	15.5	
Tibia left	IGB 2-34	72	13	22	19.5	9.5	25
Tibia right	IGB 2-35	71.5	12[c]			7.5[c]	
Mt II right	IGB 2-41	34.7	7.2	9	6.5	6	
Mt III right	IGB 2-42	40	8.5	10.5[d]	7.7	6	
Mt III left	IGB 2-43	39.8	9[e]	10.5[e]	7.5	5.5	
Tibia right (Paratype)	IGB 2-48	60.5	7	11[f]	11	4.5	17

[a] Laterally incomplete. [b] Distorted. [c] Slightly damaged. [d] Posteriorly slightly incomplete. [e] Slightly rotated. [f] Somewhat eroded.

Figure 11. Furcula of *A. kyrgyzicus*, IGB 2-23, in anterior (A), ventral (B), and posterior (C) views. Abbreviations: bm?, possible bite mark; epi, epicleideal process; fa, facet. Scale bar is 2 cm.

length of the rami and is defined ventrally by a poorly developed ridge, which becomes slightly more conspicuous towards the lateral ends. Only a small piece of the very thin epicleideal process is preserved on the left side of the bone. On the posterior side of the right ramus, there is a conspicuous, obliquely oriented flat area of *c.* 15 mm width, which is bordered medially and laterally by sharp edges (Fig. 11C). Under magnification, the bone fibres are ripped at these edges, as if the bone was cut, and the upper bone layer seems to be stripped away. This area might thus represent a bite mark, where some of the bone was ripped away with the overlying flesh during scavenging of the carcass, or it might also be a trample mark (see Fiorillo 1987).

The element described here represents the first furcula known for a metriacanthosaurid. In general shape, especially in respect to the wide angle between the two rami, it is most similar to furculae of *Allosaurus* (Chure and Madsen 1996), whereas other non-avian theropods have more pronounced angles and/or a more rounded outline of the furcula angle (Norell *et al.* 1997, Makovicky and Currie 1998, Lipkin *et al.* 2007, Nesbitt *et al.* 2009).

Manus: The manus is represented only by a manual phalanx and a partial ungual (Fig. 12). Unfortunately, metriacanthosaurid forelimbs are generally poorly known, and only a few manual elements have been described for *Sinraptor* (Currie and Zhao 1993). A possible exception is *Xuanhanosaurus*, which has an almost complete forelimb, with a partial manus, and was found to be a metriacanthosaurid by Carrano *et al.* (2012). However, the phylogenetic position of this taxon is uncertain, as it was found as a possible piatnitzkysaurid in some recent phylogenetic hypotheses (Rauhut *et al.* 2016, Dai *et al.* 2020) and can take several positions within carnosaurs in our analysis (including as a metriacanthosaurid in the equal weights analysis, see below).

A rather short and robust manual phalanx (IGB 2-24) represent the first phalanx of the second digit of the left manus (Fig. 12A–F). It is 80 mm long, 38 mm wide, and 40 mm high proximally, and 32 mm wide and 27 mm high distally. As in some other theropods, e.g. *Allosaurus* (Madsen 1976), *Asfaltovenator* (MPEF-PV 3440), *Xuanhanosaurus* (IVPP V 6729), and *Acrocanthosaurus* (Currie and Carpenter 2000), the phalanx is markedly asymmetrical (Fig. 12A, D), though to a much greater extent than in these taxa. Thus, the proximal articular surface is divided into a large, high oval lateral concavity and a much smaller, triangular medial facet that is concave dorsoventrally, but slightly convex mediolaterally (Fig. 12E). Both facets are divided by a dorsoventrally oriented ridge, with the medial being somewhat offset ventrally from the lateral one. Whereas the dorsal margin of the proximal articulation forms a gently convex arch in dorsal view, the ventral margin extends further proximally and forms a pointed proximal end in elongation of the ridge subdividing the facets, which is slightly displaced medially from the midline of the bone. The shaft of the phalanx is constricted to a minimal height and width of 22 mm and slightly obliquely laterodistally oriented. Its cross-section is semioval to triangular proximal to the distal articular end, with a flattened ventral and a narrowing, dorsally-rounded dorsal margin. A markedly rugose tuberosity is found just distal to the proximal end on the ventral part of the medial side, as in *Xuanhanosaurus* (IVPP V 6729), *Asfaltovenator* (MPEV PV 3440), and *Acrocanthosaurus* (Currie and Carpenter 2000), and another, smaller one at about half-length of the bone on its ventrolateral margin. The most conspicuous feature, however, is a ventral sulcus that is placed just lateral to the pointed ventral margin of the proximal articular surface (Fig. 12D). This sulcus extends over half the length of the phalanx, slightly mediodistally directed and distally narrowing, and is defined by a marked step medially and an expanded, overhanging flange laterally. Although a shallow sulcus is also present on the ventral side of phalanx II-1 in *Allosaurus* (USNM 4734; DINO 11541) and *Acrocanthosaurus* (NCSM 14345), it is much broader and less well defined in these taxa. The most similar morphology is found in *Xuanhanosaurus* (IVPP V 6729), which also has well-developed medial and lateral tubercles on the proximal end of the ventral side of phalanx II-1, in which, however, the ventral sulcus is less enclosed than in *Alpkarakush*.

The distal articular end is gynglimoidal, with the lateral condyle extending considerably more distally than the medial condyle. A small, triangular extensor groove is present dorsally just proximal to the gynglimus. Well-developed collateral ligament grooves are present on both sides. In lateral view, the lateral condyle is semicircular, whereas the medial condyle is only slightly lower but much shorter proximodistally in medial view.

The manual ungual (IGB 2-47) is notably short and curved (Fig. 12G, H). Based on its size and morphology, it is probably an ungual of the third digit. The proximal end is high oval, with a straight ventral margin. It is subdivided into lateral and medial concavities by a weakly developed dorsoventral ridge. The articular surface is almost twice as high as wide. A stout, but low and little projecting flexor tubercle is present just distal to the articular end on the ventral side. It is offset from the rim of the articulation by a shallow mediolateral groove. The flexor tubercle is less developed than in *Allosaurus* (Madsen 1976) or *Sinraptor* (Currie and Zhao 1993), although in the latter case, this might have to do with possible different positions of the unguals compared. Distal to the flexor tubercle, the ungual rapidly narrows dorsoventrally, considerably more so than in any ungual of *Allosaurus*, for example (Gilmore 1920, Madsen 1976). Dorsally, the dorsal margin of the ungual is not offset from the articular end by a groove or lip and curved directly ventrally from the articular end, in contrast to many coelurosaurian theropods, where the unguals first curve upwards, so that the highest point of the ungual is placed above the rim of the articular facet if the latter is held vertically. Well-developed and largely symmetrically arranged claw grooves are present on either side of the ungual. In comparison with the part dorsal to the claw groove, the part directly ventral to it bulges outwards. This is also the case in the area where the bone becomes dorsoventrally narrower from the flexor tubercle, so that here the area directly ventral to the claw groove was wider than the ventral margin of the ungual. More distally, the ventral side is broad and mediolaterally rounded. The ungual was strongly recurved, but the tip is missing, so nothing can be said about its total length or the position of the tip in relation to the articular end.

Ilium: Large parts of the left ilium are preserved, missing mainly the preacetabular process and most of the pubic peduncle (IGB 2-25; Figs 13, 14). The iliac blade is high above the acetabulum (*c.* 29 cm, excluding the supraacetabular crest), but slopes steeply posteroventrally (Fig. 13A), so that the posterior end of the iliac blade is only slightly more than a third of the height of this bone above the acetabulum (*c.* 11 cm). This slope is more pronounced than in *Siamotyrannus* (Buffetaut *et al.* 1996), *Sinraptor* (Currie and Zhao 1993), and *Yangchuanosaurus hepingensis* (Gao 1999), but similar to *Yangchuanosaurus magnus* (Dong *et al.* 1983). A lateral ridge on the acetabular blade above the acetabulum, as it is present in *Siamotyrannus* (Buffetaut *et al.* 1996), is absent. The acetabulum was large (*c.* 20 cm anteroposteriorly), almost two-thirds of the length of the postacetabular process (*c.* 33 cm). The supraacetabular crest is hood-like, strongly overhanging the acetabulum and covering its dorsal part in lateral view (Fig. 13A), as in non-tetanuran theropods and other metriacanthosaurids (Dong *et al.* 1983, Currie and Zhao 1993, Gao 1999, Wu *et al.* 2009), with the exception of *Siamotyrannus* (Buffetaut *et al.* 1996, Samathi 2013). Anteroventrally, it extends almost to the pubic articulation on the pubic peduncle, as in *Metriacanthosaurus* (OUM J 12144). The ischial peduncle is robust, wider mediolaterally than long anteroposteriorly and projects ventrally and slightly posteriorly. Its articular surface has a larger, marked convexity anteriorly and a small posterior flange that is somewhat offset medially from the lateral surface of the peduncle (Fig. 13B) and has a triangular outline in ventral view. The brevis fossa is strongly reduced, similar to the condition in *Sinraptor* (Currie and Zhao 1993); it is developed as a narrow medial shelf that extends from a flattened ventral area just posterior to the base of the ischial peduncle posterodorsally (Figs 13B, 14), first expanding slightly and then narrowing again towards the posterorodorsal edge of the iliac blade, which is

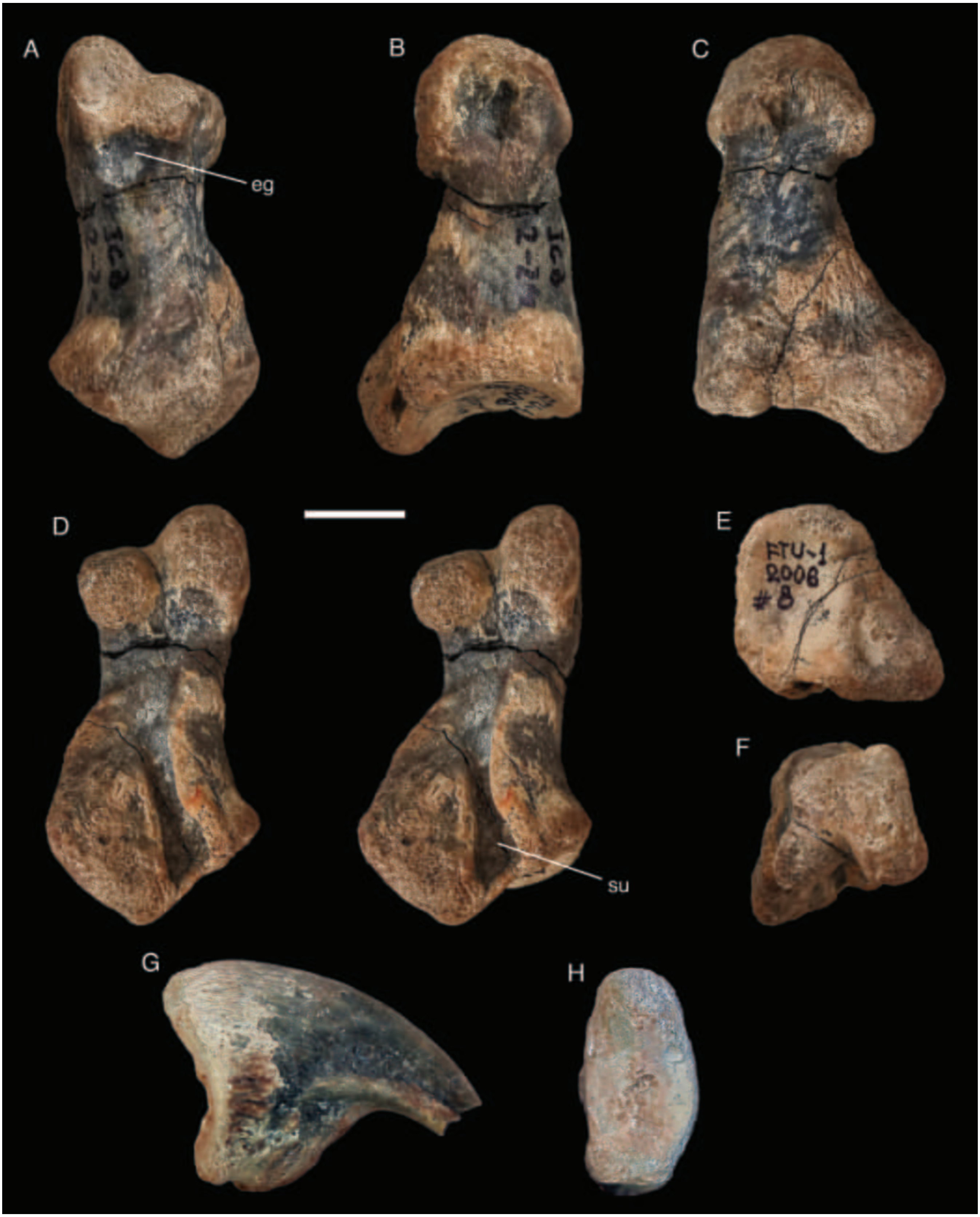

Figure 12. Manual elements of *A. kyrgyzicus*. A–F, left manual phalanx II-1, IGB 2-24, in dorsal (A), medial (B), lateral (C), ventral (D, stereophotographs), proximal (E), and distal (F) views. G, H, manual ungual IGB 2-47 in lateral (G) and proximal (H) views. Abbreviations: eg, extensor groove; su, sulcus. Scale bar is 2 cm.

Figure 13. Partial left ilium of *A. kyrgyzicus*, IGB 2-25, in lateral (A) and medial (B) views. Abbreviations: ip, ischial peduncle; mbs, medial brevis shelf; S2, attachment facet for the second sacral rib; sac, supraacetabular crest. Scale bar is 10 cm.

Figure 14. Partial left ilium of *A. kyrgyzicus*, IGB 2-25, in ventral view. Abbreviations as in Figure 13. Scale bar is 10 cm.

broken off. The lateral brevis shelf is oriented strictly ventrally, and there is no exposure of the brevis fossa in lateral view, as it is found in most megalosaurids (e.g. Britt 1991, Benson 2010) and also in *Sinraptor* (Currie and Zhao 1993), but not in other metriacanthosaurids (Dong *et al.* 1983, Buffetaut *et al.* 1996, Gao 1999, Wu *et al.* 2009).

In medial view, the medial margin of the base of the pubic peduncle is expanded medially and forms a well-developed flange that overhangs the anterodorsal part of the acetabulum medially (Fig. 13B). Above the pubic peduncle, a deep, anteriorly opening depression is present for the attachment of the sacral rib of the second sacral vertebra (Fig. 13B), as in *Allosaurus* (Madsen 1976) and *Sinraptor* (Currie and Zhao 1993). Above the acetabulum, well-developed, dorsoventrally oriented striations indicate the insertion of the sacral rib of sacral vertebra three.

Pubes: The pubes are represented by an almost complete right element (IGB 2-26), missing the proximal peduncles and the distal boot (Fig. 15A–C), a part of the shaft of the left pubis (IGB 2-28; Fig. 15D, E), and the posterior end of the pubic boot (IGB 2-29; Fig. 15F–H) of the holotype and an almost complete left and partial right pubis of the paratype (Fig. 21F–H). The right pubic shaft of the holotype is complete from the proximal expansion towards the peduncles to the distal expansion towards the pubic boot (Fig. 15A–C). The preserved length is 73 cm, with approximately 10–15 cm missing at the distal end and some 5 cm missing at the proximal end. The almost complete left pubis of the paratype is 74 cm long. The shaft of the right pubis of the holotype is long and slender, being notably bowed anteriorly (Fig. 15A, C), more so than in *Sinraptor* (Currie and Zhao 1993) and *Siamotyrannus* (Buffetaut *et al.* 1996), but comparable to *Allosaurus* (Gilmore 1920, Madsen 1976), many carcharodontosaurs (e.g. Stromer 1931, Canale *et al.* 2022) or *Tyrannosaurus* (Brochu 2003), although the pubic shafts are considerably more slender than in all of these taxa. In other metriacanthosaurids, the pubic shafts are straight (Dong *et al.* 1983, Gao 1999, Wu *et al.* 2009). Proximally, the shaft is almost round in cross-section, being *c.* 58 mm deep anteroposteriorly and 56 mm wide mediolaterally. More distally, it becomes more slender, with a minimal anteroposterior depth of *c.* 48 mm, before it then gradually expands again in its distal half towards the distal boot (Fig. 15A), which is missing in the type, but partially preserved in articulation of the distal left and right pubic shafts in the paratype (Fig. 21F–H). A robust pubic apron was obviously present, but is largely broken away (Fig. 15B, C). It is developed as a flange that extends medially from the anterior edge of the medial side of the pubic shaft. The pubic apron ends considerably above the distal expansion for the pubic boot, so that that the pubes were separated distally anteriorly, as in *Sinraptor* (Currie and Zhao 1993) and *Siamotyrannus* (Samathi 2013).

The paratype shows that the pubic boot was steeply angled posteroproximally (Fig. 21G, H), as in *Sinraptor* (Currie and Zhao 1993), but more so than in *Yangchuanosaurus shangyuensis* (Dong *et al.* 1983), *Siamotyrannus* (Buffetaut *et al.* 1996), or *Shidaisaurus* (Wu *et al.* 2009). *Yangchuanosaurus hepingensis* seems to have an intermediate condition (Gao 1999). In the distal shaft, a wide longitudinal depression appears on the posterolateral side of the shafts, between the narrow lateral side of the latter and the posterior expansion of the boot. The distal shaft is expanded mediolaterally to form a wide, distal expansion that is rounded triangular in outline in distal view, being wider anteriorly, and has a flat medial side, where the expansions of the left and right sides met. Thus, the articulated pubic boots are heart shaped in outline in distal view (Fig. 21I), as in *Sinraptor* (Currie and Zhao 1993). Only the anteroproximal part of the posterior expansion of the pubic boots are preserved in the paratype. Here, the left and right boots are fused (Fig. 21H, I). A largely symmetrical, ventrally flattened bone is here interpreted as the posterior part of the conjoined pubic boots of the holotype (IGB 2-29; Fig. 15F–H). If correctly identified, the pubic boot would have been more prominently developed than in *Sinraptor*. At the proximal break, the bone is mediolaterally slender and anteroposteriorly elongate. No suture is visible, confirming that the posterior parts of the left and right pubic boots were completely fused, as in other basal tetanurans (e.g. Currie and Zhao 1993, Sereno *et al.* 2008). The lateral walls of the posterior pubic boots are slightly dorsoventrally concave so that the lateral margins of the boot form a slight lateral lip (Fig. 15G); this concavity is consistent with the development of a posterolateral depression in the distal pubic shafts in the paratype. A concavity of the lateral side of the pubic boot and the resulting lateral lip are also present in *Sinraptor* (Currie and Zhao 1993) and

Figure 15. Pubes and ischia of *A. kyrgyzicus*. A–C, partial right pubis, IGB 2-26, in lateral (A), anterior (B), and medial (C) views. D, E, fragmentary left pubis, IGB 2-28, in lateral (D) and medial (E) views. F–H, distal end of conjoined pubic boots, IGB 2-29, in right lateral (F), proximal (G), and distal (H) views. I–M, articulated ischia, IGB 2-30, in right lateral (I; note that proximal part of right ischium is missing, so that the medial side of the proximal left element is visible), posterior (J), and left lateral (K) views, and proximal end of left ischium in proximal view (L) and conjoined ischial boot in distal view (M). Abbreviations: eb, expansion for pubic boot; co, concavity; ia, ischial articulation; ib, ischial boot; in, incision; ip, iliac peduncle; op, obturator process; pa, pubic apron; pdf, posterodorsal flange; pp, pubic peduncle; pt, pubic tubercle. Scale bar is 10 cm.

Siamotyrannus (Buffetaut *et al.* 1996, Samathi 2013). In ventral view, the cojoined boots are rather slender posteriorly but gradually expand anteriorly; the ventral surface is rugose and slightly indented in its midline.

Proximally, the flange of the pubic apron flexes posteriorly towards the obturator plate of the pubis, which is broken away. However, there is no flange on the more proximal posterior margin of the pubis of either the holotype or the paratype, indicating that the obturator foramen was either very large, or not enclosed by bone, as is also the case in other metriacanthosaurids (Dong *et al.* 1983, Currie and Zhao 1993, Buffetaut *et al.* 1996). The shaft becomes mediolaterally flattened and expands anteroposteriorly towards the proximal end. Anteriorly, a rather weakly developed pubic tubercle is present (Figs 15A, 21G). It is more proximally placed than the twist of the pubic apron into the obturator plate, and is developed as an elongate, anteriorly directed crest, as in other metriacanthosaurids (Dong *et al.* 1983, Currie and Zhao 1993, Buffetaut *et al.* 1996, Gao 1999). Although there is a notable flexure of the pubis at the level of the pubic tubercle (Figs 15B, 21F), it is not as marked as in some other theropods (e.g. *Condorraptor*; Rauhut 2005).

Ischia: Left and right ischia of the holotype are largely complete and preserved in articulation (IGB 2-30; Fig. 15I–M), with only a minor part of the shaft of the left ischium missing due to erosion, so that the iliac peduncle of the left ischium is preserved in isolation (IGB 2-31). Of the paratype, only a part of the proximal portion of the right ischium is preserved (IGB 2-53; Fig. 21J), missing both peduncles and most of the shaft. The holotype ischium is 68 cm long from the iliac peduncle to the distal extremity. The proximal end is 25 cm long anteroposteriorly and was divided into the dorsally directed, short, but anteroposteriorly broad iliac peduncle and the much longer, slender, anteriorly directed pubic peduncle (Fig. 15I, K). The pubic peduncle is longer than the articular surface between the ischium and ilium, and about twice as long as the iliac peduncle, which contrasts with the much shorter condition of this peduncle in *Sinraptor* (Currie and Zhao 1993), *Yangchuanosaurus hepingensis* (Gao 1993), and *Monolophosaurus* (Zhao and Currie 1993), but is similar to *Shidaisaurus* (Wu *et al.* 2009) and *Allosaurus* (Madsen 1976). The iliac articulation is maximally 8 cm wide and has a large, semioval, cup-shaped concavity posteriorly for the reception of the convex ventral surface of the ischial peduncle of the ilium (Fig. 15L), thus forming a peg-in-socket articulation, as in many abelisauroids (Carrano and Sampson 2008) and carcharodontosaurids (Carrano *et al.* 2012), but apparently not in *Sinraptor* (Currie and Zhao 1993). This articulation expands far lateral to the lateral surface of the ischium more distal to it. Anterior to the concavity, a broad, anterodorsally facing and laterally tapering surface represents the posteroventral margin of the acetabulum; towards the pubic peduncle, this margin becomes rapidly narrower, and while the mediolateral width of the acetabulum is *c.* 85 mm at the iliac-ischium articulation, it is only *c.* 15 mm at the dorsal rim of the pubic peduncle (Fig. 15L). At the posterior margin of the base of the iliac peduncle, a marks depression on the lateral side marked the insertion area of the m. flexor tibialis internus (Hutchinson 2001a), as it is also present in *Siamotyrannus* (Buffetaut *et al.* 1996). The paratype ischium furthermore shows a marked, large, oval tubercle with a slightly rugose surface below this depression just above the base of the shaft; this area is poorly preserved in the holotype.

Whereas the iliac peduncle extends only for *c.* 6 cm above the ventral margin of the acetabulum, the pubic peduncle extends anterior for *c.* 14 cm from the posterior margin of this structure. It is semioval in cross-section, with a minimal height of *c.* 7 cm, although small parts of the thin ventral margin might be missing. The pubic articulation forms an anteriorly directed flat surface with a semioval, ventrally slightly tapering outline that is 7 cm high and 3.5 cm wide. The obturator plate is largely reduced to only a relatively small anteroventrally projecting obturator process at the base of the ischial shafts (Fig. 15I, K), as in *Allosaurus* (Madsen 1976), *Sinraptor* (Currie and Zhao 1993), *Yangchuanosaurus magnus* (Dong *et al.* 1983), and *Yangchuanosaurus hepingensis* (Gao 1999). The obturator process is roughly rectangular in shape, with a straight anteroventral edge and a notable incision between its ventral margin and the ischial shaft, as it is typically present in non-coelurosaurian theropods (Rauhut 2003), including *Sinraptor* (Currie and Zhao 1993) and *Yangchuanosaurus hepingensis* (Gao 1999).

The shaft of the ischium is long and slender, and slightly curved anteroventrally in lateral view, as in *Megalosaurus* (Benson 2010) and *Siamotyrannus* (Buffetaut *et al.* 1996, Samathi 2013). It is semioval in outline, being deeper anteroposteriorly than wide mediolaterally, and with a flattened medial surface for the contact with the opposite element. This flat contact extends over almost the entire length of the ischial shafts (Fig. 15J), so there is no ischial apron, as it is present in some megalosaurids (Benson 2010). From the beginning of the interischial suture to slightly distal of the half length of the shafts, the posterodorsal margin of each ischium thins out, so that the joined ischia form a distinct, well developed posterodorsal median flange (Fig. 15K). Such a flange on the posterodorsal surface of the articulated ischia is also present in *Shidaisaurus* (Wu *et al.* 2009), *Yangchuanosaurus* (Dong *et al.* 1983, Gao 1999), *Sinraptor* (Currie and Zhao 1993), and *Siamotyrannus* (Buffetaut *et al.* 1996, Samathi 2013), and thus probably represents a synapomorphy of metriacanthosaurids, as it is absent in *Allosaurus* (Gilmore 1920, Madsen 1976) and carcharodontosaurs (Coria and Currie 2006, Brusatte *et al.* 2008, Canale *et al.* 2022). Distally, the shafts become more compressed mediolaterally, but gradually expand anteroposteriorly, until a marked expansion at the distal end forms a large ischial boot (Fig. 15I, K), as it is also present in other metriacanthosaurids (Dong *et al.* 1983, Currie and Zhao 1993, Gao 1999, Wu *et al.* 2009). This boot is more anteriorly than posteriorly expanded and has a gently convex ventral outline in lateral view. In ventral view, the anterior ends of the ischia ae fused into a pointed anterior end of the boot, whereas there is a notable groove between the left and right ischium in the posteriorly widening posterior two-thirds of the boot (Fig. 15M). Whereas the minimal anteroposterior width of the ischial shaft is *c.* 5.5 cm just distal to its proximal base, the ischial boot expands to a maximal anteroposterior length of *c.* 22.5 cm.

Femur: Both femora of the holotype are completely preserved (IGB 2-32, 2-33; Fig. 16), with the head of the left femur having been found in the acetabulum of the left ilium. The femur is a robust bone and only moderately curved in lateral or medial view (Fig. 16B, D, H), similar to the situation in

Metriacanthosaurus (OUM J 12144), *Sinraptor* (Currie and Zhao 1993), *Yangchuanosaurus hepingensis* (Gao 1999), and other basal tetanurans. The femoral head is directed anteromedially at an angle of approximately 25°, as in many non-neotetanuran theropods, but in contrast to the strictly medially directed femur in most coelurosaurs and allosauroids. In anterior view, the femoral head of the left femur is distinctly proximomedially directed (Fig. 16A), as in carcharodontosaurids (Brusatte and Sereno 2008), *Metriacanthosaurus* (OUM J 12144) and, to a lesser degree, *Yangchuanosaurus hepingensis* (Gao 1999). In the right femur, the femoral head has been tectonically sheared off and glued back in a position appearing to indicate a horizontal orientation of the head (Fig. 16G). However, this position probably derives from the reconstruction of that part of the proximal femur, and we consider the left femur to show the original orientation. In proximal view, the femoral head is gently convexly rounded mediolaterally, and widens gradually from the greater trochanter laterally towards the medial side of the head (Fig. 16E). The greater trochanter narrows to a slightly posterolaterally directed point. Its proximal surface is very gently convex anteroposteriorly and slightly posteroproximally directed. The medial end of the head is expanded both anteriorly and posteriorly, with the anterior side forming a rounded angle of approximately 90° between the anterior and medial margin of the head, while the posterior edge forms the medial boundary of a well-developed, oblique ligament groove on the posterior side of the femoral head (Fig. 16C). Between these edges, the medial margin of the head is convexly rounded in proximal view. A well-developed oblique groove (‘proximal articular groove’ of Carrano *et al*. 2002) is present on the proximal surface of the femur (Fig. 16E), in contrast to most allosauroids and coelurosaurs (Benson 2010), although a similar groove might be present in *Sinraptor* (based on fig. 22C in Currie and Zhao 1993). In posterior view there is a narrow incision between the head and the shaft at the distal end of the head, in continuation of the oblique ligament groove.

The lesser trochanter is aliform (‘wing-like’) and separated from the proximal shaft by a small incision in lateral view (Fig. 16D). Its proximal end is placed at the level of the distal margin of the femoral head, in contrast to the more proximally placed lesser trochanter in *Yangchuanosaurus shangyuensis* (Dong *et al.* 1983), *Sinraptor* (Currie and Zhao 1993), *Metriacanthosaurus* (OUM J 12144), *Allosaurus* (Madsen 1976), and coelurosaurs (Rauhut 2003), but as in *Yangchuanosaurus hepingensis* (Gao 1999). A small, triangular, slightly anterolaterally directed accessory trochanter is present at the base of the lesser trochanter (Fig. 16B, D, H, I), as in species of *Yangchuanosaurus* (Dong *et al.* 1983, Gao 1999), whereas such an accessory trochanter seems to be absent in *Sinraptor* (Currie and Zhao 1993). This position bears a large, low, mound-like swelling on the lateral side at the distal end of the lesser trochanter, probably for the insertion of the m. iliofemoralis externus, as in other tetanurans (Hutchinson 2001b). Proximal and slightly posterior to this mound, a flat area with marked anterior and posterior edges and a rectangular cross-section extends from the lesser trochanter towards the shaft, into which it fades just at the level of the proximal end of the mound. The fourth trochanter is developed as a robust, elongate semioval flange on the posteromedial side of the femoral shaft, just above the mid-length of the bone (Fig. 16B, D, H, I). In contrast to some theropods (e.g. *Baryonyx*; Charig and Milner 1997; *Suchomimus*, MNN Gad 500), there is no groove or depression medial to the fourth trochanter, but notable, posteriorly directed striations are present on the lateral side of the trochanter. Distal to the fourth trochanter, the shaft is mediolaterally compressed; although this might be somewhat exaggerated by compaction, this is observed in both femora. In *Sinraptor* (Currie and Zhao 1993), *Yangchuanosaurus hepingensis* (Gao 1999), and *Metriacanthosaurus* (OUM J 12144), the femoral shaft is wider mediolaterally than anteroposteriorly.

Distally, the shaft becomes more massive and rounded triangular in cross-section, before it then notably expands towards the distal articular end. A well-developed, semioval medial epicondylar crest (*sensu* Carrano *et al.* 2002, medio-distal crest of other authors, e.g. Juárez-Valieri *et al.* 2007) is present above the distal end (Fig. 16A, G). This crest is more prominent than in most other theropods, with the exception of abelisauroids (e.g. Carrano *et al.* 2002, Juárez-Valieri *et al.* 2007), but including other metriacanthosaurids, such as *Sinraptor* (Currie and Zhao 1993), *Yangchuanosaurus hepingensis* (Gao 1999), and *Metriacanthosaurus* (OUM J 12144). However, it is more robustly developed than in abelisaurids and notably offset from the distal end (by *c.* 15 cm), more so than in e.g. *Masiakasaurus* (Carrano *et al.* 2002), a morphology that seems to be unique for the new taxon. An elongate, flat triangular surface on the medial side, as it is found medial to the epicondylar crest in many theropods (see Rauhut and Carrano 2016), is absent. The anterior side of the femur is completely flat at the level of the epicondylar crest, but just distal to it, a narrow, deep, sharply defined groove begins and extends to the distal end of the femur, where it is confluent with the intercondylar groove on the distal surface of the bone (Fig. 16A, G). This groove is markedly different from the large medial depression present on the anterior side of the distal femur for the attachment of the m. femorotibialis (Hutchinson 2001b) that is present in numerous theropods (Rauhut 2003), including *Sinraptor* (Currie and Zhao 1993), as it is considerably narrower, deeper, and defined by an abrupt step from the anterior surface medially and a sharp ridge laterally. The distal end of the femur is well rounded in both medial and lateral view, and subdivided by an anteroposteriorly oriented intercondylar groove into a slightly broader lateral and a narrower medial condyle. In posterior view, the distal condyles are separated by a broad and deep intercondylar groove that extends proximally up to the level of the proximal end of the crista tibiofibularis, where it ends rather abruptly. The crista tibiofibularis is narrower than the tibial condyle and extends more proximally than the latter. An unusual feature of this crest is a medial expansion distally, which gives the crest a triangular outline in distal view, with a medially directed tip that overhangs the intercondylar groove posteriorly (Fig. 16F).

Tibia: Both tibiae of the holotype are preserved (IGB 2-34, 2-35; Fig. 17A–H), and the right tibia of the paratype is also present (IGB 2-48; Fig. 21A–E). Apart from differences in robustness and a slight difference in the development of the distal end (see below), the holotype and paratype tibiae are virtually identical, so the following description is mainly based on the holotype elements. The holotype tibiae are stout and considerably shorter than the femur. The shaft is slightly curved laterally, so

Figure 16. Femora of *A. kyrgyzicus*. A–F, right femur, IGB 2-33, in anterior (A), medial (B), posterior (C), lateral (D), proximal (E), and distal (F) views. G–I, left femur, IGB 2-32, in anterior (G), lateral (H), and medial (I) views. Abbreviations: IV, fourth trochanter; at, accessory trochanter; ec, epicondylar crest; gt, greater trochanter; lt, lesser trochanter; mt, medial tip; olg, oblique ligament groove; pag, proximal articular groove. Scale bar is 10 cm.

that the medial side is gently concave and the lateral side convex over almost their entire length (Fig. 17B, D), as in *Condorraptor* (Rauhut 2005) and *Sinraptor* (Currie and Zhao 1993). The proximal end is strongly anteroposteriorly expanded. Anteriorly, the well-developed cnemial crest arises gradually from the tibial shaft (Fig. 17A). Proximally, it accounts for *c.* 9.5 cm of the total anteroposterior length of the proximal end of *c.* 21 cm and extends slightly further proximally than the posterior part of the tibia. In lateral view, its outline is subrectanguar. A well-developed, oblique ridge is present on the lateral side of the cnemial crest proximally (Fig. 17A, E), being slightly offset from the anterior end. In anterior view, the cnemial crest flexes slightly laterally, although to a lesser degree than in *Sinraptor* (Currie and Zhao 1993). Posteriorly, the expansion of the proximal tibia is more abrupt, forming an overhanging lip over the proximal part of the posterior side of the shaft. The medial proximal trochanter and the laterally placed fibular trochanter are separated by a shallow concavity on the proximal surface, and a small incision at the posterior rim, as it is often present in theropods (Rauhut 2003). Anteriorly, the fibular condyle is separated from the cnemial crest by a moderately developed incisura tibialis (Fig. 17E). In proximal view, the fibular condyle is semicircular posteriorly and has a slightly lower, angular edge anteriorly that is confluent with a bulge extending proximally from the fibular flange. The latter is proximally placed on the lateral side of the tibia shaft, ending no more than 26 cm from the proximalmost point of the bone (Fig. 17A, B, G, H). In contrast to many tetanuran theropods, including *Sinraptor* (Currie and Zhao 1993), where it is often clearly demarcated, it arises rather gradually out of the shaft distally. As in *Megalosaurus*, *Piatnitzkysaurus*, and *Sinraptor* (see Benson 2010), it is anteroposteriorly widened and bulbous, rather than developed as a thin lamina, as is the case in most other theropods. The flange is rounded in anterior or posterior outline and is only about 10 cm long. Proximally, it again fades gradually into a notable swelling on the lateral side of the proximal end of the tibia, which continues up to the proximal articular end (Fig. 17A, B), as is also the case in many megalosauroids (Benson 2010) and *Sinraptor* (Currie and Zhao 1993), but unlike the fibular flange that is completely offset from the proximal end in many neotetanurans. In lateral view, the fibular flange and the bulge are flanked by notable longitudinal depressions both anteriorly and posteriorly.

Distal to the fibular flange, the shaft of the tibia has a rounded, rather massive outline, before it becomes gradually more anteroposteriorly flattened distally. However, the shaft remains considerably more robust than the more anteroposteriorly compressed shafts of many coelurosaur tibiae throughout its length. Although the anterior side is only slightly convex mediolaterally in the distal half of the shaft, the posterior side remains strongly convex, and the ratio of mediolateral width to anteroposterior depth is *c.* 1.35 at the mid-shaft, which is higher than in *Neovenator* (1.22; Brusatte *et al.* 2008) and *Acrocanthosaurus* (1.29; Stovall and Langston 1950), but less than in *Sinraptor* (1.45; Currie and Zhao 1993). Throughout the length of the shaft, a narrow, flattened to slightly mediolaterally concave area on the lateral margin of the anterior side marks the contact between tibia and fibula.

Distally, the tibia expands notably mediolaterally, from a minimal shaft width of *c.* 8.5 cm to a maximal distal width of 19.5 cm. The expansion is slightly more marked laterally than medially, and the lateral malleolus reaches slightly further distally than the medial, as in *Sinraptor* (Currie and Zhao 1993). Whereas the lateral expansion forms a gentle curve from the shaft into the malleolus, there is a more marked flexure point on the medial side, where the proximally concave margin of the expansion flexed into an almost straight medial margin. This is opposite to the condition in *Sinraptor*, where the medial side expands gradually and the lateral expansion is slightly offset from the shaft (Currie and Zhao 1993). In distal view, the articular surface of the tibia is broad triangular in outline, with a slightly anteriorly flexed anteromedial edge and a much shorter posteromedial than posterolateral side (Fig. 17F). From the posteromedial angle of the distal outline, a broad and well-defined groove extends anterolaterally, but does not reach the anterior end distal surface. A depression in this position is present in many theropods, but it is often less well defined as a sharp and deep groove, with the exception of *Sinraptor* (Currie and Zhao 1993). Medial to this groove, the distal end is notably convex in anterior view, whereas it remains rather flat over two-thirds of its width laterally, and then flexes proximolaterally. On the anterior side of the distal tibia, an oblique step extending from the mediodistal corner laterally marks the bracing for the ascending process of the astragalus (Fig. 17B, F), as is present in most basal tetanurans (Rauhut 2003). In the holotype, this step extends to approximately the mid-width of the distal tibia and becomes more prominent up to this point. It then flexes proximally and rapidly fades into the shaft. In the paratype tibia, the shelf is notably shorter and flexes proximally in the medial third of the distal expansion (Fig. 21D); apart from relative robustness, this is the only notable difference between the holotype and paratype tibiae. In *Sinraptor*, the flexure of the step is more marked and even further laterally placed than in *Alpkarakush* (Currie and Zhao 1993).

Fibula: The left fibula is almost completely preserved in two pieces (IGB 2-36, 2-37; Fig. 17I–M), with only an estimated 1–2 cm of the shaft missing. The fibula is a very slender bone, with a minimal anteroposterior shaft diameter of 30 mm. The proximal end is considerably expanded, more posteriorly than anteriorly, to a maximal anteroposterior width of 135 mm. The proximal articular surface is widest anteriorly, where it forms a both anteroposteriorly and mediolaterally convex condyle that is *c.* 5.5 cm wide mediolaterally and 4.5 cm long anteroposteriorly. A small, triangular process extends from this condyle anteromedially in proximal view (Fig. 17L). Posterior to this convex area, the proximal articular surface narrows rapidly and becomes notably anteroposteriorly concave. In its posterior third, it is again anteroposteriorly convex and narrows to a posteromedially directed point. The lateral surface of the proximal end showsd notable longitudinal striations. It is flat in its central part, curves abruptly anteriorly towards the anterior margin and forms a thin, medially positioned posterior flange posteriorly. Anteriorly, there is a small, thickened flange at the anteromedial edge where the expanded part of the fibula fades into the shaft. Just proximal to the iliofibularis tubercle, there is a notable deflection in the shaft, distal to which it extends slightly more posterodistally. Such a deflection is absent in *Sinraptor* (Currie and Zhao 1993) and *Yangchuanosaurus shangyuensis* (Dong *et al.* 1983). The iliofibularis tubercle is developed as

Figure 17. Tibiae and fibula of *A. kyrgyzicus*. A–F, left tibia, IGB 2-34, in lateral (A, stereophotographs), anterior (B), medial (C), posterior (D), proximal (E), and distal (F) views. G, H, right tibia, IGB 2-35, in anterior (G) and lateral (H) views. I–M, left fibula, IGB 2-36, 2-37, in lateral (I), anterior (J), medial (K), proximal (L), and distal (M) views. Abbreviations: af, anteromedial flange; cc, cnemial crest; d, depression; fc, fibular crest; fic, fibular condyle; g, groove; if, iliofibularis tubercle; in, incision; it, incisura tibialis; ri, ridge; st, step for bracing of ascending process of astragalus; sw, swelling. Scale bar is 10 cm.

Figure 18. Tarsal elements of *A. kyrgyzicus*. A–E, left astragalocalcaneum, IGB 2-38, in proximal (A, stereophotographs), lateral (B), medial (C), anterior (D), and distal (E) views. F, right astragalocalcaneum, IGB 2-39, in anterior view. G, left astragalocalcaneum in articulation with the tibia in anterior view. H, partial left distal tarsal IV in distal view. Abbreviations: ap, ascending process; ff, fibular facet; g, groove; og, oval groove; su, partially visible suture between astragalus and calcaneum; tf, tibia facet; tu, tubercle. Scale bar is 5 cm.

an elongate, slightly obliquely curved, broad, and low ridge on the anterolateral margin of the fibular shaft, starting *c.* 20 cm distal to the proximal end (Fig. 17I, J). The ridge is *c.* 8 cm long and borders a very shallow depression on the anterior side of the shaft laterally (Fig. 17J). This depression is *c.* 17 mm wide, proximomedially-distolaterally oriented, and bordered medially by a small, longitudinal rugosity. Distal to the iliofibularis tubercle, the fibular shaft narrows notably, from an anteroposterior width of *c.* 5 cm proximal to it to a width of 3.5 cm distal from the tubercle. This notable change in anteroposterior width is absent in *Sinraptor* (Currie and Zhao 1993), but seems to be present also in *Yangchuanosaurus shangyuensis* (Dong *et al.* 1983). From here, the shaft gradually narrows to its minimal width of 30 mm, until it then expands again towards the distal end in its distalmost fifth. This expansion is first moderate and gradual, until the appearance of an anteromedial flange some 11.5 cm above the distal end marks an anteromedial twist of the long axis of the distal end in relation to the proximal end (Fig. 17I). Such a flange is also present in *Sinraptor* (Currie and Zhao 1993). Further distally, the fibula also expands posteriorly and laterally, to form a rather massive, distally well-rounded distal articular end, which is 7.5 cm long anteroposteriorly and up to 5 cm wide mediolaterally. In distal view, the articular surface is triangular to teardrop shaped, tapering posterolaterally and with a flat posteromedial surface (Fig. 17M).

In medial view, a large depression is present in the expanded proximal end of the fibula (Fig. 17K), as in many tetanuran theropods (Rauhut 2003), including *Sinraptor* (Currie and Zhao 1993). This depression covers almost the entire medial surface of the proximal end and is bordered anteriorly by a thickened rim, whereas it gradually fades out posteriorly, unlike the both anteriorly and posteriorly clearly defined depression in some theropods, such as ornithomimosaurs (e.g. Rauhut 2003: fig. 47b) or *Deltadromeus* (SGM Din 2). Distally, the depression tapers and ends in a rather well-defined point, just proximal to the level of the iliofibularis tubercle. Distal to this point, the medial surface is very slightly concave anteroposteriorly up to the level where the anteromedial flange starts distally. Here, a low, obliquely posterodistally extending step separates this concave surface from a more flat, only posteriorly very slightly concave distal medial surface.

Astragalocalcaneum: Both astragalocalcanei are completely preserved (IGB 2-38, 2-39; Fig. 18A–G). The astragalus and calcaneum are largely fused, only in the left element is a suture still visible anteriorly (Fig. 18D), but becomes difficult to follow posteriorly. The elements are generally very similar to the corresponding but unfused elements in *Sinraptor* (Currie and Zhao 1993). The astragalocalcaneum has a maximum width of *c.* 19 cm, of which 14.7 cm are accounts for by the astragalus, so that the calcaneum only accounted for 22.6% of the width of the compound element, very similar to this value in *Sinraptor* (22.5%, Currie and Zhao 1993). The astragalar condyle expands anteroproximally, so that the body of the astragalus extends also anterior to the tibia (Fig. 18G), as is typical in tetanurans, and not only distal to it, as in non-tetanuran theropods. Most of the proximal articular surface of the astragalus is made up by the facet for the distal tibia, which forms a marked, mediolaterally elongate and anteroposteriorly concave facet along the posterior side of the bone (Fig. 18A). This facet is anteroposteriorly widest on the medial side, where it also curves slightly anteromedially and gradually narrows laterally. At the posteromedial edge of the tibia facet, a stout, anterolaterally directed tubercle is present (Fig. 18A, C), which fits into the groove in the distal articular surface of the tibia. A similar tubercle is also present in *Sinraptor*, where it seems to be less angular, though (Currie and Zhao 1993). Anterior to the tibia facet, the well-developed, laminar ascending process of the astragalus is found. It is triangular in outline in anterior view, with a vertical lateral margin, and approximately as high as the astragalar body below it, as in *Sinraptor* (Currie and Zhao 1993). As in most non-coelurosaurian theropods, the base of the ascending process is restricted to the lateral part of the astragalar body. The process is slightly offset anterior from the anterodistal articular condyle by a low step, and a large, mediolaterally elongate oval groove is present at its base (Fig. 18D), similar to the condition in *Sinraptor* (Currie and Zhao 1993). The proximomedial margin of the ascending process is flattened, where it abuts the oblique step on the anterior side of the distal end of the tibia. Lateral to the ascending process, a both anteroposteriorly and mediolaterally concave, laterally widening facet marks the contact between the astragalus and the fibula.

Posterolaterally, the tibia facet extends onto the posterior side of the calcaneum, where it is bordered anteriorly by an oblique ridge that extends from the posterolateral edge of the ascending process towards the posterolateral corner of the calcaneum and separates the tibia facet from the fibular facet. The latter occupies most of the proximal surface of the calcaneum and widens lateroposterioly. Medially it is confluent with the fibular facet on the astragalus.

The distal condyles of the astragalocalcaneum are strongly convex anteroposteriorly. In anterior view, there is a constriction between the medial part of the astragalus and the lateral astragalocalcaneal condyles. A well-developed groove is present across the anterior face of the distal condyles over the medial two-thirds of the width of the astragalocalcaneum (Fig. 18D, G), as in many basal averostrans (Rauhut 2003). The level of this groove roughly coincides with the astragalar articulation with the medial malleolus of the distal tibia, as in other tetanurans (Rauhut and Pol 2017). In distal view, there is also a constriction between the medial part of the astragalar condyle and the lateral astragalocalcaneal condyle. However, this constriction is restricted to the anterior margin of the condyles, the posterior margin is largely straight (Fig. 18E). Furthermore, the medial side is considerably more and more abruptly anteriorly expanded than the lateral side, in contrast to *Sinraptor*, where the two expansions are subequal (Currie and Zhao 1993). The maximum anteroposterior width of the astragalocalcaneum condyles is *c.* 95 mm medially, this width is minimally *c.* 67 mm in the constricted part, before the condyles expand again to a width of *c.* 75 mm laterally. The medial surface of the astragalus is more or less flat proximodistally and very slightly convex anteroposteriorly, whereas there is a large, semioval depression on the lateral side of the calcaneum (Fig. 18B).

Pes: The foot is represented by a partial left distal tarsal IV (IGB 2-40; Fig. 18H), metatarsals II (IGB 2-41; Fig. 19A–F) and III (IGB 2-42; Fig. 19G, H) of the right and metatarsal III of the left side (IGB 2-43; Fig. 19I–N), a pedal phalanx (IGB

Figure 19. Metatarsals of *A. kyrgyzicus*. A–F, right metatarsal II, IGB 2-41, in anterior (A), medial (B), posterior (C), lateral (D), proximal (E), and distal (F) views. G, H, right metatarsal III in anterior (G) and distal (H) views. I–N, left metatarsal III in proximal (I), distal (J), anterior (K), lateral (L), posterior (M), and medial (N) views. Abbreviations: clf, collateral ligament fossa; oe, overhanging edge; rp, rugose patch; tub, tubercle. Scale bar is 5 cm.

2-44; Fig. 20A–E), and two pedal unguals (IGB 2-45, 2-46; Fig. 20F–L). The distal tarsal IV is represented by its anterolateral half (Fig. 18H). As in other theropods (e.g. Madsen 1976, Currie and Zhao 1993, Rauhut and Pol 2017), this tarsal seems to have been roughly trapezoidal in outline, with a mediolaterally wider anterior part. The anterolateral corner is rounded and forms an angle of approximately 8590°, whereas the anteromedial corner of the bone forms a sharp angle of approximately 60°. In between these two corners, the anterior margin of the bone is gently convexly rounded. In anterior view, the anterolateral side of the bone is proximomedially thickened to almost double the thickness of the anteromedial corner. The proximal surface of the tarsal is gently concave, whereas the distal surface is largely flat, with slightly proximally flexed margins towards the anterolateral and anteromedial corners. Low, but well defined, parallel anteroposteriorly oriented ridges are present on the distal surface, these are most prominent on the lateral side of the bone.

Figure 20. Pedal phalanges of *A. kyrgyzicus*. A–E, right pedal phalanx II-2, IGB 2-44, in dorsal (A), medial (B), ventral (C), distal (D), and proximal (E) views. F–I, ungual of right digit II, IGB 2-45, in lateral (F), proximal (G), dorsal (H), and ventral (I) views. J–L, pedal ungual, IGB 2-46, in medial or lateral (J), dorsal (K), and ventral (L) views. Abbreviations: cg, claw groove; clg, collateral ligament groove. Scale bar is 2 cm.

The metatarsus is elongate and slender. The length of metatarsal III is about 56% of the length of the tibia, which is slightly longer than in *Sinraptor* (53%; Currie and Zhao 1993), considerably longer than in *Allosaurus* (47%; Gilmore 1920), and only slightly less than in *Albertosaurus* (60%; Parks 1928), all theropods with a roughly comparable femoral length. Metatarsal II is about 87% of the length of metatarsal III. The shaft is almost straight in anterior and posterior view, being only very slightly flexed medially in its distal part (Fig. 19A, C), similar to the condition in *Sinraptor* (Currie and Zhao 1993). In medial or lateral view, it is slightly flexed anterodistally, especially along its posterior surface (Fig. 19B, D); this flexure is more pronounced than in *Sinraptor* (Currie and Zhao 1993). The proximal end is considerably expanded both anteriorly and posteriorly, and also towards the medial side. Thus, whereas the minimal anteroposterior shaft width is *c.* 46 mm, the maximal anteroposterior expansion of the shaft is *c.* 100 mm. In medial view, the anterior expansion forms a gradual concave arch, whereas the posterior expansion is only slightly concave at its base and then forms a rather sharp and straight posterior edge. The expansion towards the medial side is restricted to the proximalmost part of the metatarsal and here forms a marked medial concavity in anterior view. In relation to the anteroposterior expansion, this expansion is less marked, reaching a maximal mediolateral width of 60 mm, in contrast to a minimal mediolateral shaft width of *c.* 40 mm. In proximal view, the proximal articular surface is semioval in outline, with a flat lateral margin, a slightly drawn-out anterolateral corner, and a robust posterior flange laterally (Fig. 19E), similar to the condition in *Sinraptor* (Currie and Zhao 1993) and *Allosaurus* (Gilmore 1920, Madsen 1976), although the flexure from the main part of the surface into the posterior flange is more angular in the latter. The articular surface is very slightly anteroposteriorly concave in its central portion, whereas the surface flexes slightly distally on the anterolateral corner and the posterolateral flange. The lateral side of the proximal metatarsal is flattened where it would have contacted metatarsal III. It shows weakly developed rugosities on this contact surface, which are developed as low, rugose proximodistal ridges.

The shaft of metatarsal II is deeper anteroposteriorly than wide mediolaterally. The lateral side is flattened over most of its length,

Figure 21. Remains of the paratype of *A. kyrgyzicus*. A–E, right tibia, IGB 2-48, in anterior (A), lateral (B), proximal (C), and distal (D) views, and detail of the anterior side of the distal end (E). F–I, articulated pubes, IGB 2-49–2-52, in anterior (F), left lateral (G), posterior (H), and distal (I) views. J, fragment of the right ischium, IGB 2-53, in lateral view. Abbreviations: cc, cnemial crest; eb, expansion of pubic boot; fc, fibular crest; fic, fibular condyle; in, incision; pa, pubic apron; pt, pubic tubercle; ri, ridge; st, step. Scale bars are 5 cm.

with a slight twist in the flattened surface just below mid-length, with the distal part facing slightly more anterolaterally than the proximal part. Only the distalmost section of the lateral side, adjacent to the distal articular condyle, becomes anteroposteriorly convex. The cross-section of the shaft is thus semioval at mid-length, narrowing slightly posteriorly. The anterior surface is flattened proximally and towards the distal articular end, with a transversely convex section in between. An elongate oval, slightly rugose patch is on the anterolateral side of the bone, just below the proximal expansion (Fig. 19A). A similar patch seems also to be present in *Sinraptor* (Currie and Zhao 1993). The medial surface is generally convex anteroposteriorly and becomes narrower towards the distal end. The ventral side of the shaft bulges posteriorly in the mid-shaft section. Proximally, below the posterior flange of the articular surface, the posterior side met the lateral side in a sharp posterolateral edge, which disappears into the shaft at the level where the proximal expansion starts. Just below, above the mid-length of the shaft, there is a posteriorly flattened, elongate, slightly rugose patch on the posterior side of the shaft (Fig. 19C). This patch ends at about the mid-length of the metatarsal, distal to which, a rugose, elongate oval is found on the posterolateral side of the bone; its proximal end coincides with the twist in orientation of the lateral side described above. This rugose area flexes more onto the posterior side distally and ends some 3 cm proximal to the expansion of the distal condyles.

The distal end forms a notably mediodistally directed articular condyle, with the medial orientation resulting from the fact that the distal articular surface extends more distally laterally than medially, not from a medial flexure on the distal shaft (Fig. 19A, C). The distal condyle forms an anteroposteriorly strongly convex arch that extends approximately as far proximally on the anterior and on the posterior side, similar to the condition in *Sinraptor* (Currie and Zhao 1993). The actual articular surface is marked by slight steps on the anterior, medial, and posterior surfaces, distal to which the surface is notably smooth, indicating the presence of articular cartilage. In distal view, the articular surface widens posteriorly, where it is split into a wide lateral and a much narrower lateral part by a deep, wide U-shaped posterior embayment (Fig. 19F), as in *Sinraptor* (Currie and Zhao 1993). In contrast to some theropods, the narrow medial part of the articular surface does not flay medially in its posterior part. The lateral margin of the articular surface is markedly concave anteroposteriorly, and several marked, but shallow and narrow grooves extend from that margin medially over the lateral surface of the articular end. Well-developed collateral ligament fossae are present both medially and laterally, with the lateral one being larger and placed into a funnel-shaped depression that covers the entire anteroposterior height of the lateral side of the distal end (Fig. 19D). On the anterolateral side, a low, slightly mediolaterally elongate tubercle is present at the proximal end of this depression. Medially, the dorsal margin of the collateral ligament groove bulges medially and is slightly rugose.

Left and right metatarsals III are extremely similar in their size, relative dimensions, and morphology (Fig. 19G–N). The shaft is straight over most of its length in anterior view, but shows a slight, but notable lateral flexion in its distal fourth (Fig. 19G, K), as in *Sinraptor* (Currie and Zhao 1993). In medial or lateral view, the shaft remains straight over its entire length. Proximally, the bone is notably flattened anteromedially-posterolaterally, and the proximal end strongly expands anterolaterally-posteromedially, with the expansion being more marked anterolaterally than posteromedially. Anterolaterally, there is an abrupt expansion of the proximal shaft into a small, rectangular flat anterior surface just distal to the proximal articular surface, with the latter slightly expanding onto the anterolateral side, especially at the anteromedial corner of this area. This rectangular surface shows low, but notable longitudinal striations, and it continues to the lateral surface, where there is a small flat area showing the same striations and being offset distally from the shaft by an oblique step. Posteromedially, the expansion of the proximal end of the metatarsal forms a sharp posteromedial edge. The proximal articular surface shows the hourglass shape that is typical of basal tetanuran metatarsal III, having widened anterolateral and posteromedial portions that are separated by a constricted middle part (Fig. 19I). However, in comparison with taxa such as *Allosaurus* (Gilmore 1920, Madsen 1976) or *Acrocanthosaurus* (Stovall and Langston 1950), the proximal end is very slender, and the posteromedial expansion is much less marked, resembling *Sinraptor* in that respect (Currie and Zhao 1993). The proximal articular surface thus has a long and very slightly concave anteromedial margin that would have contacted metatarsal II and anteriorly flexes into the anterolateral margin at an angle of approximately 70°. The anterolateral margin is relatively short and meets the lateral margin at an angle of approximately 120°. The lateral margin has a straight anterior half and a strongly concave, indented posterior half where metatarsal II would have overlapped the posteromedial process of metatarsal IV. Posteriorly, this margin meets the posterior margin at an angle of approximately 105°. The posterior margin is the shortest margin of the proximal articular surface and meets the anteromedial margin in a sharp angle of approximately 40°. The proximal articular surface is flat mediolaterally, but slightly concave in its central part anteroposteriorly. Anteromedially and posteromedially, the surface flexes slightly distally.

The shaft of metatarsal III is marked by the strong anteromedial-posterolateral flattening of its proximal half, which is twisted in respect to the more conventionally oriented distal half, as in *Sinraptor* (Currie and Zhao 1993) and *Allosaurus* (Madsen 1976). Thus, the proximal shaft has a very narrow, anteroposteriorly rounded posteromedial side below the sharp posteromedial crest towards the articular end described above. The anteromedial side is large, expands proximally and is very slightly anteroposteriorly convex (Fig. 19K, N). The anterolateral side is flattened and shows a low and broad, anterolaterally directed tubercle some 9 cm below the proximal end (Fig. 19K). Below this tubercle, a marked edge separates the anterolateral from the posterolateral side; this edge persists into the distal half of the shaft, extending posteriorly as the anterolateral side twists to become the lateral side in the distal shaft. The posterolateral side of the proximal shaft is similar in expansion as the anteromedial side, and has a marked anteroposterior concavity in its posterior two-thirds, but becomes slightly transversely convex towards the distal half of the shaft. Towards the distal half of the shaft, the anteromedial side twists to become the anterior side of the bone. Distal to its mid-length, metatarsal III is wider mediolaterally (*c.* 47 mm) than deep anteroposteriorly (*c.*

38 mm) and has a flattened anterior side. The medial side gradually flexes into the posterior and then the posterolateral side, only laterally, this side remains separated from the narrow, flat lateral side by the posterolateral edge described above. Where the shaft flexes laterally, the anteromedial edge is thickened and forms a notable edge that slightly overhangs the medial side (Fig. 19N). Towards the distal end, the shaft becomes more markedly anteroposteriorly flattened, more markedly so than in *Sinraptor* (Currie and Zhao 1993).

The distal articular end of metatarsal III is mediolaterally broadened. The roller-like distal articular surface extends approximately as far proximally both dorsally and ventrally, and, as in metatarsal II, the area covered by articular cartilage is marked by a slight step and a markedly smooth surface distal to it. In distal view, the articular surface is trapezoidal in outline, being dorsoventrally higher medially than laterally (Fig. 19H, J), as in *Sinraptor* (Currie and Zhao 1993). It is flat mediolaterally, without a distinction of medial and lateral condyles. The ventral margin is markedly concave, mainly due to the posteromedial edge, which is drawn out posteriorly into a point. Well-developed collateral ligament grooves are present both medially and laterally, placed in large depressions on either side at the level of the articular end. On the medial side, the anterior margin of the ligament groove is thickened and overhangs the groove. Only a very faint, broad extensor groove is present on the anterior side directly distal to the articular surface.

The single non-ungual pedal phalanx recovered (IGB 2-44; Fig. 20A–E) most probably represents phalanx II-2 of the right foot, as it closely resembles this element in *Sinraptor* (Currie and Zhao 1993). It is a robust element, maximally 95 mm long and with a minimal mediolateral width of 40 mm. The proximal articular end is trapezoidal in outline, being wider ventrally than dorsally, and with rounded edges (Fig. 20E), missing the sharply angled lateroventral corner seen in this phalanx in *Sinraptor* (Currie and Zhao 1993). It is subdivided by a low vertical ridge into two dorsoventrally notably concave facets of nearly subequal size. The articular end is 54 mm wide and 43 mm high. In dorsal view, the shaft is constricted, more so from the lateral than from the medial side. On the medial side, a marked, rugose tubercle is present ventral from the half height of the proximal articular end. The distal articular surface forms a well-developed gynglimus, with only a very faint extensor groove on the dorsal surface proximal to it. The distal articular surface extends proximally considerably more ventrally than dorsally and is ventrally mediolaterally broader than dorsally (Fig. 20D), as in *Sinraptor* (Currie and Zhao 1993). The articular surface is subdivided into a medial and lateral condyle by a deep, broad dorsoventrally oriented groove. The lateral condyle is slightly broader mediolaterally than the medial condyle and extends further distally, so that the articular end is asymmetrical in dorsal view. The medial condyle is considerably narrower, but slightly higher and more ventrally expanded than the lateral condyle. Large, well-developed collateral ligament grooves are present on either side of the phalanx, being displaced dorsally from the mid-height of the distal articular end (Fig. 20B). The posterior margin of the medial ligament groove is somewhat thickened and projects medially. The distal articular end is maximally 45 mm wide and 42 mm high.

The pedal unguals are broad and ventrally flattened, with only a moderate curvature in medial or lateral view. The larger ungual IGB 2-45 (Fig. 20F–I) most probably represents the ungual of the right digit II, whereas IGB 2-46 (Fig. 20J–L) is most likely an ungual of digit IV. As in some theropods, such as *Sinraptor* (Currie and Zhao 1993), the ungual of digit II is markedly asymmetrical and slightly curved medially in dorsal view (Fig. 20H). The proximal articular surface is round to subquadrangular in outline (Fig. 20G), with a considerably proximally expanded dorsal edge that forms a proximally rounded point in dorsal view (Fig. 20H). A ridge subdividing the facet into two concavities is only rudimentarily developed dorsally. The cross-section of the claw at mid-length is semioval, tapering medioventrally. Well-developed, single claw grooves are present, with the lateral one being placed slightly higher than the medial one. Proximally, a small tubercle is present at the end of the claw groove on either side. Ventrally, only a slightly elevated, rugose patch at the proximal end indicates the insertion of the flexor tendon (Fig. 20I); a flexor tubercle or a ventral groove (as it is present in abelisaurids) is absent, as in *Sinraptor* (Currie and Zhao 1993). This ungual is maximally 40 mm wide and 44 mm high proximally. Its length is 115 mm as measured in a straight line from the tip to the end of the dorsal proximal process (maybe missing 5 mm at the damaged tip), or 130 (+ *c.* 5) mm along the dorsal curve.

The smaller ungual IGB 2-46 is symmetrical and has a round proximal articular facet, with slight indentations on either side just above the mid-height. The dorsal proximal expansion is less prominently developed than in the other ungual. The claw grooves are symmetrically arranged and face dorsolaterally and dorsomedially, respectively (Fig. 20K). Ventral to them the ungual is markedly broadened in respect to the dorsal part; this broadening disappears proximally at the end of the claw grooves, giving the ungual an arrowhead shape in ventral view. As in the other ungual, the flexor tubercle is only developed as a small raised patch with a mildly rugose surface ventrally (Fig. 20L). This ungual is maximally 43 mm wide and 38 mm high proximally, and 90 mm long in a straight line (also missing maybe 5 mm at the tip), or 95 (+ 5) mm along the dorsal curve.

Bone histology

The analyses with the fluorescence spectrometer revealed a high content of manganese, barium and calcium. Manganese is certainly the main source for the dark staining of the bone.

Femur IGB 2-33: The bone wall thickness is 14.4 mm in the thinnest part of the bone wall and 21.1 mm in the lateral corner. Including the potentially pathological tissue in the medullary cavity (inner unit, see below), the maximum thickness increased to 25.1 mm in the lateral corner.

The observable bone tissue could be separated into an inner, middle, and outer unit (Fig. 22). The inner unit, developed within the medullary cavity, consisted of a highly irregularly vascularized tissue with only sparse compaction of the wide vascular canals (Fig. 23A, B). The osteocyte lacunae were very abundant and mostly irregularly shaped, except within bands of lamellar tissue, where they were mostly spindle shaped. There were at least three such bands present in the lateral side (Fig. 23B), but the middle and outer band merged together into a single band

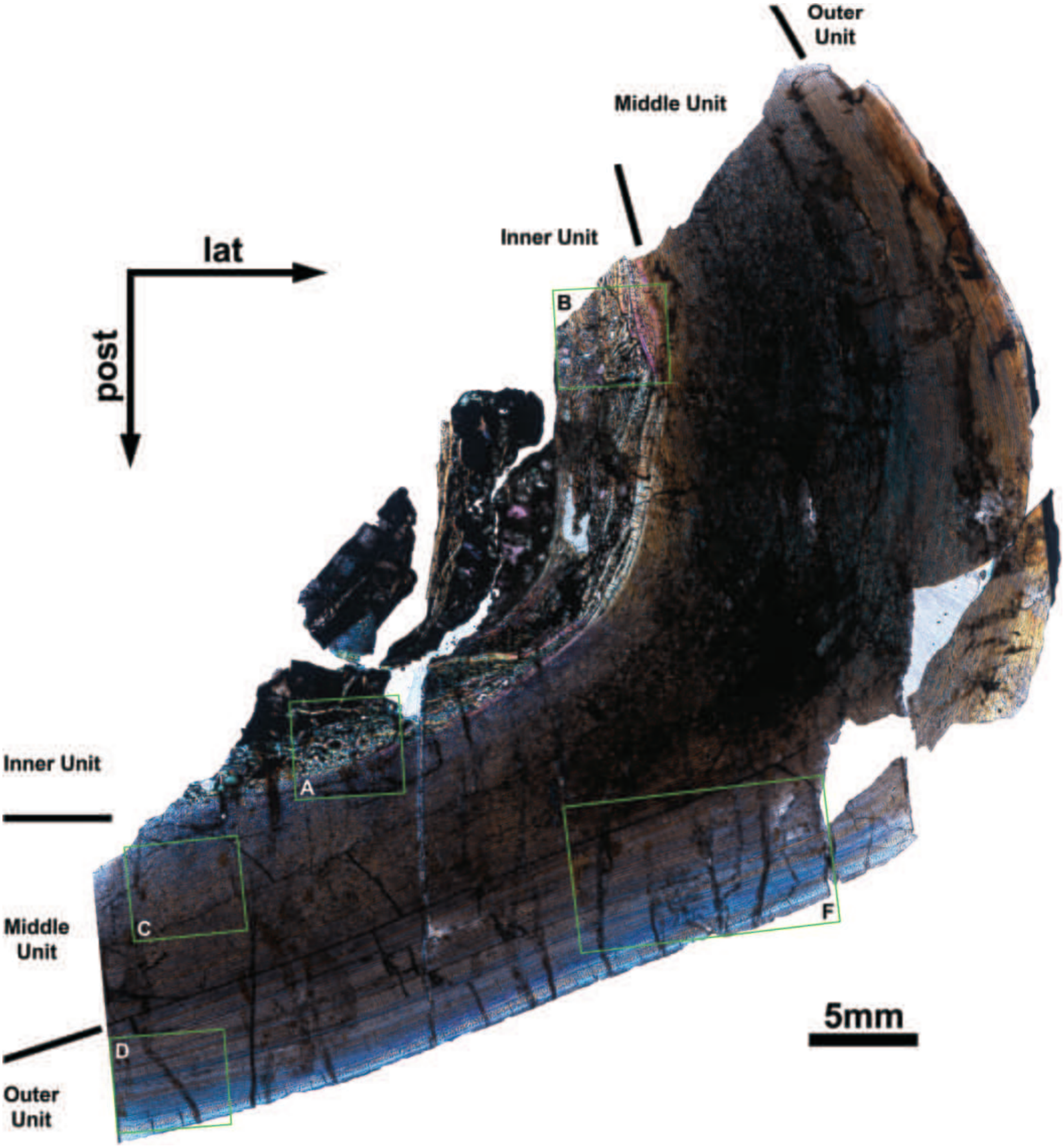

Figure 22. Overview of the mid-diaphyseal section of the right femur of *A. kyrgyzicus*, posterolateral thin section, under circumpolarized light and with a lambda filter. Frames indicate the location of the component images of Figure 23. Abbreviations: lat, lateral; post, posterior.

and then split again towards the posterior side (Fig. 22). The outer band clearly corresponded to an inner circumferential layer (ICL), although it became subsequentially less distinct and more interrupted by vascular canals towards the posterior side of the bone wall. The outer edge of the ICL was clearly resorptive laterally, whereas there was an almost continuous transition between coarse and slightly compacted cancellous endosteal bone tissue and external periosteal bone tissue in the area of the posterolateral wall (Fig. 23A).

The middle unit, which represents the inner part of the periosteally deposited bone wall, comprised about half the thickness of the latter posterolaterally and more than two-thirds of the thickness laterally (Fig. 22). Although the middle unit was partly obscured by dark manganese-rich mineral, it was clear that this unit consisted of highly vascularized, fibrolamellar bone tissue. The vascular canals were mainly oriented laminar to plexiform, rarely reticular, with well-developed primary osteons (Fig. 23C). The degree of organization slightly increased externally as well

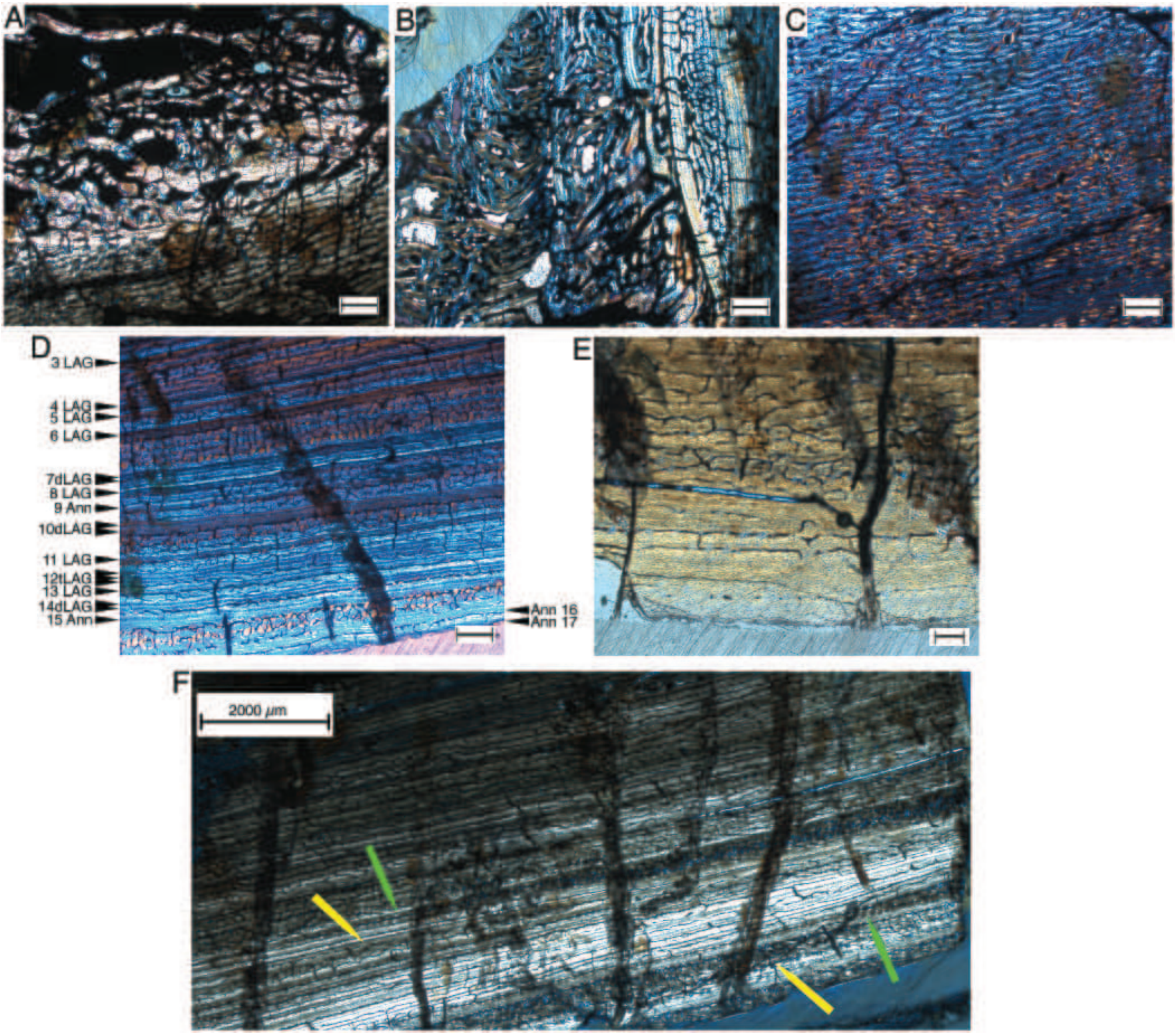

Figure 23. Component images of the posterolateral thin section of the right femur of *A. kyrgyzicus* under circumpolarized light and with a lambda filter. A, Transition from coarse cancellous bone tissue of the inner unit (top) to fibrolamellar tissue of the middle unit (bottom). B, Pathological bone tissue of up to three 'generations', direction towards the outer bone surface is to the right. C, Typical, well-vascularized fibrolamellar bone tissue with scattered secondary osteons of the middle unit, direction towards the outer bone surface is to the lower right. D, Zonal bone tissue of the outer unit with numerous growth marks (arrows). Individual growth marks were counted as one, if at least one row of vascular canals separates them from their neighbours. The count starts here with three, because the first clear growth marks are outside the top edge of the component image. Direction towards the outer bone surface is to the lower right. E, Component image of the posterior thin section (not figured) with a preserved outer edge of the bone wall. Note the distinct decrease of vascularization towards the outer edge (bottom) with at least three annuli, but the absence of a series of growth marks in quick succession without vascular canals in between as in a typical EFS. Direction towards the outer bone surface is to the bottom. F, Merging (yellow arrows) and widening (green arrows) of growth zones in the outer unit. Direction towards the outer bone surface is to the lower right. Abbreviations: Ann, Annulus; dLAG, double line of arrested growth; LAG, line of arrested growth; tLAG, triple line of arrested growth. Scale bars in A–E are 500 micrometres.

as from the lateral corner to the posterolateral wall, as the usual mode of variation between bone wall units (Hübner 2012). Secondary osteons were present, but scattered widely and almost never overlapped each other. The overall number of secondary osteons was higher in the lateral corner than in the posterolateral bone wall. The middle unit was almost azonal, without lines of arrested growth (LAG) or annuli. The first traceable growth mark represented the border to the outer unit, although weak zonation in terms of variability in vascular orientation was already present internal to it.

The outer unit, extending from the first clearly visible growth mark internally to the outer edge of the periosteally deposited bone wall (Fig. 22), also consisted mainly of fibrolamellar bone tissue. However, it was strongly separated into zones with laminar to reticular, well-developed primary osteons in the fast-growing zones. Parallel-fibred annuli and/or lines of arrested growth

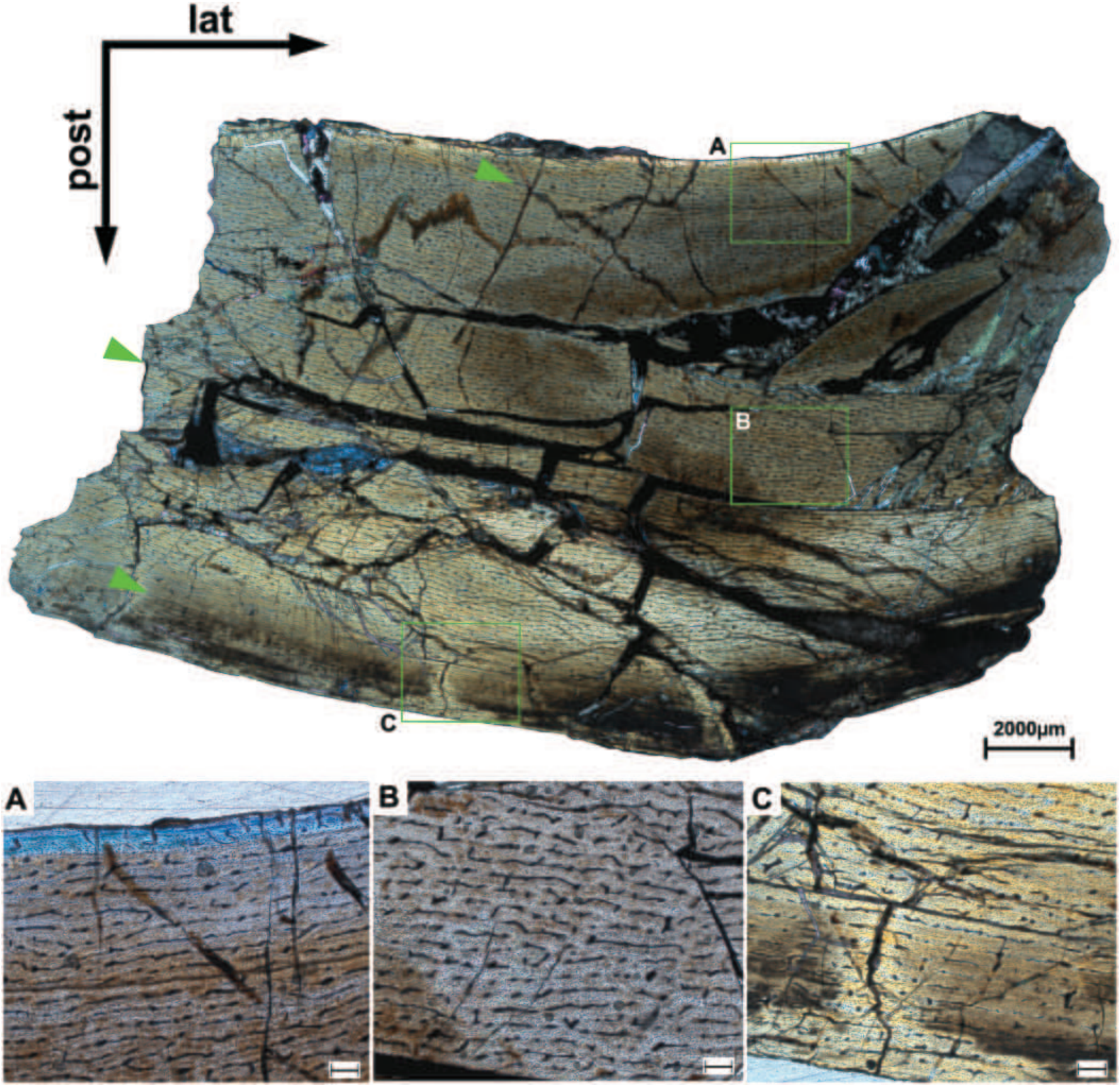

Figure 24. Overview of posterior section of right tibia IGB 2-48, under circumpolarized light and with a lambda filter. Frames indicate the location of the component images below. Growth marks are indicated by arrows. A, Inner part of the periosteal bone wall showing the well-developed (blue-coloured) band of ICL as well as a single LAG (lower third of image). Direction towards the outer bone surface is to the bottom. B, Details of the typical bone tissue within the periosteal bone wall. Direction towards the outer bone surface is to the bottom. C, Outer area of the periosteal bone wall with slightly more abundant longitudinal primary osteons and an annulus, marked by the dark crack in the middle of the image. Direction towards the outer bone surface is to the lower left. Abbreviations: lat, lateral, pos, posterior. Scale bars in A–C are 200 micrometres.

(LAGs) were present in between (Fig. 23D). The latter were rarely interrupted by vascular canals. Secondary osteons were isolated and scarce, but were more abundant in the lateral corner. None reached the periosteal surface, however. The innermost growth mark was mostly blackish and obscured posteriorly (Fig. 22) but could be followed towards the lateral corner, where it was developed as a double LAG. The spacing of the fast-growing zones was irregular, but there was a clear decrease in average thickness about halfway towards the surface posterolaterally (Fig. 23D). However, the growth zones became generally thinner from the posterolateral wall to the lateral corner and growth marks even merged together. The best account for growth marks was visible in the posterolateral bone wall. Depending on the area of the count, between 15 and 17 growth marks were present, developed as annuli and LAGs, in one case even a triple LAG (Fig. 23D). Where preserved, the outer edge of the bone wall lacked

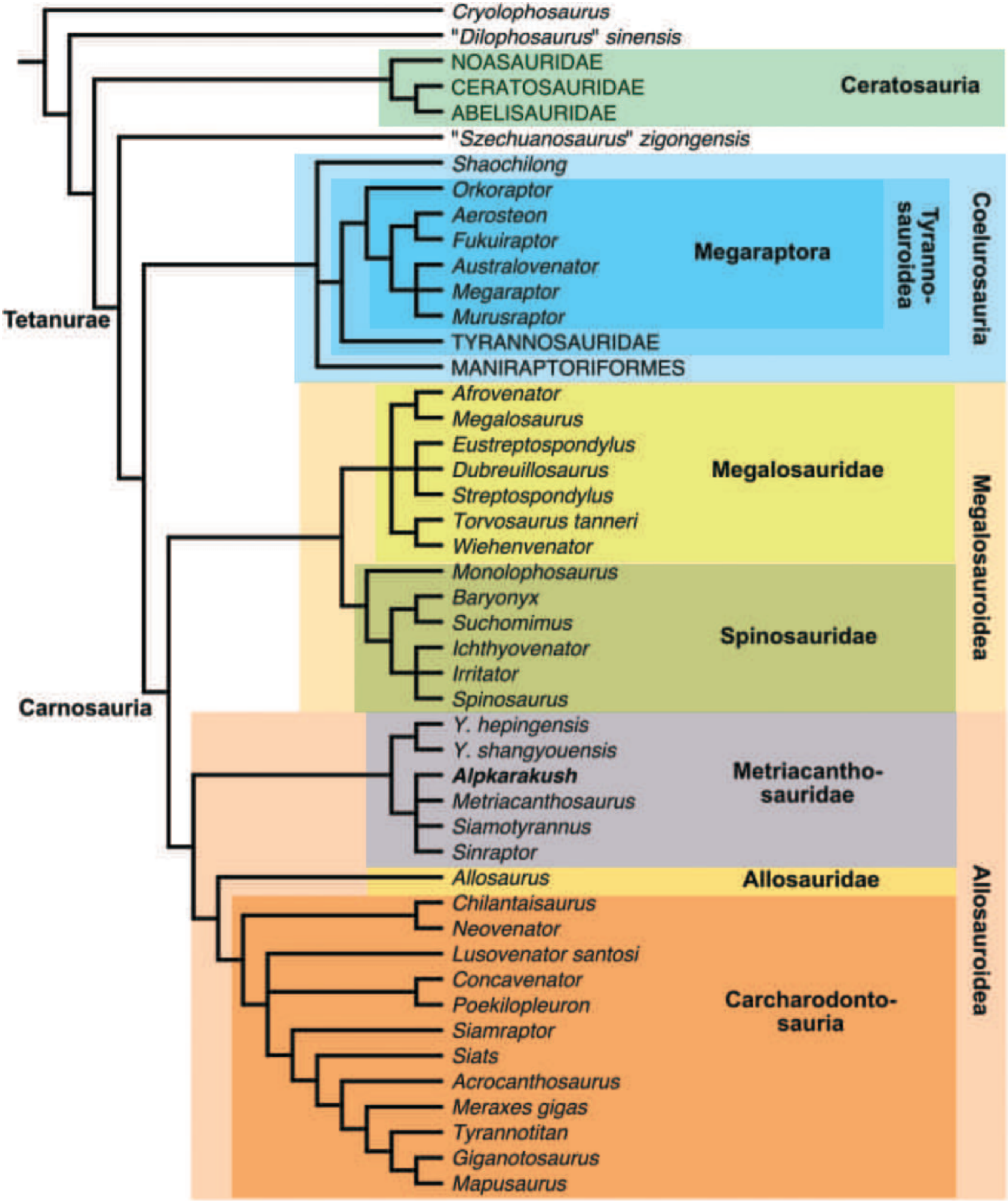

Figure 25. Phylogenetic position of *A. kyrgyzicus*. Simplified reduced consensus tree resulting from the equally weighted parsimony analysis. For full results see Supporting information, Fig. S2.

a typical External Fundamental System (EFS), but the vascularization was already very scarce with mostly longitudinal primary osteons in a laminar order arranged in between thicker, avascular, parallel-fibred tissue (Fig. 23E).

An unusual feature in the outer unit was the termination of two of the fast-growing zones at the transitional area between the posterolateral wall and the lateral corner, combined with a distinct increase in thickness of two other zones in the same area

(Fig. 23F). In addition, these fast-growing zones, together with at least a third zone, consist almost exclusively of woven-fibred tissue and contain unusually highly disorganized vascular canals with mainly reticular and sometimes even radial orientations (Fig. 23F). In the lateral and posterior sides of the bone wall, there was at least a single area with this fast-growing tissue present, respectively.

Tibia IGB 2-48: The bone wall in the sampled posterior area is *c.* 13.5 mm thick. There was no clear separation between the main histological units (Fig. 24) as in the femur of the holotype. Only a distinct band of ICL was present internally along the whole course of the sampled area (Fig. 24A). The ICL was penetrated occasionally by mostly radial simple vascular canals.

The periosteal bone wall consisted of fibrolamellar bone tissue with numerous, well-developed primary osteons and abundant osteocyte lacunae. The vascular pattern was mainly laminar to plexiform with local occurrences of reticular or even short radial canals (Fig. 24B). The spatial density of vascular canals decreased towards the outer periphery, whereas the percentage of longitudinal canals increased (Fig. 24C). Secondary osteons were completely absent.

Three growth marks were present, widely spaced from each other (Fig. 24). The innermost growth mark was a LAG, which was partially resorbed by the expanding medullary cavity, and the middle and outer growth marks were developed as annuli. There was no EFS developed at the outer edge (Fig. 24C).

Phylogenetic position of *Alpkarakush*

The phylogenetic analysis using equal weights resulted in the recovery of 12 154 equally parsimonious trees with a length of 4792 steps. The strict consensus tree of these trees (Supporting information, Fig. S1) shows a reasonably good resolution, but with a major polytomy at the base of Tetanurae, in which most basal tetanuran taxa were unresolved. Reduced consensus methods removed numerous taxa at the base of Tetanurae, and the following description was based on the reduced consensus tree. As our matrix was mainly designed to resolve the phylogenetic position of *Alpkarakush* within basal tetanurans, we will focus on this part of the tree; unexpected results, e.g. in the Coelurosauria, might at least partially be caused by incomplete taxon and/or character sampling for this part of the tree.

The results of our analysis (Supporting information, Fig. S2; Fig. 25) mainly conformed to other recent phylogenetic analyses of theropod dinosaurs, with a monophyletic clade Coelophysoidea at the base of Neotheropoda, followed by monophyletic Ceratosauria and Tetanurae. *Cryolophosaurus* and '*Dilophosaurus*' *sinensis* (considered to be a junior synonym of *Sinosaurus triassicus* by some authors; see Xing *et al.* 2014, Zhang *et al.* 2023), which were sometimes regarded as early Tetanurans (e.g. Carrano *et al.* 2012) or, in the case of '*D*'. *sinensis*, early ceratosaurs (Wang *et al.* 2017), were here found to be outside Averostra, as subsequent sister taxa to this clade. Within Tetanurae, the poorly known '*Szechuanosaurus*' *zigongensis* is found as the earliest branching taxon, followed by a dichotomy of two major clades, the Coelurosauria and Carnosauria (*sensu* Rauhut and Pol 2019), the latter including Megalosauroidea and Allosauroidea. This result thus resembles that found by Rauhut (2003), Cau (2018), and Rauhut and Pol (2019), whereas many recent phylogenetic analyses found the Megalosauroidea to be sister taxon of a clade uniting Allosauroidea and Coelurosauria, in a clade termed Neotetanurae or Avetheropoda (see e.g. Carrano *et al.* 2012, Rauhut *et al.* 2016, Dai *et al.* 2020), and Wang *et al.* (2017) even found the Allosauroidea of the above analyses to be paraphyletic, with the Metriacanthosauridae forming the sister taxon to an Allosauria-Coelurosauria clade. Within Carnosauria, the taxa usually grouped in the Piatnitzkysauridae (*Marshosaurus*, *Piatnitzkysaurus*, *Condorraptor*, and, sometimes, *Xuanhanosaurus*) were all removed by reduced consensus methods, as was the supposed early allosauroid *Asfaltovenator*. The remaining carnosaurs were thus placed either in the Megalosauroidea or the Allosauroidea, which form sister taxa. The taxonomic composition of the two clades largely conformed to that found in other recent analysis, with a few notable exceptions. *Monolophosaurus*, which has been recovered in varying positions within basal tetanurans in recent years, was placed in the Megalosauroidea. In respect to Allosauroidea, the megaraptorans, which were found to be derived allosauroids within the Neovenatoridae by Benson *et al.* (2010) and several subsequent analyses (e.g. Carrano *et al.* 2012, Zanno and Makovicky 2013, Malafaia *et al.* 2020) were placed as an early branching clade within Tyrannosauroidea, as argued by Novas *et al.* (2013) and subsequent authors. Likewise, *Shaochilong*, regarded as a carcharodontosaurid in recent years (Brusatte *et al.* 2009, 2010, Carrano *et al.* 2012), was found to be a coelurosaur, as in some previous analyses (e.g. Rauhut 2003). Furthermore, the poorly known Middle Jurassic French taxon *Poekilopleuron* was found to be an early carcharodontosaurid, rather than a megalosaurid, as is the case in most recent analyses.

Within megalosauroids, two subclades were recovered, the Spinosauridae and the Megalosauridae. *Monolophosaurus* was found as the earliest branching spinosaurid, as in the equal weights analysis of Schade *et al.* (2023). The remaining spinosaurids were subdivided into the Baryonichinae (*Baryonyx*, *Suchomimus*), and the Spinosaurinae (with a polytomy between *Irritator*, *Ichthyovenator* and *Spinosaurus*). Within megalosaurids, a polytomy was recovered between a *Wiehenvenator-Torvosaurus* clade, a *Megalosaurus-Afrovenator* clade, and a clade that recovered *Dubreuillosaurus*, *Eustreptospondylus*, and *Streptospondylus* in a polytomy. Allosauroidea were subdivided into Metriacanthosauridae and Allosauria, with the latter including *Allosaurus*, the Neovenatoridae (including *Neovenator* and *Chilantaisaurus*), and the Carcharodontosauridae.

Alpkarakush was found to be a metriacanthosaurid. In general, metriacanthosaurid interrelationships were poorly resolved, with only two distinct subclades within this clade, one consisting of the two species of the genus *Yangchuanosaurus*, and the other, conforming to the subfamily Metriacanthosaurinae, of a polytomy including *Sinraptor*, *Metriacanthosaurus*, *Siamotyrannus*, and *Alpkarakush*. The other taxon found within Metriacanthosauridae, *Shidaisaurus*, could attain various positions in relation to these clades and their subtaxa. *Shidaisaurus* was either found as an early branching metriacanthosaurid, outside the *Yangchuanosaurus*-Metriacanthosaurinae clade, as sister taxon to the *Sinraptor*/*Metriacanthosaurus*/*Siamotyrannus*/*Alpkarakush* clade, or as sister taxon to *Metriacanthosaurus*.

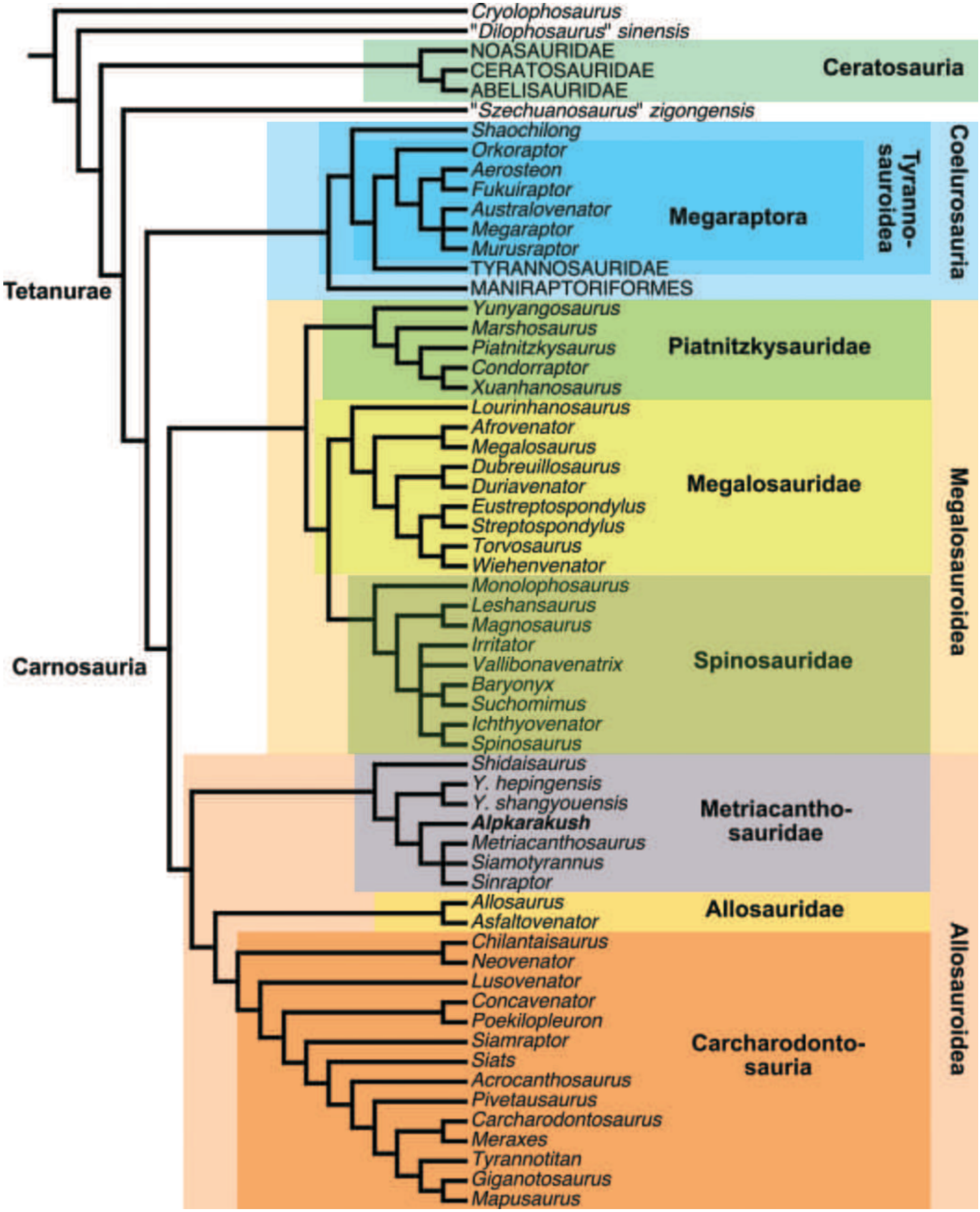

Figure 26. Phylogenetic position of *A. kyrgyzicus*. Simplified strict consensus tree resulting from the implied weighing parsimony analysis with k = 12. For full results see Supporting information, Fig. S3.

The analyses using implied weights found few most parsimonious trees, with scores of 208.21175 (k = 12; 3 Most Parsimonious Trees [MPT]), 251.68722 (k = 9; 1 MPT), 319.46481 (k = 6; 5 MPT), and 443.57498 (k = 3; 30 MPT). The strict consensus tree resulting from the analysis with k = 12 (Supporting information, Fig. S3; Fig. 26) was in general agreement with the reduced consensus tree of the equally weighted analysis, but showed considerably better resolution. At higher weighing strengths, changes in topology were mainly found within Megalosauroidea, but also between some metriacanthosaurids and a few other taxa (Supporting information, Figs S4–S6). The most severe reordering of taxa was found at k = 3, in which the Megalosauridae were found as the earliest branching tetanurans, followed by metriacanthosaurids and Allosauria, whereas the Spinosauridae were recovered as the earliest branching coelurosaurs (Supporting information, Fig. S6). Most of these changes seem to reflect the fragmentary nature of the unstable taxa, for which changing weights in a single character might then have severe consequences for their phylogenetic position. This might especially be the reason for the unstable relationships within Megalosauroidea; of the 23 taxa included in this clade in the k = 12 analysis, only two have more than 50% coded characters (*Eustreptospondylus*: 55%; *Monolophosaurus*: 51%), whereas for six taxa (*Duriavenator*, *Magnosaurus*, *Streptospondylus*, *Torvosaurus guerneyi*, *Xuanhanosaurus*, *Yungyangosaurus*) only 10% or less of the characters could be coded. Within metriacanthosaurids, it was mainly the very fragmentary *Metriacanthosaurus* (6.5% coded characters) that changed position (being found as sister taxon to *Shidaisaurus* at the base of the clade in weighing concavities below 10), although *Alpkarakush* (25% coded characters) also changed position and was found to be sister taxon of *Siamotyrannus* (6.8% coded characters) in these analyses. However, as the implied weighing analysis with k = 12 was closest to the equally weighted analysis, just with improved resolution, and Goloboff *et al.* (2018) found the weighted analysis to perform best at this concavity (see also Ezcurra 2024), our following tree description and discussion is based on the strict consensus tree of the three MPTs resulting from this analysis. At least in respect to metriacanthosaurids, this tree was also the most consistent with the stratigraphic occurrences of the taxa.

The consensus tree from the implied weighing analysis with k = 12 was very well resolved, with just two polytomies in carnosaurs, one between *Irritator*, *Vallibonavenatrix*, the Baryonychinae, and a subclade containing *Spinosaurus* and *Ichthyovenator*, and one in metriacanthosaurids between *Sinraptor*, *Siamotyrannus*, and *Metriacanthosaurus*. Furthermore, there was an additional three-taxa polytomy outside Carnosauria, within megaraptorans. Apart from the better resolution, the results were almost identical to those found in the unweighted analysis, so this tree is used to discuss character distribution and possible evolutionary implications.

Within Carnosauria, the implied weighting analysis found a basal dichotomy into Megalosauroidea and Allosauroidea. Within the former clade, a monophyletic Piatnitzkysauridae formed the earliest branching subclade; this clade included the genera *Yungyangosaurus*, *Marshosaurus*, *Piatnitzkysaurus*, *Xuanhanosaurus*, and *Condorraptor*. The other megalosauroids were placed in either the Spinosauridae or the Megalosauridae. Megalosauridae included the genera *Lourinhanosaurus*, *Megalosaurus*, *Afrovenator*, *Duriavenator*, *Dubreuillosaurus*, *Wiehenvenator*, *Torvosaurus*, *Streptospondylus*, and *Eustreptospondylus*, whereas *Monolophosaurus* and a clade including the poorly known *Magnosaurus* and *Leshansaurus* were found as an early branching Spinosauridae, rather than in Megalosauridae. As in the unweighted analysis, Allosauroidea was subdivided into Metriacanthosauridae and Allosauria. *Asfaltovenator* was here found as an allosaurid, sister taxon to *Allosaurus*, but otherwise the taxonomic composition and phylogenetic relationships within Allosauria correspond to those found in the unweighted analysis. Within metriacanthosaurids, the implied weighting analysis recovered the Chinese *Shidaisaurus* as the earliest branching taxon, followed by the genus *Yangchuanosaurus* with its two species. *Alpkarakush* was confirmed as a metriacanthosaurid and represented the sister taxon to a clade uniting the remaining metriacanthosaurids *Sinraptor*, *Siamotyrannus*, and *Metriacanthosaurus*.

Characters that support the inclusion of *Alpkarakush* in the Metriacanthosauridae include the following: posterior margin of the infratemporal fenestra straight or only slightly convex (judged from the morphology of the quadratojugal and the facet for the contact with the squamosal on this bone; unknown in *Shidaisaurus*); mesial carina of lateral teeth extended to base of crown (unknown in *Shidaisaurus*); flexor tubercle in manual unguals reduced and less than one-third of the height of the articular facet (apart from *Alpkarakush* only known in *Sinraptor* within metriacanthosaurids; also present in *Asfaltovenator*); medial brevis shelf poorly developed and not visible in lateral view; angle between proximal part of ischial shaft and pubic peduncle of ischium less than 110°; presence of a posterior midline crest on the articulated ischia; presence of a strongly expanded ischial boot; presence of an oval fossa on the base of the ascending process of the astragalus; pedal ungual II asymmetrical (shared with *Sinraptor*, unknown in other metriacanthosaurids).

Within Metriacanthosauridae, *Alpkarakush* furthermore shows the following synapomorphies with other taxa or subclades of this clade, which were absent in other members: ventral prong of the quadratojugal ends anterior to or level with the posterior rim of the infratemporal fenestra (shared with *Sinraptor* and unknown in *Siamotyrannus* and *Metriacanthosaurus*, whereas the prong extended further posteriorly in *Yangchuanosaurus*; although the jugal was not preserved, the length of its ventral posterior prong can be estimated from the articular facet on the quadratojugal); posterior process of the postorbital broader mediolaterally than high dorsoventrally (shared with *Sinraptor* and unknown in *Siamotyrannus* and *Metriacanthosaurus*; also present in derived carcharodontosaurids); transverse dimensions of mid-sacral vertebrae reduced in relation to first and last sacral (shared with all metriacanthosaurids more derived than *Shidaisaurus*); lateral groove present on pubic boot (present in *Sinraptor* and *Siamotyrannus*); fibular crest on tibia bulbous (shared with *Sinraptor* and *Metriacanthosaurus*).

Biogeographic analysis

As outlined in the Material and methods, the biogeographic analysis was carried out on the basis of the trees resulting from the

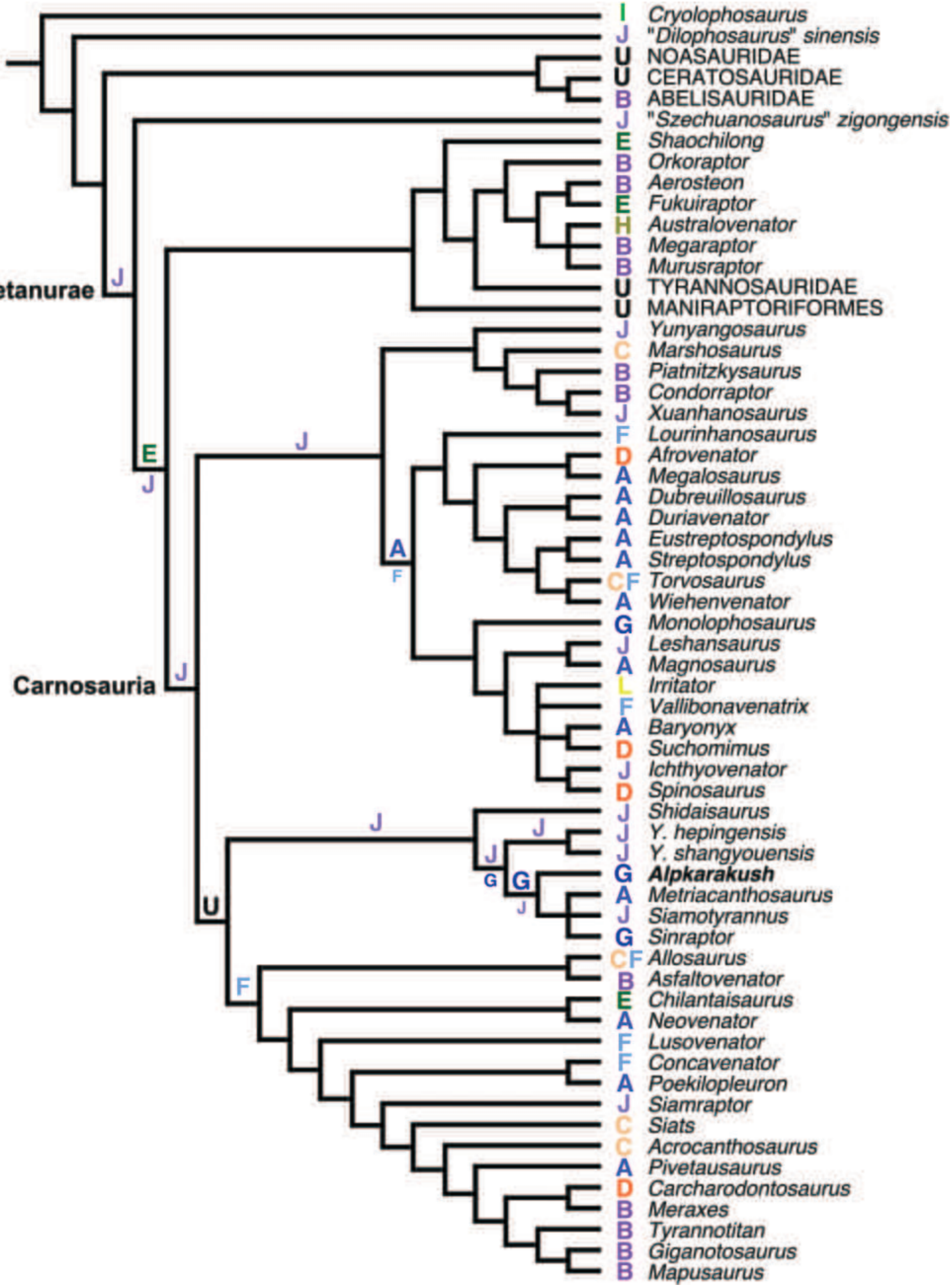

Figure 27. Biogeographic reconstructions for selected clades, resulting from the S-DIVA analysis. Legend: A, north-eastern Europe; B, southern South America; C, North America; D, northern Africa; E, north-eastern Asia; F, south-western Europe; G, Central Asia; H, Australia; I, Antarctica; J, South-East Asia; L, Central South America. For further details on these regions see the Material and methods section. For full results of the S-DIVA analysis see Fig. S7 in the Supporting information.

phylogenetic analysis using implied weights with a k = 12. Since our focus lies on the phylogenetic position and biogeographic implications for *Alpkarakush*, we restrict the presentation of the biogeographic results to the Carnosauria. For a full documentation of the results of the S-DIVA analysis see the Supporting information.

The S-DIVA analysis (Fig. 27) identified South-East Asia as the ancestral territory of Tetanurae, and eastern Asia in general (50% North-East Asia, 50% South-East Asia) as the original area for Avetheropoda (the clade including Coelurosauria and Carnosauria). Likewise, a South-East Asian origin for Carnosauria was also indicated. Within Carnosauria, the area of origin of megalosauroids was problematic, as all three included clades (Piatnitzkysauridae, Spinosauridae, and Megalosauridae) have wide distributions, with megalosaurids being especially diverse in the Middle and Late Jurassic of Europe (see also Rauhut *et al.* 2016, 2018, 2020), and consequently, Europe was identified as area of origin of this clade. However, given that the South-East Asian *Yunyangosaurus* was found as the earliest branching piatnitzkysaurid, and the central Asian *Monolophosaurus* as the earliest branching spinosaurid, an Asian origin of the Megalosauroidea in general, followed by a rapid dispersal over much of Pangaea, seems likely. The area of origin of Allosauroidea was identified as 50% South-East Asia and 50% south-west Europe; given that very little is known about Central Asian theropods, an origin somewhere between eastern Asia and Europe seems likely. For metriacanthosaurids, the area of origin was clearly identified as South-East Asia, followed by a dispersal into central Asia.

DISCUSSION

Age assessment and histology of the holotype and paratype of *A. kyrgyzicus*

The general bone histology of the holotype femur of *A. kyrgyzicus*, with highly vascularized fibrolamellar bone tissue, is similar to other large theropods, such as *Allosaurus* (e. g. Bybee *et al.* 2006), *Acrocanthosaurus* (D'Emic *et al.* 2012), or *Tyrannosaurus* (e.g. Horner and Padian 2004). The minimum age at the time of death can be estimated with 17 years. However, possible resorption of additional growth marks by the expanding medullary cavity during growth, the weak zonation in the middle unit of the femoral bone wall, and the slightly higher counts of growth marks in other areas of the posterolateral bone wall strongly indicate an older age. For the assessment of skeletal maturity, two lines of evidence indicate that the *A. kyrgyzicus* holotype was an almost fully grown, large subadult individual. On the one hand, there was a strong zonation present, with subsequentially thinner fast-growing zones in between distinct annuli and LAGs in the outer unit of the bone wall (Fig. 15D), which terminate at the outer edge of the femur with a zone of generally scarce vascularization in combination with thicker bands of parallel-fibred tissue. On the other hand, there was no distinct EFS present (Fig. 15E), indicating that the individual was still slowly growing at the time of death.

The histology of the tibia of the smaller individual revealed a much younger age than the holotype. This was indicated by the absence of secondary remodelling, only three preserved growth marks with wide distances between them (Fig. 16), and the comparatively high vascularization at the periphery of the bone wall (Fig. 17C). That tibia thus belonged to a large juvenile or a small subadult.

The unusual tissue of the inner unit in the holotype femur of *A. kyrgyzicus* could be interpreted as medullary bone (MB) tissue. However, several recent studies have revealed that a clear separation between MB and pathological bone (PB) tissue is currently not unambiguously possible, especially when only single elements of a skeleton and/or only parts of the cross section could be sampled (e. g. O'Connor *et al.* 2018, Canoville *et al.* 2020). In contrast, some observed characters might indicate that this tissue is of pathological origin. The first character is the combination of this endosteal tissue with highly disorganized tissue in up to three fast-growing zones in the outer unit. This combination of inner and outer pathological tissue was found in several dinosaur specimens (see e.g. Chinsamy and Tumarkian-Deratzian 2009, Hedrick *et al.* 2016) although the here described specimen shows only moderate development of this tissue in the external bone unit, which is also incorporated into the periosteal bone wall. Thus, the individual has not died from these events. Moreover, the presence of up to three bands of lamellar tissue within the inner unit, matching with the number of the unusually fast-growing zones externally indicates more than one event of possible trauma or infection affecting the femur in life, which also does not fit the fast development and subsequent fast resorption of MB tissue (e. g. Canoville *et al.* 2020).

Considerations on the association of two individuals of *Alpkarakush*

As mentioned above, the only larger vertebrate remains found at locality FTU-1 that clearly cannot be referred to the type individual of *A. kyrgyzicus* are fragmentary remains of a smaller theropod. These remains include an almost complete right tibia, most parts of both pubes that were articulated distally, and a fragment of the proximal shaft of the right ischium. These remains were found in the same layer and in close association with the remains of the larger individual; the pubes of the small individual were appressed to the shaft of the femur of the type of *Alpkarakush*, and field photographs show that the tibiae of the large and the small individual were also found in direct association within the same layer. In comparison with the type of *Alpkarakush*, the sizes of the preserved elements of the smaller specimen were consistent with these bones representing a single individual. Most notably, *Alpkarakush* seems to have a remarkably short tibia, which is only about 81% of the length of the femur, whereas this ratio is about 88% in *Sinraptor* (Currie and Zhao 1993), 89% in *Yangchuanosaurus shangyuensis* (Dong *et al.* 1983), and approximately 87% even in the gigantic carcharodontosaurid *Meraxes* (Canale *et al.* 2022). This is also reflected in the length of the tibia as compared to the pubis, the only two elements present in both holotype and paratype. The ratio between pubis and tibia length is about 1 in *Allosaurus* (Gilmore 1920) and *Meraxes* (Canale *et al.* 2022), and approximately 0.9 in *Sinraptor* (Currie and Zhao 1993). However, the more complete right pubis of the holotype is, as preserved, already longer (73 cm) than the tibia of this individual (72 cm), and if an estimated 15–20 cm is missing in the former bone (as mentioned in the description), the pubis/tibia ratio of this animal would be between 1.22 and 1.29. This ratio is 1.22 in the paratype specimen, and thus fits with the unusual proportions of the holotype. It might be worth noting that the pubis also seems to be longer than the tibia in *Yangchuanosaurus shangyuensis*, but, based on measurements from the photographs in Dong *et al.* (1983), the ratio between these bones seems to be around 1.13 in this animal, and therefore still considerably lower than in *Alpkarakush*. A similar pubis/tibia ratio as in *Alpkarakush* has only been described in *Ceratosaurus*, in which this ratio is 1.21 (Gilmore 1920). Thus, the unusually high pubis/tibia ratio might be another diagnostic feature of *A. kyrgyzicus* and a strong argument for considering both individuals from locality FTU-1 as representing the same taxon.

Apart from these proportions, anatomical comparisons also support a referral to the same taxon. The second theropod individual is approximately 15–20% smaller than the large individual (based on the length of the tibia), but the tibia is considerably less robust. However, the overlapping morphology of preserved elements of the small individual correspond well with that of the larger individual. The proximal end of the pubes is identical in the development of the pubic tubercle and in general shape, as were the shafts of these elements. Distally, the pubes of the small individual were more complete than the better-preserved right element of the holotype; here the elements agree in the distally open pubic apron, which ends above the distal expansion towards the pubic boot, and the unusual longitudinal groove on the posterolateral side of the distal pubic shafts seen in the small individual is indicated by a concavity in this area towards the distal break in the pubis of the holotype individual. In the ischium, the beginning of a posterior midline crest is preserved in the ischium of the small individual, a metriacanthosaurid synapomorphy that is also present in the large individual. The tibia of the smaller theropod shows the same semioval and bulbous fibular crest as the tibiae of the type, and also the stout ridge connecting this crest with the proximal end. Furthermore, both the morphologies of the proximal articular end and the distal malleoli were very similar. Thus, although none of the autapomorphic characters of the holotype individual are preserved in the small individual, the character combination is consistent with the morphology of the former, including unusual characters that were rarely found in theropods, such as the groove on the distal pubis or the bulbous fibular crest. Thus, there can be little doubt that the two specimens represent the same taxon.

The single anatomical difference between the tibiae of the holotype and the smaller individual is the less laterally expanded ridge for the bracing to the ascending process of the astragalus on the anterior side of the distal end, which can thus be related to ontogenetic variation. This indicates that the ascending process of the astragalus was relatively broader in the juvenile than in the adult and extended over more of the width of the astragalar body. An ascending process that extends over the entire breadth of the astragalar body was found as a coelurosaurian synapomorphy (Rauhut 2003), so this condition in a juvenile non-coelurosaur might indicate heterochronic processes in the evolution of the coelurosaurian tarsus, as it has been proposed for other parts of the skeleton (e.g. Rauhut *et al.* 2012). More detailed osteological comparisons of ontogenetic changes in basal tetanurans for which both juvenile and adult material is known (e.g. *Allosaurus*; see Bybee *et al.* 2006) would be needed to confirm such ontogenetic trends.

Given the histological results, it thus seems most likely that the locality FTU-1 preserves an association of a large subadult and a considerably younger juvenile specimen of the same species. As noted above, the material comes from fine grained sediments arranged in various fining upwards cycles, which we interpret as distal floodplain deposits, and apart from the two theropod specimens, only isolated elements of very small vertebrates were found, including lungfish teeth and remains of turtle shells. The close association of the two individuals and general taphonomy of the site thus indicate that the animals probably died and were deposited contemporaneously. Given the depositional setting, alternative hypotheses, such as a chance association by water currents or an animal that suddenly died while scavenging on the other individual, seem to be less likely. This might indicate a juvenile accompanied by a large subadult (a sexually mature individual with an estimated mass of *c.* 1250 kg, following the equation provided by Campione *et al.* 2014), possibly one of the parents. In summary, this association suggests that juveniles of *Alpkarakush* travelled together with adults to at least an early subadult stage. Gregarious behaviour, including an association of juveniles and adults, has been suggested for a number of theropods, both on the basis of trackway evidence (e.g. Barco *et al.* 2006, Lockley *et al.* 2015, Heredia *et al.* 2020) as well as skeletal associations (e.g. Currie 2000, Coria and Currie 2006, Currie and Eberth 2010).

Metriacanthosaurid distribution and evolution

The identification of the first large-bodied predatory dinosaur from the Jurassic of Central Asia west of China as a metriacanthosaurid underlines the ecological importance that these animals seem to have had in Middle to Late Jurassic dinosaur faunas of Asia. According to our phylogenetic results, the currently oldest known and also earliest branching metriacanthosaurid is *Shidaisaurus jinae* from the Bajocian Chuanjie Formation of southern China (Wu *et al.* 2009). *Alpkarakush* represents the second oldest known representative of the clade, whereas the Chinese *Yangchuanosaurus* and *Sinraptor* as well as the British *Metriacanthosaurus* were Late Jurassic in age, and the youngest known metriacanthosaurid is *Siamotyrannus* from the Barremian Sao Khua Formation of Thailand. The occurrence of metriacanthosaurids in both southern China and Kyrgyzstan already in the Middle Jurassic again underlines the very rapid diversification of tetanurans during this time (see Rauhut *et al.* 2016, Rauhut and Pol 2019). The biogeographic analysis indicates a largely South-East Asian early evolution of tetanurans, and metriacanthosaurids seem to have originated in this area in the latest early to early Middle Jurassic and then dispersed westwards from there during the course of the Middle Jurassic to reach Europe in the Late Jurassic. Although rare megalosauroids were also present in the Middle and Late Jurassic of Asia (*Monolophosaurus* from the Callovian Wucaiwan Formation of Xinjiang, western China, *Yanyungosaurus* from the Middle Jurassic of the Xintiangou Formation of south-eastern China, and *Leshansaurus* from the Late Jurassic of Sichuan, China), the majority of large-bodied theropodan apex predators in dinosaur faunas of that age in this continent seem to be metriacanthosaurids. Interestingly, in the Late Jurassic of Europe, the only large-bodied theropod taxon from north-eastern Europe (outside the Iberian Peninsula) is *Metriacanthosaurus*, although isolated remains of large probable megalosaurids were also present (Carrano *et al.* 2012, Rauhut *et al.* 2018). Metriacanthosaurids were so far completely unknown from the rather well-sampled faunas of the Late Jurassic of south-western Europe (Iberian Peninsula, especially Portugal) and also from the Morrison Formation of the western USA, where the large predatory dinosaur niche is occupied by allosaurids and, in apparently considerably lower numbers, large megalosaurids and ceratosaurs (Foster 2003, Mateus *et al.* 2006, Rauhut *et al.* 2018). Allosaurids have so far not been reported from either north-eastern Europe or Asia. This might indicate a possible barrier for the exchange of apex predators (geographical or ecological) between northern and south-western Europe at that time. Of course, the absence of metriacanthosaurids in south-western Europe and North America, as well as the absence of allosaurids in Asia might also simply be due to sampling failure. However, the Morrison Formation is certainly the best sampled Late Jurassic terrestrial unit globally (see Foster 2020), and the Lusitanian Basin of Portugal has yielded by far the most diverse dinosaur fauna from the Late Jurassic of Europe (see Mocho *et al.* 2019, Malafaia *et al.* 2020, Rotatori *et al.* 2022, and references therein), so this explanation seems rather unlikely for at least these two units.

The joint occurrence of early carcharodontosaurids in the Late Jurassic of south-western Europe (Malafaia *et al.* 2020) and eastern Africa (Rauhut 2011) as well as the occurrence of the probable piatnitzkysaurid *Marshosaurus* in the Late Jurassic of North America (see Carrano *et al.* 2012) might further even indicate that western Laurasian large theropod faunas might have been more similar to Gondwanan faunas than to their Asian counterparts. An argument against this interpretation might be the placement of *Xuanhanosaurus* from the Oxfordian of China in the Piatnitzkysauridae in our implied weights analysis (see also Rauhut *et al.* 2016). However, *Xuanhanosaurus* is only known from fragmentary remains, including a few anterior dorsal vertebrae and an almost complete forelimb (Dong 1984, see also Rauhut 2003, Carrano *et al.* 2012), which severely limits comparisons with other early tetanurans, in which forelimbs and especially mani were rarely found. This is especially true for metriacanthosaurids, for which so far only a few manual elements were known in *Sinraptor* (Currie and Zhao 1993). The marked similarities between manual phalanx II-1 in *Xuanhanosaurus* and *Alpkarakush* might lend support to a metriacanthosaurid identification of the former, as it was also found in at least some trees in our unweighted analysis. More forelimb material of metriacanthosaurids and a more detailed analysis of *Xuanhanosaurus* would be needed to solve this issue.

Another argument against a western Laurasian–Gondwanan faunal connection might be the distribution of smaller, coelurosaurian theropods, which were, in the Late Jurassic, diverse in Laurasia (see Ding *et al.* 2020), but seem to be at least extremely rare in Gondwana during that time (Rauhut and Pol 2021, 2022). This distribution might at least partially be a sampling artifact, as the Late Jurassic theropod fossil record from Gondwana is still abysmal (see Rauhut and Pol 2021). However, any biogeographic scenario should be seen as tentative, especially since many of the clades in question probably already originated in the Middle or even the late Early Jurassic.

Our phylogenetic analysis differs from other recent phylogenies of basal tetanurans (e.g. Carrano *et al.* 2012, Rauhut *et al.* 2016, Dai *et al.* 2020) in respect to the phylogenetic position of '*Szechuanosaurus*' *zigongensis*, which was found to be placed inside the metriacanthosaurid genus *Yangchuanosaurus* in these analyses. In contrast, this taxon was recovered as the earliest branching taxon within Tetanurae in our analysis, as in Rauhut (2003). Unfortunately, '*Szechuanosaurus*' *zigongensis* has so far only received a preliminary description, which probably accounts for this phylogenetic uncertainty. This taxon comes from the probably Oxfordian Lower Shaximiao Formation (see introduction) and its identification as a metriacanthosaurid would thus further increase the diversity and abundance of this clade in the Late Jurassic of Asia. In order to account for this possibility, we ran a second phylogenetic and biogeographic analysis with '*S*.' *zigongensis* being constrained to the Metriacanthosauridae. The results were in general agreement with our analysis with only a few notable exceptions. Thus, relationships between megalosauroids are somewhat shaken up, with the poorly known Chinese theropod *Yunyangosaurus* from the Middle Jurassic of south-eastern China (Dai *et al.* 2020), which is recovered as the earliest branching piatnitzkysaurid in our unconstrained analysis, being placed within megalosaurids and several other fragmentary known taxa changing position within Megalosauria. However, relationships within Allosauroidea remain stable, with the only difference that, due to the constraint, '*Szechuanosaurus*' *zigongensis* is placed within Metriacanthosauridae, as the earliest branching member within this clade. In respect to biogeography, the origin of Tetanurae is still reconstructed for eastern Asia (though without specification if south- or north-eastern Asia), and the area of origin for metriacanthosaurids is identified as South-East Asia. Thus, the interpretation that metriacanthosaurids originated in this area and spread from there remains robust also under these constrains.

CONCLUSIONS

A partial skeleton of a large (*c.* 7–8 m body length) theropod dinosaur from the late Middle Jurassic Balabansai Formation of Kyrgyzstan represents the first diagnosable theropod taxon from the Jurassic of Central Asia west of China, and is here described as a new taxon, *Alpkarakush kyrgyzicus*. Phylogenetic analysis places the new taxon in the Metriacanthosauridae, further underlining the diversity and wide distribution of this clade in the Jurassic of Asia. *Alpkarakush* seems to have been generally similar to the western Chinese metriacanthosaurid *Sinraptor*, with the presence of a pronounced postorbital supraorbital rugosity and relatively elongated distal hindlimbs if compared to other allosauroids (length of metatarsal II is approximately 45% of femoral length in *Alpkarakush*, similar to the almost 47% in *Sinraptor*, whereas this ratio is 38.5% in *Allosaurus* and the carcharodontosaurid *Meraxes*; Gilmore 1920, Currie and Zhao 1993, Canale *et al.* 2022). Metriacanthosaurids apparently originated in South-East Asia in the latest early or early Middle Jurassic, and rapidly became the dominant clade of theropodan apex predators in many ecosystems in this continent in the

Jurassic. In order to better understand Jurassic theropod diversity and evolution, more finds from areas between Central Europe and western China, especially from Central Asia are needed.

SUPPORTING INFORMATION

Supplementary data is available at *Zoological Journal of the Linnean Society* online.

ACKNOWLEDGEMENTS

We thank Alexander Averianov and Thomas Martin for discussions, and Zhanyl Durovna Namazbekova, Natalia Viktrovna Proshina, Maria Vasilevna Volkovskaia, Bakytbek Zhenaliev, Zhypargul Anarbaeva, Kurmanbek Sulaiman, Alexander Cherenkov, and Ishen Bektenov for help during fieldwork and preparation of materials. We are very thankful to Pia Kain (Friedenstein Stiftung Gotha), who made the casts of the bone pieces sampled for the histological analysis and for her training and strong support during the processing of the thin sections. We also thank Aurore Canoville (same institution) for very helpful discussions regarding the pathological nature of the inner tissue in the holotype femur. Thoughtful comments by Fernando Novas and an anonymous reviewer greatly helped to improve the manuscript. This work was supported by the Deutsche Forschungsgemeinschaft (DFG) under grant HU 2096/4-1/RA 1012/32-1/WI 2133/6-1 (to T.R.H., O.W., and O.W.M.R.), INTAS Young Scientist Fellowship 04-83-3029 and a Paleontological Society Sepkoski Grant (to A.A.B.), and the National Academy of Sciences of the Kyrgyz Republic, which is gratefully acknowledged.

DATA AVAILABILITY

All the data underlying this article are available in the article and its online supplementary materials. In addition, 3D models of important elements of the new taxon are deposited on Morphosource (www.morphosource.com).

REFERENCES

Aliev MM, Genkina RZ, Dubrovskaya EN *et al.* *[Jurassic Continental Deposits of Western Central Asia (Dating, Partition, Correlation)].* Moscow: Nauka, 1981. [in Russian]

Alifanov VR, Averianov AO. *Ferganasaurus verzilini* gen. et sp. nov., a new neosauropod (Dinosauria, Saurischia, Sauropoda) from the Middle Jurassic of Fergana Valley, Kirghizia. *Journal of Vertebrate Paleontology* 2003;**23**:358–72. https://doi.org/10.1671/0272-4634(2003)023[0358:fvgesn]2.0.co;2

Averianov AO. *Sunosuchus* sp. (Crocodylomorpha, Goniopholididae) from the Middle Jurassic of Kirghisia. *Journal of Vertebrate Paleontology* 2000;**20**:776–9.

Averianov AO, Bakirov AA. [Results and perspectives of the study of dinosaur assemblages in Kyrgyzstan]. *Izvestiya Natsional'noi Akademii Nauk Kyrgyzskoi Respubliki* 2000;**2**:22–4. [in Russian]

Averianov AO, Krasnolutskii SA. Stegosaur remains from the Middle Jurassic of West Siberia. *Proceedings of the Zoological Institute RAS* 2009;**313**:153–67. https://doi.org/10.31610/trudyzin/2009.313.2.153

Averianov AO, Bakirov AA, Martin T. First definitive stegosaur from the Middle Jurassic of Kyrgyzstan. *Paläontologische Zeitschrift* 2007;**81**:440–6. https://doi.org/10.1007/bf02990255

Averianov AO, Krasnolutskii SA, Ivantsov SV. A new basal coelurosaur (Dinosauria: Theropoda) from the Middle Jurassic of Siberia. *Proceedings of the Zoological Institute RAS* 2010;**314**:42–57. https://doi.org/10.31610/trudyzin/2010.314.1.42

Averianov AO, Martin T, Bakirov AA. Pterosaur and dinosaur remains from the Middle Jurassic Balabansai Svita in the Northern Fergana Depression, Kyrgyzstan (Central Asia). *Palaeontology* 2005;**48**:135–55. https://doi.org/10.1111/j.1475-4983.2004.00437.x

Averianov AO, Martin T, Evans SE *et al.* First Jurassic Choristodera from Asia. *Naturwissenschaften* 2006;**93**:46–50. https://doi.org/10.1007/s00114-005-0061-2

Averianov AO, Martin T, Skutschas PP *et al.* Amphibians from the Middle Jurassic Balabansai Svita in the Fergana depression, Kyrgyzstan (central Asia). *Palaeontology* 2008;**51**:471–85. https://doi.org/10.1111/j.1475-4983.2007.00748.x

Bakirov AA. [Middle Jurassic vertebrate fauna of Kyrgyzstan]. In: *Theses of Reports of Young Scientists and Post-Graduates of the National Academy of Sciences of the Kyrgyz Republic at the Scientific-Practical Conference 'Start to Science'*, p. 67–8. Bishkek: Ilim, 2009. [In Russian].

Bakirov AA. [Middle Jurassic (Callovian) dinosaurs of Northern Fergana (Kyrgyzstan)]. In: *Geodynamics, Mineralization and Geoecological Problems of the Tien Shan. Materials of the International Conference dedicated to the 70th anniversary of the Institute of Geology of the National Academy of Sciences of the Kyrgyz Republic*, p. 51–5. Bishkek: Ilim, 2013. [In Russian].

Bakirov AA. Brief introduction on the dinosaurs from Kyrgyzstan. *Abstracts for International Symposium on Cretaceous Biota and the K-Pg boundary in Jiayin of Heilonjiang, China and the 2nd Jiayin Forum on Fossil Protection*, Aug. 18-21, 2019, p. 72–6. 2019.

Barco JL, Canudo JI, Ruiz-Omeñaca JI. New data on *Therangospodus oncalensis* from the Berriasian Fuentesalvo Tracksite (Villar del Río, Soria, Spain): an example of gregarious behaviour in theropod dinosaurs. *Ichnos* 2006;**13**:237–48. https://doi.org/10.1080/10420940600843682

Benson RBJ. A description of *Megalosaurus bucklandii* (Dinosauria: Theropoda) from the Bathonian of the UK and the relationships of Middle Jurassic theropods. *Zoological Journal of the Linnean Society* 2010;**158**:882–935. https://doi.org/10.1111/j.1096-3642.2009.00569.x

Benson RBJ, Carrano MT, Brusatte SL. A new clade of archaic large-bodied predatory dinosaurs (Theropoda: Allosauroidea) that survived to the Latest Mesozoic. *Naturwissenschaften* 2010;**97**:71–8. https://doi.org/10.1007/s00114-009-0614-x

Bonaparte JF. Jurassic tetrapods from South America and dispersal routes. In: Jacobs LL (ed.), *Aspects of Vertebrate History.* Flagstaff, AZ: Museum of Northern Arizona Press, 1980, 73–97.

Bonaparte JF. Les Dinosaures (Carnosaures, Allosauridés, Sauropodes, Cétiosauridés) du Jurassique moyen de Cerro Cóndor (Chubut, Argentine). *Annales de Paléontologie* 1986;**72**:247–289, 326–386.

Bonaparte JF. Mesozoic vertebrates of South America. In: Sun A, Wang Y (eds), *Sixth Symposium on Mesozoic Terrestrial Ecosystems and Biota, Short Papers.* Beijing: China Ocean Press, 1995, 89–90.

Bonaparte JF, Novas FE. *Abelisaurus comahuensis*, n. g., n. sp., Carnosauria del Cretacio tardio de Patagonia. *Ameghiniana* 1985;**21**:259–65.

Bonaparte JF, Novas FE, Coria RA. *Carnotaurus sastrei* Bonaparte, the horned, lightly built carnosaur from the Middle Cretaceous of Patagonia. *Contributions in Science* 1990;**416**:1–41. https://doi.org/10.5962/p.226819

Britt BB. Theropods of Dry Mesa Quarry (Morrison Formation, Late Jurassic), Colorado, with emphasis on the osteology of *Torvosaurus tanneri*. *BYU Geology Studies* 1991;**37**:1–72.

Brochu CA. Osteology of *Tyrannosaurus rex*: insights from a nearly complete skeleton and high-resolution computed tomographic analysis of the skull. *Memoir (Society of Vertebrate Paleontology)* 2003;7:1–138. https://doi.org/10.2307/3889334

Brusatte SL, Sereno PC. Phylogeny of Allosauroidea (Dinosauria: Theropoda): comparative analysis and resolution. *Journal of Systematic Palaeontology* 2008;**6**:155–82. https://doi.org/10.1017/s1477201907002404

Brusatte SL, Benson RBJ, Chure DJ *et al.* The first definitive carcharodontosaurid (Dinosauria: Theropoda) from Asia and the delayed ascent of tyrannosaurids. *Naturwissenschaften* 2009;**96**:1051–8. https://doi.org/10.1007/s00114-009-0565-2

Brusatte SL, Benson RBJ, Hutt S. The osteology of *Neovenator salerii* (Dinosauria: Theropoda) from the Wealden Group (Barremian) of the Isle of Wight. *Monograph of the Palaeontographical Society* 2008;**631**:1–75.

Brusatte SL, Carr TD, Norell MA. The osteology of *Alioramus*, a gracile and long-snouted tyrannosaurid (Dinosauria: Theropoda) from the Late Cretaceous of Mongolia. *Bulletin of the American Museum of Natural History* 2012;**366**:1–197. https://doi.org/10.1206/770.1

Brusatte SL, Chure DJ, Benson RBJ *et al.* The osteology of *Shaochilong maortuensis*, a carcharodontosaurid (Dinosauria: Theropoda) from the Late Cretaceous of Asia. *Zootaxa* 2010;**2334**:1–46.

Buffetaut E, Suteethorn V, Tong H. The earliest known tyrannosaur from the Lower Cretaceous of Thailand. *Nature* 1996;**381**:689–91. https://doi.org/10.1038/381689a0

Bybee PJ, Lee AH, Lamm E-T. Sizing the Jurassic theropod *Allosaurus*: assessing growth strategy and evolution of ontogenetic scaling of limbs. *Journal of Morphology* 2006;**267**:347–59. https://doi.org/10.1002/jmor.10406

Campione NE, Evans DC, Brown CM *et al.* Body mass estimation in non-avian bipeds using a theoretical conversion to quadruped stylopodial proportions. *Methods in Ecology and Evolution* 2014;**5**:913–23. https://doi.org/10.1111/2041-210x.12226

Canale JI, Apesteguia S, Gallina PA *et al.* New giant carnivorous dinosaur reveals convergent evolutionary trends in theropod arm reduction. *Current Biology* 2022;**32**:3195–202.e5. https://doi.org/10.1016/j.cub.2022.05.057

Canoville A, Schweitzer MH, Zanno LE. Identifying medullary bone in extinct avemetatarsalians: challenges, implications and perspectives. *Philosophical Transactions of the Royal Society of London, Series B: Biological Sciences* 2020;**375**:20190133. https://doi.org/10.1098/rstb.2019.0133

Carrano MT, Benson RBJ, Sampson SD. The phylogeny of Tetanurae (Dinosauria: Theropoda). *Journal of Systematic Palaeontology* 2012;**10**:599. https://doi.org/10.1080/14772019.2012.713753

Carrano MT, Loewen MA, Sertich JJW. New materials of *Masiakasaurus knopfleri* Sampson, Carrano and Forster, 2001, and implications for the morphology of the Noasauridae. *Smithsonian Contributions to Paleobiology* 2011;**95**:1–53. https://doi.org/10.5479/si.00810266.95.1

Carrano MT, Sampson SD. The phylogeny of Ceratosauria (Dinosauria: Theropoda). *Journal of Systematic Palaeontology* 2008;**6**:183–236.

Carrano MT, Sampson SD, Forster CA. The osteology of *Masiakasaurus knopfleri*, a small abelisauroid (Dinosauria: Theropoda) from the Late Cretaceous of Madagascar. *Journal of Vertebrate Paleontology* 2002;**22**:510–34. https://doi.org/10.1671/0272-4634(2002)022[0510:toomka]2.0.co;2

Cau A. The assembly of the avian body plan: a 160-million-year long process. *Bollettino della Società Paleontologica Italiana* 2018;**57**:1–25.

Cerroni MA, Canale JI, Novas FE. The skull of *Carnotaurus sastrei* Bonaparte 1985 revisited: insights from craniofacial bones, palate and lower jaw. *Historical Biology* 2020;**33**:2444–85. https://doi.org/10.1080/08912963.2020.1802445

Charig AJ, Milner AC. *Baryonyx walkeri*, a fish-eating dinosaur from the Wealden of Surrey. *Bulletin of the Natural History Museum, London (Geology)* 1997;**53**:11–70.

Chinsamy A, Raath MA. Preparation of fossil bone for histological examination. *Palaeontologia Africana* 1992;**29**:39–44.

Chinsamy A, Tumarkin-Deratzian AR. Pathologic bone tissues in a turkey vulture and a nonavian dinosaur: implications for interpreting endosteal bone and radial fibrolamellar bone in fossil dinosaurs. *Anatomical Record* 2009;**292**:1478–84. https://doi.org/10.1002/ar.20991

Choiniere JN, Clark JM, Forster CA *et al.* A basal coelurosaur (Dinosauria: Theropoda) from the Late Jurassic (Oxfordian) of the Shishugou Formation in Wucaiwan, People's Republic of China. *Journal of Vertebrate Paleontology* 2010a;**30**:1773–96. https://doi.org/10.1080/02724634.2010.520779

Choiniere JN, Xu X, Clark JM *et al.* A basal alvarezsauroid theropod from the early Late Jurassic of Xinjiang, China. *Science* 2010b;**327**:571–4. https://doi.org/10.1126/science.1182143

Chure DJ, Madsen JH. On the presence of furculae in some non-maniraptoran theropods. *Journal of Vertebrate Paleontology* 1996;**16**:573–7. https://doi.org/10.1080/02724634.1996.10011341

Coria RA, Currie PJ. The braincase of *Giganotosaurus carolinii* (Dinosauria: Theropoda) from the Upper Cretaceous of Argentina. *Journal of Vertebrate Paleontology* 2002;**22**:802–11.

Coria RA, Currie PJ. A new carcharodontosaurid (Dinosauria, Theropoda) from the Upper Cretaceous of Argentina. *Geodiversitas* 2006;**28**:71–118.

Cullen TM, Canale JI, Apesteguia S *et al.* Osteohistological analyses reveal diverse strategies of theropod dinosaur body-size evolution. *Proceedings Biological Sciences* 2020;**287**:20202258. https://doi.org/10.1098/rspb.2020.2258

Currie PJ. Possible evidence of gregarious behavior in tyrannosaurids. *Gaia* 2000;**15**:271–7.

Currie PJ, Carpenter K. A new specimen of *Acrocanthosaurus atokensis* (Theropoda, Dinosauria) from the Lower Cretaceous Antlers Formation (Lower Cretaceous, Aptian) of Oklahoma, USA. *Geodiversitas* 2000;**22**:207–46.

Currie PJ, Eberth DA. On gregarious behavior in *Albertosaurus*. *Canadian Journal of Earth Sciences* 2010;**47**:1277–89. https://doi.org/10.1139/e10-072

Currie PJ, Zhao X-J. A new carnosaur (Dinosauria, Theropoda) from the Jurassic of Xinjiang, People's Republic of China. *Canadian Journal of Earth Sciences* 1993;**30**:2037–81. https://doi.org/10.1139/e93-179

D'Emic MD, Melstrom KM, Eddy DR. Paleobiology and geographic range of the large-bodied Cretaceous theropod dinosaur *Acrocanthosaurus atokensis*. *Palaeogeography, Palaeoclimatology, Palaeoecology* 2012;**333–334**:13–23. https://doi.org/10.1016/j.palaeo.2012.03.003

Dai H, Benson RBJ, Hu X *et al.* A new possible megalosauroid theropod from the Middle Jurassic Xintiangou Formation of Chongqing, People's Republic of China and its implication for early tetanuran evolution. *Scientific Reports* 2020;**10**:139. https://doi.org/10.1038/s41598-019-56959-x

Ding A, Pittman M, Upchurch P *et al.* The biogeography of coelurosaurian theropods and its impact on their evolutionary history. *Bulletin of the American Museum of Natural History* 2020;**440**:117–57.

Dong Z. [A new theropod dinosaur from the Middle Jurassic of Sichuan Basin]. *Vertebrata PalAsiatica* 1984;**22**:213–8. [in Chinese].

Dong Z, Tang Z. [A new mid-Jurassic theropod (*Gasosaurus constructus* gen. et sp. nov.) from Dashanpu, Zigong, Sichuan Province, China]. *Vertebrata PalAsiatica* 1985;**23**:77–83. [in Chinese].

Dong Z, Zhou S, Zhang Y. [The dinosaurian remains from Sichuan Basin, China]. *Palaeontologia Sinica* 1983;**162**:1–145. [in Chinese].

Ezcurra MD. Exploring the effects of weighting against homoplasy in genealogies of palaeontological phylogenetic matrices. *Cladistics* 2024;**40**:242–81. https://doi.org/10.1111/cla.12581

Filippi LS, Méndez AH, Gianechini FA *et al.* Osteology of *Viavenator exxoni* (Abelisauridae; Furileusauria) from the Bajo de la Carpa Formation, NW Patagonia, Argentina. *Cretaceous Research* 2018;**83**:95–119.

Fiorillo AR. Trample marks: caution from the Cretaceous. *Current Research in the Pleistocene* 1987;**4**:73–5.

Foster JR. Paleoecological analysis of the vertebrate fauna of the Morrison Formation (Upper Jurassic), Rocky Mountain Region, USA. *Bulletin of the New Mexico Museum of Natural History & Science* 2003;**23**:1–95.

Foster JR. *Jurassic West. The Dinosaurs of the Morrison Formation and their World.* 2nd edn. Bloomington, IN: Indiana University Press, 2020.

Foth C, Rauhut OWM. Re-evaluation of the Haarlem *Archaeopteryx* and the radiation of maniraptoran theropod dinosaurs. *BMC Evolutionary Biology* 2017;**17**:236. https://doi.org/10.1186/s12862-017-1076-y

Gao Y. [A new species of *Szechuanosaurus* from the Middle Jurassic of Dashanpu, Zigong, Sichuan]. *Vertebrata PalAsiatica* 1993;**31**:308–14. [in Chinese]

Gao Y. *[A Complete Carnosaur Skeleton from Zigong, Sichuan - Yangchuanosaurus hepingensis].* Chengdu: Sichuan Science and Technology Press, 1999. [in Chinese]

Gauthier J. Saurischian monophyly and the origin of birds. *Memoirs of the Californian Academy of Science* 1986;**8**:1–55.

Gilmore CW. Osteology of the carnivorous Dinosauria in the United States National Museum, with special reference to the genera

Antrodemus (*Allosaurus*) and *Ceratosaurus*. *Bulletin of the United States National Museum* 1920;**110**:i–159. https://doi.org/10.5479/si.03629236.110.i

Godefroit P, Sintisa SM, Dhouaily D *et al.* A Jurassic ornithischian dinosaur from Siberia with both feathers and scales. *Science* 2014;**345**:451–5.

Goloboff PA, Morales ME. TNT version 1.6, with a graphical interface for MacOS and Linux, including new routines in parallel. *Cladistics* 2023;**39**:144–53. https://doi.org/10.1111/cla.12524

Goloboff PA, Torres A, Arias JS. Weighted parsimony outperforms other methods of phylogenetic inference under models appropriate for morphology. *Cladistics* 2018;**34**:407–37. https://doi.org/10.1111/cla.12205

He X. *[The Vertebrate Fossils of Sichuan]*. Chengdu: Sichuan Scientific and Technological Publishing House, 1984. [in Chinese]

Hedrick BP, Gao C, Tumarkin-Deratzian AR *et al.* An injured *Psittacosaurus* (Dinosauria: Ceratopsia) from the Yixian Formation (Liaoning, China): implications for *Psittacosaurus* biology. *Anatomical Record* 2016;**299**:897–906. https://doi.org/10.1002/ar.23363

Hendrickx C, Mateus O, Araújo R. The dentition of megalosaurid theropods. *Acta Palaeontologica Polonica* 2015;**60**:627–42.

Hendrickx C, Mateus O, Araújo R *et al.* The distribution of dental features in non-avian theropod dinosaurs: taxonomic potential, degree of homoplasy, and major evolutionary trends. *Palaeontologia Electronica* 2019;**22**:1–110.

Hendrickx C, Stiegler J, Currie PJ *et al.* Dental anatomy of the apex predator *Sinraptor dongi* (Theropoda: Allosauroidea) from the Late Jurassic of China. *Canadian Journal of Earth Sciences* 2020;**57**:1127–47. https://doi.org/10.1139/cjes-2019-0231

Heredia AM, Diaz-Martinez I, Pazos PJ *et al.* Gregarious behaviour among non-avian theropods inferred from trackways: a case study from the Cretaceous (Cenomanian) Candeleros Formation of Patagonia, Argentina. *Palaeogeography, Palaeoclimatology, Palaeoecology* 2020;**538**:109480. https://doi.org/10.1016/j.palaeo.2019.109480

Horner JR, Padian K. Age and growth dynamics of *Tyrannosaurus rex*. *Proceedings Biological Sciences* 2004;**271**:1875–80. https://doi.org/10.1098/rspb.2004.2829

Hu D, Clarke J, Eliason C *et al.* A bony-crested Jurassic dinosaur with evidence of iridescent plumage highlights complexity in early paravian evolution. *Nature Communications* 2018;**9**:217.

Hu D, Hou L, Zhang L *et al.* A pre-*Archaeopteryx* troodontid theropod from China with long feathers on the metatarsus. *Nature* 2009;**461**:640–3. https://doi.org/10.1038/nature08322

Hübner TR. Bone histology in *Dysalotosaurus lettowvorbecki* (Ornithischia: Iguanodontia) – variation, growth, and implications. *PLoS One* 2012;**7**:e29958. https://doi.org/10.1371/journal.pone.0029958

Huene F. The carnivorous Saurischia in the Jura and Cretaceous Formations, principally in Europe. *Revista del Museo de La Plata* 1926;**29**:35–167.

Hutchinson JR. The evolution of pelvic osteology and soft tissues on the line to extant birds (Neornithes). *Zoological Journal of the Linnean Society* 2001a;**131**:123–68. https://doi.org/10.1111/j.1096-3642.2001.tb01313.x

Hutchinson JR. The evolution of femoral osteology and soft tissues on the line to extant birds (Neornithes). *Zoological Journal of the Linnean Society* 2001b;**131**:169–97. https://doi.org/10.1111/j.1096-3642.2001.tb01314.x

Juárez-Valieri RD, Fiorelli LE, Cruz LE. *Quilmesaurus curriei* Coria, 2001 (Dinosauria, Theropoda). Su validez taxonómica y relaciones filogenéticas. *Revista del Museo Argentino de Ciencias Naturales* 2007;**9**:59–66.

Ksepka DT, Norell MA. The illusory evidence for Asian Brachiosauridae: new material of *Erketu ellisoni* and a phylogenetic reappraisal of basal Titanosauriformes. *American Museum Novitates* 2010;**3700**:1–27. https://doi.org/10.1206/3700.2

Lamm E-T. Preparation and sectioning of specimens. In: Padian K, Lamm E-T (eds), *Bone Histology of Fossil Tetrapods: Advancing Methods, Analysis and Interpretation*. Berkeley CA: University of California Press, 2013, 55–160.

Li K, Liu J, Yang C *et al.* Dinosaur assemblages from the Middle Jurassic Shaximiao Formation and Chuanjie Formation in the Sichuan-Yunnan Basin, China. *Volumina Jurassica* 2011;**9**:21–42.

Lipkin C, Sereno PC, Horner JR. The furcula in *Suchomimus tenerensis* and *Tyrannosaurus rex* (Dinosauria: Theropoda: Tetanurae). *Journal of Paleontology* 2007;**81**:1523–7. https://doi.org/10.1666/06-024.1

Lockley MG, McCrea RT, Alcala L *et al.* A preliminary report on an assemblage of large theropod tracks from the Cretaceous Dakota Group, western Colorado: evidence for gregarious behavior. *New Mexico Museum of Natural History & Science Bulletin* 2015;**67**:179–83.

Maddison WP, Maddison DR. *Mesquite: A Modular System for Evolutionary Analysis. Version 3.81*, 2023. http://mesquiteproject.org

Madsen JH. *Allosaurus fragilis*: a revised osteology. *Utah Geological and Mineralogical Survey Bulletin* 1976;**109**:3–163.

Madsen JH, Welles SP. *Ceratosaurus* (Dinosauria, Theropoda). A revised osteology. *Miscellaneous Publication, Utah Geological Survey* 2000;**00-2**:1–80.

Makovicky PJ, Currie PJ. The presence of a furcula in tyrannosaurid theropods, and its phylogenetic and functional implications. *Journal of Vertebrate Paleontology* 1998;**18**:143–9. https://doi.org/10.1080/02724634.1998.10011040

Malafaia E, Mocho P, Escaso F *et al.* A new carcharodontosaurian theropod from the Lusitanian Basin: evidence of allosauroid sympatry in the European Late Jurassic. *Journal of Vertebrate Paleontology* 2020;**40**:e1768106. https://doi.org/10.1080/02724634.2020.1768106

Mallison H, Wings O. Photogrammetry in paleontology—a practical guide. *Journal of Paleontological Techniques* 2014;**12**:1–31.

Marsh OC. Principal characters of American Jurassic dinosaurs. Part V. *American Journal of Science (ser. 3)* 1881;**21**:417–23.

Martin T, Averianov AO. Mammals from the Middle Jurassic Balabansai Formation of the Fergana Depression, Kyrgyzstan. *Journal of Vertebrate Paleontology* 2010;**30**:855–71. https://doi.org/10.1080/02724631003758045

Mateus O, Walen A, Antunes MT. The large theropod fauna of the Lourinha Formatuion (Portugal) and its similarity to that of the Morrison Formation, with a description of new species of *Allosaurus*. *New Mexico Museum of Natural History and Science Bulletin* 2006;**36**:123–9.

Mocho P, Royo-Torres R, Ortega F. A new macronarian sauropod from the Upper Jurassic of Portugal. *Journal of Vertebrate Paleontology* 2019;**39**:e1578782. https://doi.org/10.1080/02724634.2019.1578782

Nesbitt S, Turner A, Spaulding M *et al.* The theropod furcula. *Journal of Morphology* 2009;**270**:856–79.

Nessov LA. *[Dinosaurs of Northern Eurasia: New Data About Assemblages, Ecology and Palaeobiogeography]*. Saint Petersburgh: Izdatelstvo Sankt-Peterburgskogo Universiteta, 1995. [in Russian]

Nessov LA, Kaznishkina MN, Cherepanov GO. [Mesozoic ceratopsian dinosaurs and crocodiles of central Asia.] In: Bogdanova TN, Khozatsky LI (eds), *Theoretical and Applied Aspects of Modern Paleontology*. Moscow: Nauka, 1989, 144–54. [in Russian]

Norell MA, Makovicky P, Clark JM. A *Velociraptor* wishbone. *Nature* 1997;**389**:447. https://doi.org/10.1038/38918

Novas FE, Agnolin FL, Ezcurra MD *et al.* Evolution of the carnivorous dinosaurs during the Cretaceous: the evidence from Patagonia. *Cretaceous Research* 2013;**45**:174–215. https://doi.org/10.1016/j.cretres.2013.04.001

O'Connor PM. The postcranial axial skeleton of *Majungasaurus crenatissimus* (Theropoda: Abelisauridae) from the Late Cretaceous of Madagascar. *Society of Vertebrate Paleontology, Memoir* 2007;**8**:127–62.

O'Connor JK, Erickson GM, Norell MA *et al.* Medullary bone in an Early Cretaceous enantiornithine bird and discussion regarding its identification in fossils. *Nature Communications* 2018;**9**:5169.

Owen R. Report on British fossil reptiles. Part II. *Reports of the British Association for the Advancement of Sciences* 1842;**11**:60–204.

Parks WA. *Albertosaurus arctunguis*. A new species of therapodous dinosaur from the Edmonton Formation of Alberta. *University of Toronto Studies, Geological Series* 1928;**25**:1–42.

Paul GS. *Predatory Dinosaurs of the World.* New York, NY: Simon & Schuster, 1988.

Peng G, Ye Y, Yuhui G *et al. [Jurassic Dinosaur Faunas in Zigong.]* Zigong: Zigong Dinosaur Museum, 2005. [in Chinese]

Qin Z, Clark JM, Choiniere JN *et al.* A new alvarezsaurian theropod from the Upper Jurassic Shishugou Formation of western China. *Scientific Reports* 2019;**9**:11727. https://doi.org/10.1038/s41598-019-48148-7

Rauhut OWM. The interrelationships and evolution of basal theropod dinosaurs. *Special Papers in Palaeontology* 2003;**69**:1–213.

Rauhut OWM. Osteology and relationships of a new theropod dinosaur from the Middle Jurassic of Patagonia. *Palaeontology* 2005;**48**:87–110. https://doi.org/10.1111/j.1475-4983.2004.00436.x

Rauhut OWM. Theropod dinosaurs from the Late Jurassic of Tendaguru (Tanzania). *Special Papers in Palaeontology* 2011;**86**:195–239.

Rauhut OWM, Carrano MT. The theropod dinosaur *Elaphrosaurus bambergi* Janensch, 1920, from the Late Jurassic of Tendaguru, Tanzania. *Zoological Journal of the Linnean Society* 2016;**178**:546–610. https://doi.org/10.1111/zoj.12425

Rauhut OWM, López-Arbarello A. Archosaur evolution during the Jurassic: a southern perspective. *Revista de la Asociación Geológica Argentina* 2008;**63**:557–85.

Rauhut OWM, Pol D. A theropod dinosaur from the Late Jurassic Cañadón Calcáreo Formation of Chubut, Patagonia, and the evolution of the theropod tarsus. *Ameghiniana* 2017;**54**:539–66. https://doi.org/10.5710/amgh.12.10.2017.3105

Rauhut OWM, Pol D. Probable basal allosauroid from the early Middle Jurassic Cañadón Asfalto Formation of Argentina highlights phylogenetic uncertainty in tetanuran theropod dinosaurs. *Scientific Reports* 2019;**9**:18826. https://doi.org/10.1038/s41598-019-53672-7

Rauhut OWM, Pol D. New theropod remains from the Late Jurassic Cañadón Calcáreo Formation of Chubut, Argentina. *Journal of South American Earth Sciences* 2021;**111**:103434.

Rauhut OWM, Pol D. New theropod remains from the Late Jurassic Cañadón Calcáreo Formation of Chubut, Argentina. Palaeovertebrata, Special Volume, 2022, 164.

Rauhut OWM, Foth C, Tischlinger H *et al.* Exceptionally preserved juvenile megalosauroid theropod dinosaur with filamentous integument from the Late Jurassic of Germany. *Proceedings of the National Academy of Sciences of the United States of America* 2012;**109**:11746–51. https://doi.org/10.1073/pnas.1203238109

Rauhut OWM, Hübner TR, Lanser K-P. A new megalosaurid theropod dinosaur from the late Middle Jurassic (Callovian) of north-western Germany: implications for theropod evolution and faunal turnover in the Jurassic. *Palaeontologia Electronica* 2016;**19**:1–65.

Rauhut OWM, Piñuela L, Castanera D *et al.* The largest European theropod dinosaurs: remains of a gigantic megalosaurid and giant theropod tracks from the Kimmeridgian of Asturias, Spain. *PeerJ* 2018;**6**:e4963. https://doi.org/10.7717/peerj.4963

Rauhut OWM, Schwermann AH, Hübner TR *et al.* The oldest record of the genus *Torvosaurus* (Theropoda: Megalosauridae), from the Callovian Ornatenton Formation of north-western Germany. *Geologie und Paläontologie in Westfalen* 2020;**93**:31–43.

Ren X-X, Sekiya T, Wang T *et al.* A revision of the referred specimen of *Chuanjiesaurus anaensis* Fang *et al.*, 2000: a new early branching mamenchisaurid sauropod from the Middle Jurassic of China. *Historical Biology* 2021;**33**:1872–87. https://doi.org/10.1080/08912963.2020.1747450

Rotatori FM, Moreno-Azanza M, Mateus O. Reappraisal and new material of the holotype of *Draconyx loureiroi* (Ornithischia: Iguanodontia) provide insights on the tempo and modo of evolution of thumb-spiked dinosaurs. *Zoological Journal of the Linnean Society* 2022;**195**:125–56. https://doi.org/10.1093/zoolinnean/zlab113

Rozhdestvensky AK. [The finding of a giant dinosaur.]. *Priroda* 1968;**2**:115–6. [in Russian]

Sadleir R, Barrett PM, Powell HP. The anatomy and systematics of *Eustreptospondylus oxoniensis*, a theropod dinosaur from the Middle Jurassic of Oxfordshire, England. *Monograph of the Palaeontographical Society* 2008;**160**:1–82. https://doi.org/10.1080/25761900.2022.12131807

Samathi A. Osteology and phylogenetic position of *Siamotyrannus isanensis* (Dinosauria; Theropoda) from the Lower Cretaceous of Thailand. Unpublished MSc Thesis, Ludwig-Maximilians-Universität, 2013.

Sampson SD, Witmer LM. Craniofacial anatomy of *Majungsaurus crenatissimus* (Theropoda: Abelisauridae) from the Late Cretaceous of Madagascar. *Society of Vertebrate Paleontology, Memoir* 2007;**8**:32–102.

Schade M, Rauhut OWM, Foth C *et al.* A reappraisal of the cranial osteology of the spinosaurid *Irritator challengeri* (Dinosauria: Theropoda). *Palaeontologia Electronica* 2023;**26**:a17.

Seeley HG. On the classification of the fossil animals commonly named Dinosauria. *Proceedings of the Royal Society of London* 1887;**43**:165–71.

Seiilbek S, Sarbassov B, Ismakova A *et al.* Mythological aspects of the Kyrgyzs' ethnographic way of life in the historical epos 'Manas'. *Opción* 2018;**33**:632–51.

Sereno PC, Brusatte SL. Basal abelisaurid and carcharodontosaurid theropods from the Lower Cretaceous Elrhaz Formation of Niger. *Acta Palaeontologica Polonica* 2008;**53**:15–46. https://doi.org/10.4202/app.2008.0102

Sereno PC, Dutheil DB, Iarochene M *et al.* Predatory dinosaurs from the Sahara and Late Cretaceous faunal differentiation. *Science* 1996;**272**:986–91. https://doi.org/10.1126/science.272.5264.986

Sereno PC, Martinez RN, Wilson JA *et al.* Evidence for avian intathoracic air sacs in a new predatory dinosaur from Argentina. *PLoS One* 2008;**3**:e3303–20. https://doi.org/10.1371/journal.pone.0003303

Sereno PC, Wilson JA, Larsson HCE *et al.* Early Cretaceous dinosaurs from the Sahara. *Science* 1994;**266**:267–71. https://doi.org/10.1126/science.266.5183.267

Soto M, Perea D. A ceratosaurid (Dinosauria, Theropoda) from the Late Jurassic-Early Cretaceous of Uruguay. *Journal of Vertebrate Paleontology* 2008;**28**:439–44. https://doi.org/10.1671/0272-4634(2008)28[439:acdtft]2.0.co;2

Stovall JW, Langston WJ. *Acrocanthosaurus atokensis*, a new genus and species of Lower Cretaceous Theropoda from Oklahoma. *American Midland Naturalist* 1950;**43**:696–728. https://doi.org/10.2307/2421859

Stromer E. Ergebnisse der Forschungsreisen Prof. E. Stromers in den Wüsten Ägyptens. II. Wirbeltierreste der Baharije-Stufe (unterstes Cenoman). 10. Ein Skelett-Rest von *Carcharodontosaurus* nov. gen. *Abhandlungen der Bayerischen Akademie der Wissenschaften, Mathematisch-naturwissenschaftliche Abteilung, Neue Folge* 1931;**9**:1–23.

Sullivan RM. A taxonomic review of the Pachycephalosauridae (Dinosauria: Ornithischia). *New Mexico Museum of Natural History & Science Bulletin* 2006;**35**:347–65.

Upchurch P, Hunn CA, Norman DB. An analysis of dinosaurian biogeography: evidence for the existence of vicariance and dispersal patterns caused by geological events. *Proceedings Biological Sciences* 2002;**269**:613–21. https://doi.org/10.1098/rspb.2001.1921

Walker AD. Triassic reptiles from the Elgin area: *Ornithosuchus* and the origin of carnosaurs. *Philosophical Transactions of the Royal Society of London, Series B* 1964;**248**:53–134.

Wang J, Ye Y, Pei R *et al.* Age of Jurassic basal sauropods in Sichuan, China: a reappraisal of basal sauropod evolution. *GSA Bulletin* 2018;**130**:1493–500. https://doi.org/10.1130/b31910.1

Wang S, Stiegler J, Amiot R *et al.* Extreme ontogenetic changes in a ceratosaurian theropod. *Current Biology* 2017;**27**:144–8.

Wilson JA, Upchurch P. Redescription and reassessment of the phylogenetic affinities of *Euhelopus zdanskyi* (Dinosauria: Sauropoda) from the Early Cretaceous of China. *Journal of Systematic Palaeontology* 2009;**7**:199–239. https://doi.org/10.1017/s1477201908002691

Wu X-C, Currie PJ, Dong Z *et al.* A new theropod dinosaur from the Middle Jurassic of Lufeng, Yunnan, China. *Acta Geologica Sinica - English Edition* 2009;**83**:9–24. https://doi.org/10.1111/j.1755-6724.2009.00002.x

Xing L, Paulina Carabajal A, Currie PJ *et al.* Braincase anatomy of the basal theropod *Sinosaurus* from the Early Jurassic of China. *Acta Geologica Sinica* 2014;**88**:1653–61.

Xing L, Miyashita T, Zhang J *et al*. A new sauropod dinosaur from the Late Jurassic of China and the diversity, distribution, and relationships of mamenchisaurids. *Journal of Vertebrate Paleontology* 2015;**35**:e889701. https://doi.org/10.1080/02724634.2014.889701

Xu L, Wang M, Chen R *et al*. A new avialan theropod from an emerging Jurassic terrestrial fauna. *Nature* 2023;**621**:336–43. https://doi.org/10.1038/s41586-023-06513-7

Xu X, Clark JM, Eberth DA *et al*. The Shishugou fauna of the Middle–Late Jurassic transition period in the Junggar Basin of Western China. *Acta Geologica Sinica (English Edition)* 2022;**96**:1115–35.

Xu X, Clark JM, Forster CA *et al*. A basal tyrannosauroid dinosaur from the Late Jurassic of China. *Nature* 2006;**439**:715–8. https://doi.org/10.1038/nature04511

Xu X, Clark JM, Mo J *et al*. A Jurassic ceratosaur from China helps to clarify avian digital homologies. *Nature* 2009;**459**:940–4. https://doi.org/10.1038/nature08124

Xu X, Norell MA, Kuang X *et al*. Basal tyrannosauroids from China and evidence for protofeathers in tyrannosauoids. *Nature* 2004;**431**:680–4. https://doi.org/10.1038/nature02855

Xu X, Upchurch P, Mannion PD *et al*. A new Middle Jurassic diplodocoid suggests an earlier dispersal and diversification of sauropod dinosaurs. *Nature Communications* 2018;**9**:2700. https://doi.org/10.1038/s41467-018-05128-1

Xu X, You H-L, Du K *et al*. An *Archaeopteryx*-like theropod from China and the origin of Avialae. *Nature* 2011;**475**:465–70. https://doi.org/10.1038/nature10288

Xu X, Zheng X-T, Sullivan C *et al*. A bizarre Jurassic maniraptoran theropod with preserved evidence of membranous wings. *Nature* 2015;**521**:70–3. https://doi.org/10.1038/nature14423

Xu X, Zhou Z, Sullivan C *et al*. An updated review of the Middle-Late Jurassic Yanliao Biota: chronology, taphonomy, paleontology and paleoecology. *Acta Geologica Sinica* 2016;**90**:2229–43.

Yu Y, Harris A, Blair C *et al*. RASP (Reconstruct Ancestral State in Phylogenies): a tool for historical biogeography. *Molecular Phylogenetics and Evolution* 2015;**87**:46–9. https://doi.org/10.1016/j.ympev.2015.03.008

Yu Y, Harris AJ, He X. S-DIVA (statistical dispersal-vicariance analysis): a tool for inferring biogeographic histories. *Molecular Phylogenetics and Evolution* 2010;**56**:848–50. https://doi.org/10.1016/j.ympev.2010.04.011

Zanno LE, Makovicky PJ. Neovenatorid theropods are apex predators in the Late Cretaceous of North America. *Nature Communications* 2013;**4**:2827. https://doi.org/10.1038/ncomms3827

Zhang F, Zhou Z, Xu X *et al*. A bizarre Jurassic maniraptoran from China with elongate ribbon-like feathers. *Nature* 2008;**455**:1105–8. https://doi.org/10.1038/nature07447

Zhang Z-C, Wang T, You H-L. A new specimen of *Sinosaurus triassicus* (Dinosauria: Theropoda) from the Early Jurassic of Lufeng, Yunnan, China. *Historical Biology* 2023;**36**:857–71. https://doi.org/10.1080/08912963.2023.2190760

Zhao X-J, Currie PJ. A large crested theropod from the Jurassic of Xinjiang, People's Republic of China. *Canadian Journal of Earth Sciences* 1993;**30**:2027–36. https://doi.org/10.1139/e93-178

Zhou Z, Wang Y. Vertebrate assemblages of the Jurassic Yanliao Biota and the Early Cretaceous Jehol Biota: comparisons and implications. *Palaeoworld* 2017;**26**:241–52. https://doi.org/10.1016/j.palwor.2017.01.002

Zhou Y, Dai H, Yu H *et al*. Zircon geochronology of the new dinosaur fauna in the Middle Jurassic lower Shaximiao Formation in Chongqing, SW China. *Palaeogeography, Palaeoclimatology, Palaeoecology* 2022;**592**:110894. https://doi.org/10.1016/j.palaeo.2022.110894